

**Therapeutic Strategies of Matricellular Proteins in Cutaneous Wound Healing:  
Countervailing Chronic Wounds and Excessive Scarring.**

by

**Kyle James Sylakowski**

Bachelor of Science, California State University San Marcos, 2013

Submitted to the Graduate Faculty of the  
School of Medicine in partial fulfillment  
of the requirements for the degree of  
Doctor of Philosophy

University of Pittsburgh

2022

UNIVERSITY OF PITTSBURGH

SCHOOL OF MEDICINE

This thesis was presented

by

**Kyle James Sylakowski**

It was defended on

February 2, 2022

and approved by

Charleen T. Chu, MD, PhD, Department of Pathology

Bennett Van Houten, PhD, Department of Pharmacology & Chemical Biology

Donna Beer Stolz, PhD, Department of Cell Biology

Justin S. Weinbaum, PhD, Department of Bioengineering & Pathology

Committee Chair: Alejandro Soto-Gutiérrez, MD, PhD, Department of Pathology

Dissertation Advisor: Alan H. Wells, MD, DMSc, Department of Pathology

Copyright © by Kyle James Sylakowski

2022

# **Therapeutic Strategies of Matricellular Proteins in Cutaneous Wound Healing: Countervailing Chronic Wounds and Excessive Scarring.**

Kyle James Sylakowski, PhD

University of Pittsburgh, 2022

Cutaneous wound healing is an intricate orchestration of three overlapping phases of repair that encompass numerous cell types, signaling cascades, and microenvironment modifications to reach a successful resolution with minimal scarring. Disruption of any of these steps will create an abnormal healing response resulting in either chronic ulceration or excessive scarring. It has become evident that the extracellular matrix (ECM) and its associated components are key orchestrators during this process. A subclass of non-structural ECM proteins called matricellular proteins has taken to the forefront as possible targets for therapeutic strategies using ECM components due to their ability to mediate cell-ECM interactions. Here, we utilize two matricellular proteins significantly upregulated during the early or late phases of cutaneous wound healing – Tenascin-C (TNC) and Decorin (DCN). TNC is considered a vital *on-switch* for early phases of wound healing as it coordinates migration and survival signals of numerous cell types in the early stages of the hostile wound environment. Building upon previous work that showed TNC’s ability to promote survival of mesenchymal stem cells (MSCs) both *in vitro* and *in vivo*, we show that TNC enhances the therapeutic efficacy of MSCs through an improved ability to promote angiogenesis. DCN is the opposite of TNC as it is considered an essential *off-switch* for the tissue replacement phase of wound healing and limiting the occurrence of excessive scarring pathologies. Here we show DCN’s ability to improve wound healing outcomes and limit hypertrophic scarring *in vivo* during the resolution phase of repair. Ultimately, our work further

emphasizes the potential use of matricellular proteins as therapeutic strategies to enhance cutaneous wound healing outcomes.

**Table of Contents**

**Preface..... xii**

**1.0 Introduction..... 1**

**1.1 Skin Anatomy And Function..... 2**

**1.2 Cutaneous Wound Healing..... 5**

**1.3 Extracellular Matrix In Cutaneous Wound Healing ..... 7**

**1.3.1 ECM In The Hemostasis And Inflammation Phase Of Wound Healing. ....8**

**1.3.2 ECM In The Tissue Replacement Phase Of Wound Healing. ....10**

**1.3.3 ECM In The Resolution Phase Of Wound Healing .....12**

**2.0 Chronic Wounds ..... 15**

**2.1 Clinical Significance Of Chronic Wounds ..... 15**

**2.2 Chronic Wound Microenvironment ..... 16**

**2.3 Mesenchymal Stem Cells ..... 19**

**2.3.1 MSCs Role In Wound Repair .....19**

**2.3.2 Hostile Wound Microenvironment Challenges MSC Survival.....22**

**2.3.3 MSC Delivery Strategies For Improved Survival And Efficacy.....25**

**2.3.3.1 Matrix Components For MSC Delivery: ..... 25**

**2.3.3.2 Matricellular Protein Tenascin-C ..... 28**

**3.0 Excessive Scarring ..... 31**

**3.1 Clinical Significance ..... 31**

**3.2 Excessive Scarring Microenvironment..... 32**

**3.3 Matricellular Protein Decorin ..... 35**

<b>4.0 Hypothesis.....</b>	<b>37</b>
<b>5.0 Matricellular Protein Tenascin-C Enhances Mesenchymal Stem Cell Angiogenic And Wound Healing Ability. ....</b>	<b>39</b>
<b>5.1 Summary: .....</b>	<b>39</b>
<b>5.2 Introduction .....</b>	<b>40</b>
<b>5.3 Materials And Methods .....</b>	<b>42</b>
<b>5.3.1 Cell Culture .....</b>	<b>42</b>
<b>5.3.2 Coating Culture Plates With Col-I And TNC .....</b>	<b>45</b>
<b>5.3.3 Apoptosis Assessment .....</b>	<b>45</b>
<b>5.3.4 Preparation Of Conditioned Media.....</b>	<b>46</b>
<b>5.3.5 Cord Formation Assay.....</b>	<b>46</b>
<b>5.3.6 Scratch Assay.....</b>	<b>47</b>
<b>5.3.7 Cytokine Measurement.....</b>	<b>48</b>
<b>5.3.8 RT-PCR Analysis .....</b>	<b>48</b>
<b>5.3.9 Animal Model .....</b>	<b>49</b>
<b>5.3.10 Mouse Wounding .....</b>	<b>50</b>
<b>5.3.11 Coacervate Preparation And Mouse Injections .....</b>	<b>50</b>
<b>5.3.12 Coacervate Release.....</b>	<b>52</b>
<b>5.3.13 Histological Analyses .....</b>	<b>52</b>
<b>5.3.14 Statistical Analysis: .....</b>	<b>55</b>
<b>5.4 Results.....</b>	<b>56</b>
<b>5.4.1 Tenascin-C Protects MSCs Under Ischemic Conditions <i>In-Vitro</i>. ....</b>	<b>56</b>

5.4.2 Condition Media From MSCs Cultured On Tenascin-C Improves Endothelial Cord Formation And Motility.....	60
5.4.3 Assessment Of Culture Conditions On MSC Paracrine Activity And Gene Expression During H/ND Exposure. ....	63
5.4.4 Coacervate With TNC And MSC Improves Wound Healing <i>In Vivo</i> In Delayed Wound Healing Mouse Model.....	66
5.5 Discussion .....	72
6.0 The Matricellular Protein Decorin Delivered Intradermally With Coacervate Improves Wound Resolution In A Mouse Model Of Hypertrophic Scarring.....	75
6.1 Summary .....	75
6.2 Introduction .....	76
6.3 Materials And Methods .....	79
6.3.1 Animal Model .....	79
6.3.2 Mouse Wounding .....	79
6.3.3 Coacervate Preparation.....	80
6.3.4 Coacervate Mouse Injections .....	80
6.3.5 Coacervate Release.....	81
6.3.6 Histological Analyses .....	82
6.3.7 Statistical Analysis: .....	85
6.4 Results.....	85
6.4.1 Growth Factor Therapy Augments Initial Phases Of Healing .....	85
6.4.2 Modifying The Matrix Increased Vascularization During Tissue Replacement.....	88

<b>6.4.3 Coacervate With Decorin Improves Wound Healing Outcomes In The Resolution Phase .....</b>	<b>91</b>
<b>6.5 Discussion .....</b>	<b>94</b>
<b>7.0 Concluding Remarks And General Discussion .....</b>	<b>97</b>
<b>7.1 Significance .....</b>	<b>97</b>
<b>7.2 Future Directions: Dual Delivery Of matricellular Proteins Tenascin-C And Decorin .....</b>	<b>98</b>
<b>7.3 Future Directions: Enhancing MSC Delivery Strategies For Improved Survival And Efficacy .....</b>	<b>100</b>
<b>7.3.1 Hypoxic Preconditioning For MSC Delivery: .....</b>	<b>101</b>
<b>7.3.2 Regulating Autophagy May Be Key Mechanism For Survival And Efficacy In MSC Combinational Therapies. ....</b>	<b>102</b>
<b>Appendix A .....</b>	<b>112</b>
<b>Appendix A.1 Autophagy Analysis Methodology .....</b>	<b>112</b>
<b>Appendix B .....</b>	<b>114</b>
<b>Appendix B.1 CXCR3 Deficient Mouse Model for Wound Healing.....</b>	<b>114</b>
<b>Appendix C .....</b>	<b>117</b>
<b>Appendix C.1 Abbreviations .....</b>	<b>117</b>
<b>Bibliography .....</b>	<b>119</b>

## List of Figures

<b>Figure 1: Anatomy of the skin .....</b>	<b>5</b>
<b>Figure 2: Overview of ECM during routine wound healing.....</b>	<b>14</b>
<b>Figure 3: Phase transitions in normal and abnormal wound healing.....</b>	<b>18</b>
<b>Figure 4: Roles for mesenchymal stem cells (MSCs) during cutaneous wound healing .....</b>	<b>21</b>
<b>Figure 5: MSCs face a steep challenge when they enter the wound microenvironment.....</b>	<b>24</b>
<b>Figure 6: Confirmation of hypoxia in BioSpherix culture system. ....</b>	<b>44</b>
<b>Figure 7: Coacervate delivery study of matricellular protein TNC and MSCs on delayed wound healing mouse model. ....</b>	<b>51</b>
<b>Figure 8: Illustration overview of wound healing score assessment for cutaneous wound healing .....</b>	<b>55</b>
<b>Figure 9: TNC protects MSCs against ischemic conditions in vitro. ....</b>	<b>58</b>
<b>Figure 10: Time course comparison of culture treatments on MSC cell survival during H/ND in vitro.....</b>	<b>59</b>
<b>Figure 11: MSC-TNC CM improves endothelial cell cord formation and motility. ....</b>	<b>62</b>
<b>Figure 12: Evaluation and comparison of pro-angiogenic factors for MSC paracrine activity. ....</b>	<b>64</b>
<b>Figure 13: RT-PCR analysis of MSCs on different seeding conditions during H/ND.....</b>	<b>66</b>
<b>Figure 14: Assessment of the tissue replacement phase of CXCR3 -/- mice treated with matricellular protein TNC and MSCs embedded in coacervate. ....</b>	<b>69</b>
<b>Figure 15: Assessment of collagen alignment and maturation in CXCR3 -/- mice treated with matricellular protein TNC and MSCs embedded in coacervate. ....</b>	<b>71</b>

<b>Figure 16: Coacervate delivery study of matricellular proteins on hypertrophic mouse scarring model.....</b>	<b>81</b>
<b>Figure 17: Early wound healing phase assessment of CXCR3 -/- mice treated with matricellular proteins embedded in coacervate. ....</b>	<b>87</b>
<b>Figure 18: Assessment of the tissue replacement phase of CXCR3 -/- mice treated with matricellular proteins embedded in coacervate. ....</b>	<b>89</b>
<b>Figure 19: Additional staining to assess treatment groups on tissue replacement phase during wound healing.....</b>	<b>90</b>
<b>Figure 20: Assessment of the resolution phase of CXCR3 -/- mice treated with matricellular proteins embedded in coacervate. ....</b>	<b>94</b>
<b>Figure 21: Arrested autophagy phenotype in IHMSCs.....</b>	<b>108</b>
<b>Figure 22: IHMSC autophagosome turnover at Day 7 exposure to H/ND.....</b>	<b>109</b>
<b>Figure 23: Concept of MSC-ECM therapeutic strategy to modulate downstream autophagy mechanisms in cutaneous wound healing. ....</b>	<b>110</b>
<b>Figure 24: FVB vs CXCR3 KO mouse comparison.....</b>	<b>116</b>

## Preface

This dissertation is dedicated to my grandfather, Marvin Sylakowski, who suffered from diabetic foot ulcers in the later years of his life and ultimately succumbed to his disease in the Spring of 2019. I will never forget his passion for life and his ability to light up a room, whether it be filled with close family or strangers alike.

Completing this dissertation was one of the most challenging experiences I have ever accomplished. These pages culminate in the blood, sweat, and tears spent over these past six years, overcoming numerous obstacles in all facets: physical, mental, and psychological. I could not have done this without the support of many people in my life, and I cannot acknowledge that enough. I would first like to thank my family for their unconditional love and support over these past 31 years. To my parents, Jill and Bill Sylakowski, I would not be the man I am today without you, and it is because of you that I am resolute in my character and have the ability to achieve anything I put my mind to – thank you. To my sister Kate, thank you for coming to visit me in Pittsburgh throughout the years and for pushing me to accomplish greater goals in life; your resolve and achievements in the NAVY are truly awe-inspiring and remind me to keep moving forward. To my amazing wife, Lauren, words cannot explain how much I appreciate you standing in the trenches with me through this whole experience. Your love, guidance, patience, and calming touch were a saving grace to me in times when I needed it most. Thank you for being my rock and making me a better person. To all of my friends both new and old, thank you for your support throughout this process and over the years. It is the time spent with all of you whether it be around a campfire, at the dinner table, or in a hockey game that allows me to reset my mind and remember to enjoy life in the moment.

I would like to thank both past and present members of the Wells Lab. You have all been very encouraging and made coming to the lab a joy. I would especially like to thank Bo, Amanda, Diana, Drew, and Shao for your assistance in navigating the rigors of graduate school and for your input on the experimental design process. Of Course, All of this could not have been done without my PI Alan. Thank you for allowing me the opportunity to join and work in your lab. Furthermore, thank you for believing in me throughout the highs and lows of the Ph.D. process. With your guidance and mentorship, I have become the Scientist I am today, and I'm so very grateful. Finally, I would like to thank my thesis committee and other members of the CMP faculty for their insights on my work and for always providing help when I needed it.

## 1.0 Introduction

This chapter includes material excerpted from the following publications:

Sylakowski K., & Wells A. ECM-regulation of autophagy: the yin and yang of autophagy during wound healing. Matrix Biology. 2021; 100-101:197-206.

The skin is one of the body's most important organs as it protects everything else underneath. When the skin is damaged, it undergoes highly dynamic and coordinated phases of repair that will result in a small scar. Complications early in the repair process can cause skin failure to heal and result in the presence of an open wound or ulcer. Complications in the later phases of wound healing can cause an exuberant healing response and lead to excessive scarring. Counterbalancing abnormal wound healing events has proven challenging as this is a complex and multifactorial problem. This dissertation focuses on the role of matricellular proteins, specifically the use of Tenascin-C (TNC) and Decorin (DCN), as tools to correct abnormal wound healing events. Part one of this dissertation will build upon our lab's previous work showing that TNC can improve mesenchymal stem cell (MSC) survival both *in vitro* and *in vivo*, where we now want to determine if TNC can influence any pro-regenerative responses from the MSCs as a potential therapeutic for chronic skin wounds. The second part of this dissertation focuses on DCN's natural role in the resolution phase of wound healing to determine whether it can improve wound healing in a hypertrophic scarring mouse model. This work seeks to continue unveiling how matricellular proteins TNC and DCN can be used in and hopefully translate to novel therapeutic within cutaneous wound healing.

## 1.1 Skin Anatomy And Function

Unbeknownst to most in the general population, the skin is the largest organ in the body in terms of both surface area and weight [1]. The average adult human will have approximately 22 square feet of skin weighing roughly 8 pounds. Not only is the skin the largest organ of the body, but it is also one of the most important in terms of its functionality. The skin's most renowned function is providing a protective barrier for the body against the outside world [2, 3]. This includes protection from UV radiation, chemicals, and potential pathogens. The skin is also essential in many physiological functions. One such function is the sensation of the environment through touch [4]. The skin has specialized tactile receptors to sense changes in temperature, pressure, and pain [5]. Touch is considered one of the most important of the five senses because all animals on this earth need the ability to interact with the environment through touch to survive. Another critical function of the skin is thermoregulation [6]. To keep the body from over-heating, blood vessels near the skin will vasodilate and release heat through the skin. The skin also has specialized glands called sweat glands that help release body heat through the secretion of sweat. On the contrary, when the body starts to get cold, the blood vessels in the skin begin vasoconstriction, allowing less blood to be near the extremities and localizing it around the internal organs. Finally, the skin also plays a role in metabolism. Many chemicals can be metabolized through the skin, but one of the most important examples of metabolism is vitamin D production [7]. The primary source of endogenous vitamin D is synthesized when UV rays hit the skin and trigger its production. Vitamin D is crucial in facilitating the transportation of phosphorous and calcium into the bone and gut[8]. Moreover, without a high enough vitamin D level, affected individuals will soon contract Rickets disease [9].

The skin comprises two main layers: the epidermis and the dermis (Figure 1) [10, 11]. The epidermis is the outermost layer of the skin comprised majorly of keratinocytes. This is the first line of defense against pathological and toxic agents and prevents the gain or loss of fluids. It is arranged in four distinct stratified squamous epithelium sub-layers. The stratum basale is the bottom most layer that attaches the epidermis to the basal membrane below. Scattered throughout the stratum basale are valleys called the dermal papilla. It is at the base of the dermal papilla where mitosis occurs to create the new keratinocytes that make up the epidermis [12]. As new keratinocytes are made, they push the older keratinocytes up towards the skin's surface. The second layer is the stratum spinosum. The primary function of this layer is to provide strength and flexibility to the skin through the synthetization of cytokeratins. This additional support of these cytokeratins can often be seen with areas of the skin that undergo repeated pressure, often resulting in a callus thanks to the excess support of the cytokeratins. Another critical function of the spinosum is that melanocytes are usually found near the bottom of this layer. Melanocytes are a particular type of cell that make melanosomes. These melanosomes are then introduced into the newly differentiating basal keratinocytes as they move up the stratum elevator. The melanosomes make melanin which is secreted into the basal keratinocyte cytoplasm, allowing them to soak up harmful UV rays of the sun [13]. The third layer of the epidermis is called the stratum granulosum. In this layer, the keratinocytes are starting to become more compressed, and they appear to have a dense buildup of lipid granules [14]. These granules and this layer give the skin its primary waterproof barrier. The fourth and final layer of the epidermis is the stratum corneum [15, 16]. An important thing to note is that the epidermis is avascular and has no direct blood supply. This results in each layer having to rely on diffusion in order for the cells to get the nutrients they need. So as the keratinocytes move farther away from the basal membrane, they receive fewer nutrients.

Moreover, by the time they reach the corneum layer, all of the keratinocytes have died and become anucleated [17]. This creates a very tough and protective outer layer that will sluff off and be replaced by additional keratinocytes underneath. The lipid granules from the granulosum layer also end up drying out and forming an additional layer to help with liquid regulation [14].

The second layer of the skin is the dermis. The dermis is much more complex than the epidermis, with the addition of vascular tissues, sensory receptors, neurons, and different types of glands. Supporting all these accessory components are the two layers of the dermis: the papillary and the reticular. The papillary dermis is the top layer that comes in contact with the basement membrane [18]. Phenotypically it looks very superficial and sponge-like overall. It fills all the valleys on the opposite side of the stratum basal dermal papilla. This layer's extracellular matrix comprises collagen I and III fibrils mixed with fine elastin fibers [19]. Below the papillary dermis is the reticular dermis. Phenotypically the collagen fibrils in the reticular dermis are much more ordered and very well aligned. This aligned structure of the reticular along with thicker collagen I bundles helps to give this layer of the dermis an extreme resiliency. The primary residing cell of the dermis are dermal fibroblasts. Dermal fibroblasts are responsible for generating the connective tissue and fibers responsible for giving the dermis its mechanical properties [19], as well as replacing and missing tissue during the tissue replacement process of repair [20]. Together, both layers provide an intricate system that allows us to interact safely with the world around us.

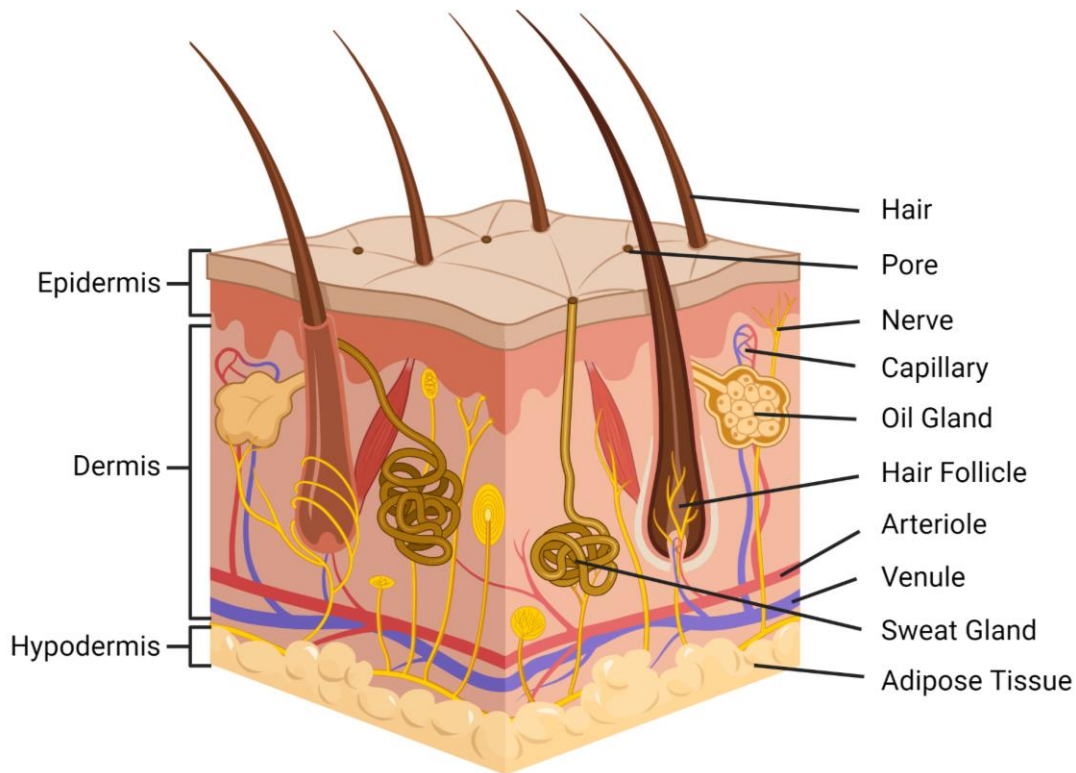


**Figure 1: Anatomy of the skin** The skin comprises two main layers - the epidermis and the dermis. The epidermis is the outermost layer of the skin and is home to a specialized subset of skin epithelial cells called keratinocytes. Keratinocytes are responsible for creating the outermost protective barrier of the skin via keratin production. The dermis is the skin's connective tissue, and it houses blood vessels, hair follicles, nerves, and other vital tissue regulating structures. This figure was created with BioRender.com.

## 1.2 Cutaneous Wound Healing

Cutaneous wound healing is how the skin will repair itself after injury. This has been broken down into two main types of healing; primary intention and secondary intention. Wound healing by primary intention occurs from wounding caused by a sharp, clean laceration, such as a surgical incision, that can be kept sterile with minimal tissue loss and have the wound edges

approximated by either sterile sutures or another type of closure adhesive [21]. These wounds also need to be closed within 4-8 hours to keep the wound bed from becoming inflamed or necrotic, but if done successfully, the healing process will be quick with minimal scarring [21]. Healing by secondary intention occurs when the injury to the skin causes too much tissue loss for the wound edges to be approximated correctly or if the wound becomes infected, causing an enhanced inflammatory state [22]. These wounds will require a more significant amount of new tissue growth to repair correctly and thus will take longer to heal. Whether a wound goes through primary intention or secondary intention, it will still pass through the same phases of repair.

The complete wound healing cascade is triggered when an injury damages the dermal layer of the skin. The subsequent wound healing response is an intricate orchestration of three overlapping phases of repair that encompass numerous cell types, signaling cascades, and microenvironment modifications to reach a successful resolution. There are three main phases of wound healing: the hemostasis/inflammation phase, the tissue replacement phase, and the resolution phase (Figure 2, 3 – left column). The first phase of wound repair is the hemostasis/inflammation phase, where the first point of concern is to stop the bleeding of ruptured blood vessels while subsequently preventing pathogenic infection. A clotting cascade is activated upon injury where blood circulating platelets and fibrinogen enzymatically converted into fibrin come together to form a fibrin clot and provide an early provisional matrix over the wounded area [23]. This fibrin clot is also biologically active, playing a significant role in signaling a localized immune response by recruiting pro-inflammatory neutrophils, macrophages ( $M0 \rightarrow M1$ ), and other leukocytes to prevent infection and clear the wound of cellular and extracellular debris.

The next phase of wound healing, the tissue replacement phase, begins with the proliferation and migration of fibroblasts, endothelial cells, epidermal cells, and other progenitor

cells into the wound bed to initiate the rebuilding of the lost and injured tissue. Fibroblasts begin producing the collagen III-rich granulation tissue as a temporary supportive matrix to replace the absent extracellular matrix; endothelial cells begin to create new blood vessels via angiogenesis; and the epidermal cells start to migrate underneath the scab to seal the wound surface and restore the epidermis permanently. At this point, the wound is considered sterile, and a transition occurs where pro-inflammatory macrophages (M1) decline and are replaced by wound healing macrophages (M2). These M2 macrophages help to produce and modulate the granulated ECM and promote further vasculature repair.

The resolution phase is the final repair phase where the provisional wound bed is replaced with a mature ECM, the excess blood vessels are pruned by up to 90% [24], and any residual proliferation and migration signals are terminated and replaced with 'stop' signals such as those acting through CXCR3 [25]. The wound bed will start to contract as fibroblasts transdifferentiate into myofibroblast to reorganize and restructure the immature collagen III to mature collagen I, restoring tensile strength back to the skin [20]. With every phase having a successful outcome, all that will remain will be a light scar to hint at what occurred.

### **1.3 Extracellular Matrix In Cutaneous Wound Healing**

Wound healing is a highly dynamic and complex process involving three major repair phases: hemostasis/inflammation, tissue replacement, and resolution. The modulation, structure, and signaling of the extracellular matrix (ECM) through all these phases is key to successful wound resolution. The dynamic nature of the ECM not only directs the transition through the phases of wound healing [26, 27] but also determines with survival and fate of the cells in the wound bed.

### **1.3.1 ECM In The Hemostasis And Inflammation Phase Of Wound Healing.**

Hemostasis is the first reaction in an activated wound healing response (Figure 2). It is initiated when an injury to the skin damages the underlying vasculature and serves as the primary mechanism to prevent extensive hemorrhaging. This is accomplished through the formation of a fibrin clot, where circulating platelets adhere to newly exposed collagen I matrix and subsequently become activated through the glycoprotein VI receptor [28]. These activated platelets undergo morphological changes to increase their surface area along with secreting additional pro-coagulation factors in the local environment. The activated platelets also begin to express binding receptors for fibrinogen, allowing for the capture of circulating plasma fibrinogen. The newly adhered fibrinogen acts as a tether for other circulating platelet cells allowing for their aggregation and activation [29]. Fibrinogen can also activate platelets through glycoprotein VI receptors like the earlier exposed collagen I fragments [28].

As circulating platelets and fibrinogen continue to build up at the injury site, they eventually form what is known as the platelet plug. As more and more platelets become activated within the platelet plug, they proceed to enhance the coagulation signaling cascade. This involves a final step where the structure of the platelet plug is further reinforced and transformed into the fibrin clot. Where additional plasma fibrinogen is enzymatically modified into fibrin and crosslinked together with plasma fibronectin to form a structural mesh that solidifies the entire structure [30], this newly formed barrier has now been termed the “Early Provisional Matrix” and is the first primary ECM framework within the activated wound healing response [23]. In addition to creating a barrier to stop the bleeding, the body also releases the matrix glycoprotein thrombospondin-1 that acts as an endogenous angiogenic inhibitor. Thrombospondin-1 adheres to the CD47 receptor of endothelial cells and subsequently downregulates their ability to undergo

enhanced autophagy, thus further limiting their ability to survive and respond to any pro-angiogenic signals coming from the early wound bed [31-33].

Once the primary goal of stopping the localized hemorrhage is accomplished, the early provisional matrix priorities shift to augment a robust inflammatory response to counter the breach in the anti-microbial barrier. The main goal of the immune system is to sterilize the wound bed against foreign pathogens and to remove all damaged tissue to prepare for a smooth transition into the tissue replacement phase. Neutrophils are one of the first immune cells to respond, sensing chemical cues in the local microenvironment from the fibrin clot and transmigrating through the vascular wall to reach the site of injury within 24 hours after injury [34, 35]. They begin the fight against infection and combat foreign pathogens through a variety of measures, including the phagocytosis of small microbes, the release of antimicrobial granules and reactive oxygen species, and the distribution of neutrophil extracellular traps (NETs)[36]. Neutrophil functions have been shown to be enhanced and altered through ECM attachment via  $\beta$ 2 integrin [37], but overall, there is much to still investigate within how the ECM dynamics influence neutrophil form and function.

Monocytes are the next major immune cell to emigrate into the wound bed. They are recruited by pro-inflammatory cytokines (IL-6, TNF alpha, CCL2, CCL5) produced by activated platelets from the fibrin clot or activated neutrophils already on site[38, 39]. Additionally, ECM-derived damage-associated modifying proteins (DAMPs) can also recruit monocytes as smaller ECM fragments can break from the wound area and into the localized vasculature [40]. Once monocytes arrive at the site of injury, they extravasate into the wound bed, relying on  $\beta$ 1 integrins to adhere to ECM proteins such as fibronectin to navigate around [41]. Once in the wound bed, they receive additional inflammatory chemical cues such as interferon-gamma and lipopolysaccharide to stimulate their polarization from M0 into the M1 -pro-inflammatory

macrophage phenotype [42]. The M1 macrophage relies heavily on its phagocytosing ability, eradicating other remnants of pathogen fragments missed by neutrophils and debriding the rest of the wound bed of damaged tissue [42].

As the composition of the original early provisional matrix becomes altered through debridement and release of ECM modifying enzymes, macrophages and early migrating fibroblasts will start to synthesize and deposit hyaluronan and versican into the matrix [43]. This is a second major modification to the wound ECM, termed the “Late Provisional Matrix.” Versican is a large proteoglycan that can be cleaved by ADAMTS proteases to elicit different responses throughout wound healing. It can attach to numerous inflammatory cell receptors and is considered a key molecule in regulating the inflammation response [44]. Hyaluronan is a glycosaminoglycan that can also play a part in all aspects of wound healing. For the immune response, it’s size dictates whether it will have pro-inflammatory effects or anti-inflammatory effects [45]. Together these two ECM proteins mark the end of the hemostatic/inflammation phase of repair as the wound transitions away from the provisional matrix to the next stage of wound healing where it will need to support the survival, proliferation, and migration of numerous cell types.

### **1.3.2 ECM In The Tissue Replacement Phase Of Wound Healing.**

As the wound reaches its final stages of sterilization and most of the damaged ECM has been removed, the late provisional matrix starts to transform into a more modular granulation tissue, ultimately setting the stage for the tissue replacement phase to begin. The overall goal of this phase of wound healing is to repopulate and restore the tissue that was once there before. This involves various cell types proliferating around the wound's edges and then migrating within to rebuild. Within the epidermal layer, keratinocytes begin to proliferate and migrate into the edges

of the provisional matrix under the eschar, creating what is known as the epithelial tongue. The keratinocytes will continue to bore through the provisional matrix until they converge with keratinocytes migrating in from the adjacent side. Once this connection is made in the epidermis, then subsequent dermal fibroblasts can come and begin to reconstruct the basement membrane below, further separating the epidermis-dermis of the skin.

In the underlying dermis, fibroblasts all along the wound margin are proliferating and migrating into the wound bed. They are tasked with creating a new stroma for the wound bed to replace the existing fibrin/platelet dense provisional matrix. The new matrix structure called the granulation matrix is made from a more accommodating collagen III environment. Collagen VI is also produced during the tissue repair phase as it helps to regulate dermal fibroblast motility and ECM matrix assembly[46, 47]. In Addition to collagen secretion, other matricellular ECM proteins such as tenascin-C, osteopontin, and fibronectin are also present to aid in migration and survival to incoming cells. The tenascin-C protein specifically has been shown to enhance the survival of mesenchymal stem cells post-transplantation into a cutaneous wound healing model. The EGF-like repeat domain of tenascin-C will bind to the EGFR receptor and promote survival via the Akt survival pathway [48, 49]. These new ECM proteins are important as the provisional matrix before this point was an acellular space which includes that lack of supporting vasculature. Hence, any cells migrating into the granulation tissue early on will face ischemic conditions and be challenged both in survival and in function.

Macrophages also play a large role in the early part of the tissue replacement stage as newly recruited monocytes and previously active M1 macrophages start to polarize towards the M2 anti-inflammatory/pro-repair phenotype. The macrophage polarization is triggered by a culmination of a few signaling pathways, with the major signals of CCL2 (MCP1) and IL-6 pathways triggering

an autophagic induction response; to help the macrophage improve their survival and help fibroblasts with granulation tissue formation [50]. M2 macrophages will also start to release growth factors such as VEGF and PDGF to help in the initiation of angiogenesis [38]. In addition to the construction of a new matrix, angiogenesis plays just as vital of a role in the tissue replacement phase as a substantial amount of energy (nutrients and oxygen) is required to rebuild the wound bed to proper form. In conjunction with the M2 macrophages, the ischemic/hypoxic conditions of the wound bed will also trigger mesenchymal stem cells to secrete higher levels of VEGF through enhanced autophagic flux [51, 52]. The ECM protein osteopontin will further support the angiogenic response by stimulating the MSCs to migrate to the injury site and promote their differentiation into endothelial cells [53].

### **1.3.3 ECM In The Resolution Phase Of Wound Healing**

The final phase of the wound healing mechanism is the resolution phase. Up to this point, both the provisional matrix and granulation matrix focused heavily on recruiting cells into the wound bed and supporting their additive functions. The focus of the matrix now will be to quell all superfluous tissue repair mechanisms and reorganize them into a more mature matrix that restores the local microenvironment to a homeostatic state.

The reorganization of the granulation matrix into the mature matrix starts with the turnover of Collagen III fibrils to collagen I. The collagen III network provided a flexible environment that allowed for an abundant amount of cell migration and function in and around the wound bed. Turnover into collagen I fibrils will enhance the tensile strength of the tissue and offer further support needed to return to normal function. This is achieved through fibroblasts differentiating into myofibroblasts which acquire higher amounts of intracellular alpha-smooth muscle actin,

allowing for stronger manipulation and contraction of the underlying ECM via integrin interactions [54]. The myofibroblasts along with remaining M2 macrophages, release a series of ECM modulating enzymes such as matrix metalloproteinases, transglutaminases, and lysyl oxidases to strategically crosslink ECM back to its collagen-1 state [54]. Subsequently, after this conversion, the majority of the myofibroblasts and M2 macrophages undergo apoptotic events and are removed from the restored wound bed.

A second component of the wound bed that is largely manipulated during the resolution phase is the underlying vasculature. The tissue replacement phase required a large amount of cellular traffic, nutrients, and cargo to come in and out of the wound bed. Consequently, these systems are not necessary anymore, resulting in vascular pruning to regress the density of blood vessels back to normal levels and allow for the remaining vasculature to fully mature. One of the critical regulators during this step is a small leucine-rich proteoglycan (SLRP) called decorin (DCN). DCN is considered a necessary shut-off switch for the pro-reparative mechanism of the tissue replacement phase, as it binds to growth factor receptors such as EGFR and VEGFR2 [55]; and limits the occurrence of hypertrophic scarring by preventing excessive repair. Upon binding VEGFR2 on endothelial cells, DCN will induce a pro-autophagic response through the AMPKa/Vps34/Peg3 signaling pathway and concurrently inhibit angiogenesis through suppressing VEGFA levels [55-57]. In conjunction with the decorin finding, the same group of researchers have since looked at other ECM proteins as they relate to the modification of endothelial cells. Similarly, endorepellin, a matrikine subdomain protein of perlecan, has also been found to signal through the VEGFR2 to induce a pro-autophagic response [58] that actively contributes to blocking the angiogenic capability in endothelial cells [59]. Additionally, the

autophagic signaling of these SLRPs leads to an apoptotic clearing of all leftover endothelial cells in the final transition from resolution to homeostasis.

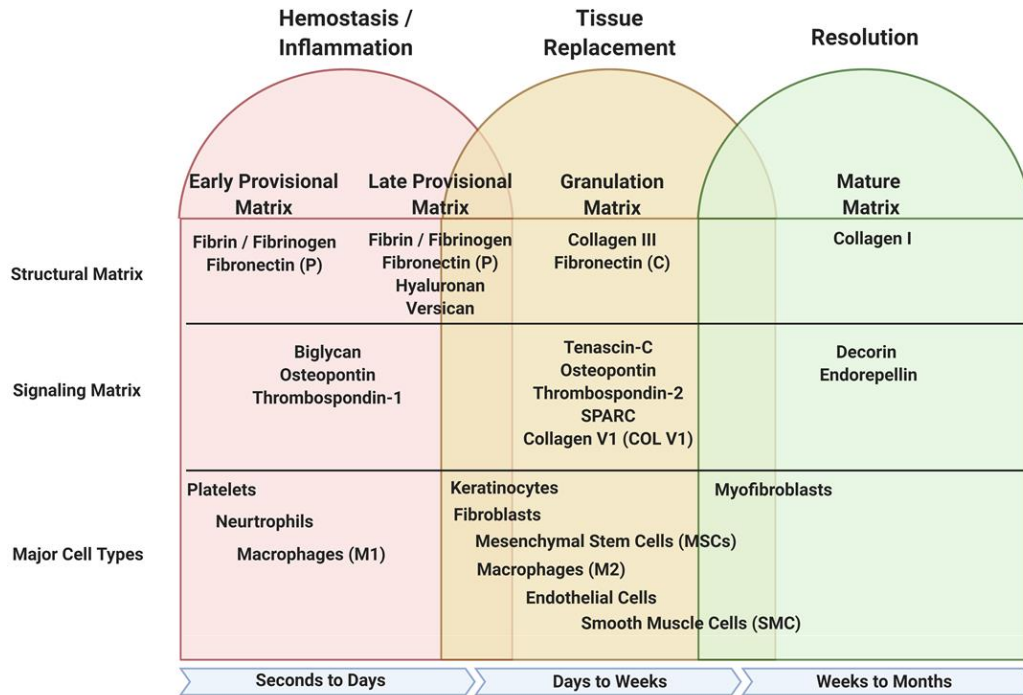


**Figure 2: Overview of ECM during routine wound healing** During the initial stages of the hemostasis/inflammation phase of repair, a provisional matrix barrier known as the fibrin clot is generated to suppress further hemorrhaging from the wound site. Concurrently with the formation of the clot, activated platelets signal to the surrounding tissue to initiate a hasty immune response recruiting neutrophils and monocyte-derived M1 macrophages to sterilize the wound and remove all damaged ECM debris. An increase of inflammatory cell manipulations along with early fibroblasts' ECM secretions further modify the provisional matrix changing it from an early to late form. The late provisional matrix further manipulates the inflammatory response, preparing it to transition from anti-inflammatory to pro-repair. During the tissue replacement phase, further modification by fibroblasts and M2 macrophages to the late provisional matrix transforms it into a granulation matrix. The granulation matrix is meant to provide easier cell movement and function as it is mostly made from a loose collagen III base with interspersed signaling ECM proteins. The last phase of repair is the resolution phase, where the ECM is recognized to its final form, vasculature is pruned, and the spare cells are removed. This figure was created with BioRender.com.

## 2.0 Chronic Wounds

This chapter includes material excerpted from the following publications:

Sylakowski K., Bradshaw A., & Wells A. Mesenchymal stem cell/multipotent stromal cell augmentation of wound healing: lessons from the physiology of matrix and hypoxia support. The American Journal of Pathology. 2020; 190 (7): 1370-1381.

Bradshaw A., Sylakowski K., & Wells A. The pro-reparative engine: stem cells aid healing by dampening inflammation. Current Pathobiology Reports. 2018; 6 (2): 109-115.

### 2.1 Clinical Significance Of Chronic Wounds

Chronic wounds are defined as wounds that fail to progress through the normal wound healing processes in an orderly and timely manner, failing to resolve within three months [60, 61]. It is estimated that 1-2 percent of the population in the developed world will suffer from a chronic wound at least once in their lifetime [62]. In the United States, 8.2 million Medicare beneficiaries require interventional wound treatments costing roughly 100 billion dollars annually [63]. These numbers are expected to grow exponentially due to the rise in morbidities such as obesity and diabetes and the overall rising median age of the U.S. population.

From the patient's perspective, the effect of chronic wounds should not be underestimated as they can have devastating tolls on their overall quality of life. Chronic wounds last an average

of 10-14 months, with 60-70% of patients having a wound that will recur after healing. [64]. Current clinical treatment of chronic wounds often requires weekly or biweekly visits by the patient to measure wound healing progress and clean the wound through debridement. In addition to prolonged hospital visits, the type of wound and area of obstruction can cause the patient to suffer from chronic pain and limited mobility. After months of treatment, this can easily cause patients' quality of life to suffer in all physical, psychological, social, and financial aspects [65].

Chronic wounds are hard to treat as there is not usually one definitive factor that drives their occurrence. Instead, several local and systematic factors will inhibit a proper wound response resulting in a chronic ulcer. Examples of some of the major factors that will affect wound healing outcomes are a type of wound or ulcer, size – both width and depth, location, mechanical factors, infection, blood supply, metabolic conditions, and radiation exposure. Different combinations of these factors and the overall health and age of the patient in question result in each chronic wound being a unique case by case event, leading to the need for further personalized treatment options.

## **2.2 Chronic Wound Microenvironment**

According to the Wound Healing Society, chronic wounds are classified into four main classifications: venous ulcers, arterial ulcers, diabetic foot ulcers, and pressure ulcers. Chronic wound pathology occurs when the tissue replacement phase of healing does not cover the wound bed and the wound healing process stalls. Several situations impact and block tissue replacement. Repeated injury, as in pressure ulcers, activates excessive matrix breakdown by matrix metalloproteinases (MMP) [66]. Insufficient vascular supply, due to diabetic atherosclerosis or pressure as in pressure ulcers, limits cellular replacement [66, 67]. Insufficient drainage, as in

venous stasis ulcers, leaves toxic components and increased MMP activity that drives premature cell apoptosis and dysfunctional matrix [66, 67]. Wound infection, even without biofilms, also leads to matrix breakdown secondary to chronic inflammatory infiltrates [68]. In all these situations, the pathological wound beds impact the survival of the parenchymal cells and conclude in the ulcers.

The circumstance that creates chronic wounds will have similar defining characteristics observed in most chronic skin ulcers (Figure 3-Middle Column) [69]. (1) They will have a prolonged and uncontrolled inflammatory response (mainly by neutrophils and M1 macrophages) which will result in high levels of proteases (MMP2, MMP9) and inflammatory markers (IFN- $\gamma$ , TNF- $\alpha$ , IL1- $\beta$ )[69-71]. These higher levels of inflammatory factors will break down the provisional matrix, generating matrix fragments, particularly collagen fibrils that drive innate infiltration in a feed-forward fashion. (2) The breakdown of the provisional matrix will reduce the migration of tissue replacement phase cells (dermal fibroblasts, endothelial cells, mesenchymal stem cells, and keratinocytes) from proliferating and migrating into the wound bed [69]. This will cause defective-re-epithelialization, the inability for the matrix to transition from provisional matrix to granulation matrix, and the overall decrease in angiogenesis [60, 70]. (3) There will also be low growth factor activity due to the lack of pro-reparative cells such as MSCs and late-stage inflammatory M2 macrophages. This process will continue in its feed-forward loop as cells around the wound edge can experience chronic hypoxia or ischemia, leading to enhanced atrophy and necrosis, further fueling the pathological inflammatory response.

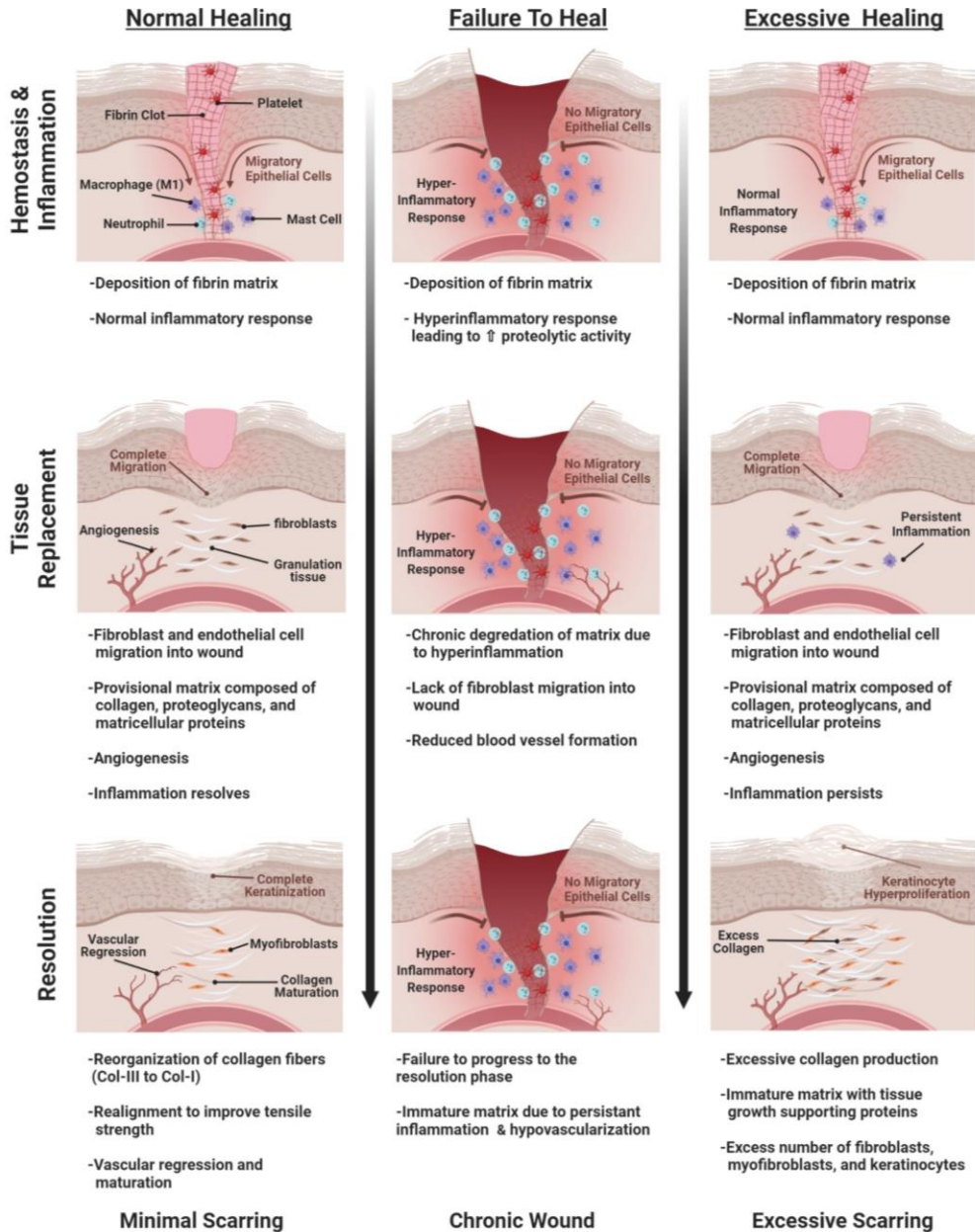


Figure 3: Phase transitions in normal and abnormal wound healing. Wound healing has three overlapping phases of repair – Hemostasis & Inflammation, Tissue Replacement, and Resolution. The successful transition of all three phases will result in a regular wound healing event with minimal scarring, as shown in the left column. When healing is stalled in the first phase of repair, this will fail to heal and the appearance of a chronic ulcer, as shown in the middle column. When obstructions in the wound healing process occur in the last two phases of repair, this can trigger an extreme healing event leading to excessive scarring, as seen in the right column (Adapted from Wells et al. 2015). This figure was created with BioRender.com.

## **2.3 Mesenchymal Stem Cells**

Mesenchymal stem cells or multipotent stromal cells were first discovered in 1970 by Friedenstein and colleagues, who recognized that a small subset of bone marrow cells had the unique ability to develop into colony-forming unit fibroblasts [72] MSCs are now characterized for their ability to self-renew, adhere to plastic, and differentiate into subsets of specialized cells particularly suited for the regeneration of mesenchymal tissues (adipocytes, osteoblasts, chondrocytes, and myoblasts) [73-79]. They are further defined by the International Society for Cell & Gene Therapy for expressing markers: CD73, CD90, and CD105; while also lacking the expression of markers CD14, CD19, CD34, CD45, CD11b, CD79a, and HLA-DR [80]. MSCs as a cellular therapy has shown clinical benefit in several disease situations through both their immunosuppressive and angiogenic properties, making them possible key players in regulating and treating chronic wounds [81, 82]. Unfortunately, the overall promise of MSCS cell therapy applications have proven disappointing in wound repair despite success in pre-clinical animal models as the stem cells are lost rapidly from the wound bed. This has resulted in new research of delivery methods focusing on improving MSC survival and performance in the hopes of overcoming these early performance pitfalls.

### **2.3.1 MSCs Role In Wound Repair**

The use of MSCs to treat dysfunctional cutaneous wounds is considered particularly promising for a number of reasons. First, the immune-tolerant site of the skin can accommodate the extended persistence of allogeneic cells. Second, skin being an externally accessible organ, repeated applications can be achieved non-invasively. In addition, the pro-reparative secretome of

MSCs can be utilized in different phases of the wound healing process (Figure 4). This is an advantage over the direct application of growth factors or other molecules as the wound bed consists of asynchronous areas of healing, where MSCs are environmentally adaptive and can produce an appropriate response for the transitioning phases of the wound bed to recreate the physiological situation. Such as in a normal skin wound, endogenous subsets of hair follicle MSCs called dermal sheath cells help repair/replace the injured dermal tissue. While MSCs from the subcutaneous fat tissue and blood supply help regulate early and mid-phase inflammation while also helping to restore dermal tissue [83, 84].

Upon infiltrating the wound, MSCs begin to secrete pro-inflammatory cytokines (CSF2, IL-6, IL-8, CCL2, CCL3) recruiting neutrophils and M1 converted macrophages to help degrade damaged tissue [84, 85] (in the Hemostasis/Inflammation phase), but also regulating the overall inflammatory response by limiting the number of activated T-cells, neutrophils, and macrophages [84, 86-88]. Upon transition into the Tissue Replacement phase, MSCs focus on secreting cytokines directed to the proliferation and migration of epithelial cells for re-epithelialization (EGF, KGF, HGF), directing new endothelial cells for angiogenesis (VEGFA, ANGPT1, PDGF-BB), and stimulating fibroblasts to produce matrix proteins that later transition to a mature provisional matrix (FGF) [84, 85, 89, 90]. MSCs also direct the polarization of monocytes into pro-reparative M2 macrophages (IL-4, IL-13, IL-10, TGF-B) to help clear remaining cellular debris and modify the temporary matrix [84, 87]. In the Resolution phase, MSCs regulate the matrix through secretion of MMPs and TIMPs, while also regulating the amount of collagen disposition through balancing TGF-B1 and TGF-B3 to prevent hypertrophic scarring [90]. These vital guiding functions are unique to MSCs because they express low levels of major histocompatibility complex class (MHC) II and lack the MHC co-stimulatory molecules which are

essential for immune cell activation (CD40, CD40L, CD80, CD86); allowing for their use in allogeneic transplant with a very low rate of rejection [91].

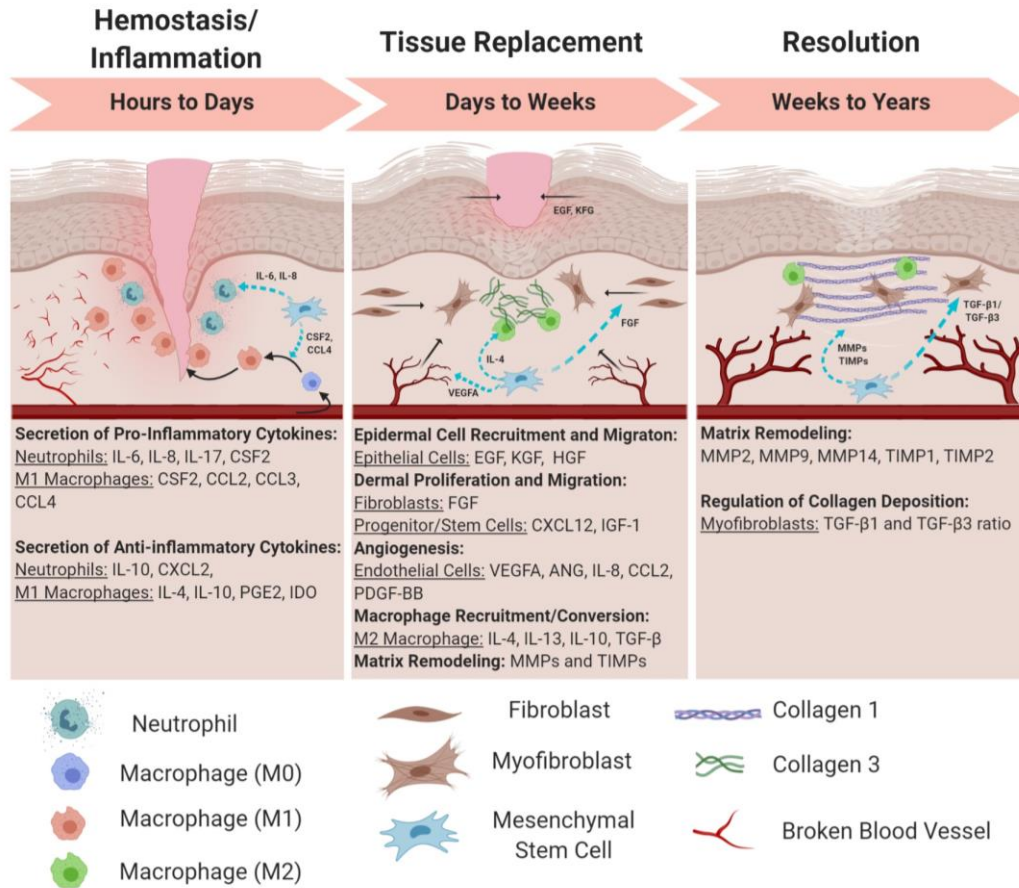


**Figure 4: Roles for mesenchymal stem cells (MSCs) during cutaneous wound healing** The hemostasis/inflammation phase relies heavily upon the pro-inflammatory machinery for sterilizing the wound and clearing damaged ECM debris. MSCs help to orchestrate a healthy initial immune response that eventually will turn over into a pro-reparative response. Upon entering the tissue replacement phase, MSCs produce various growth factors and chemokines to initiate a massive arrival of tissue-resident cell types that will begin to rebuild within the wound bed. The resolution phase is the final phase of wound healing where MSCs help to orchestrate final modifications to the extracellular matrix, vasculature, and resident cells. Biorender was used to design and create with figure. (<https://biorender.com/>)

### 2.3.2 Hostile Wound Microenvironment Challenges MSC Survival

Despite the potential benefits MSCs possess for regenerative therapies, their use must first overcome pro-apoptotic stressors within wounded tissue [48]. Younger and healthier patients have wound healing machinery and endogenous MSCs that work well enough to overcome these healing challenges. However, in older patients who suffer from diseases such as those with type 2 diabetes or metabolic syndrome, their MSCs become more susceptible to apoptosis, increased levels of ROS accumulation, and increased mitochondrial deterioration. Rendering their MSCs too dysfunctional [92] to overcome the stress of the wound bed ultimately limiting their effectiveness in the wound healing process. This is where the reliance on exogenous MSCs therapies from healthier and younger donors has come to light. However, the lack of survival of exogenously applied MSC in wounds has still been well documented in a variety of tissues, particularly the heart [93], brain [94], and kidney [95]. For the heart, a survival rate of 5% within a two-week period post-myocardial infarction (MI) treatment [93], and only a 1% survival rate one hour after injection into an ischemic kidney model [95]. Even when using an immunodeficient mouse model, Toma et al. report having less than 0.44% survival of MSCs 4 days post-MI [96]. Even skin, where immune tolerance should present less barriers to MSC, is devoid of implanted MSCs within a week [49].

The disparagingly low survival rates likely result from a variety of factors within the harsh wound microenvironment; such as the absence of trophic factors, a heightened inflammatory response, and an impaired vasculature [97, 98]. These factors induce MSC death through a variety of mechanisms, including anoikis, ischemic reactive oxygen species (ROS), loss of growth factors, or increased signaling from death cytokines [99.] (Figure 5). Our lab has previously shown that MSCs are very susceptible to ROS and pro-inflammatory death-inducing signaling complexes that

occur within the wound bed [100]. We have also shown that MSCs are metabolically glycolytic [101], so nutrient deprivation within the wound bed is also potentially detrimental to MSC survival [102, 103]. Recent evidence regarding hypoxic/ischemic stress showed that severe hypoxia (<1% O<sub>2</sub>) drives mitochondrial dysfunction resulting in apoptosis or necrosis [102, 104]. Despite numerous approaches to limit MSC death post-transplantation, whether through using growth factor preconditioning or genetic modifications [105], most efforts have had a limited impact on overall MSC survival. The death of the exogenously applied MSCs is in counterpoint to the survival of the endogenous MSCs. Therefore, we can learn from the physiological adaptations and survival mechanisms of successfully resolving wounds to develop pro-survival therapies for those who have a dysfunction of their own MSCs, the elderly, and those with co-morbidities.

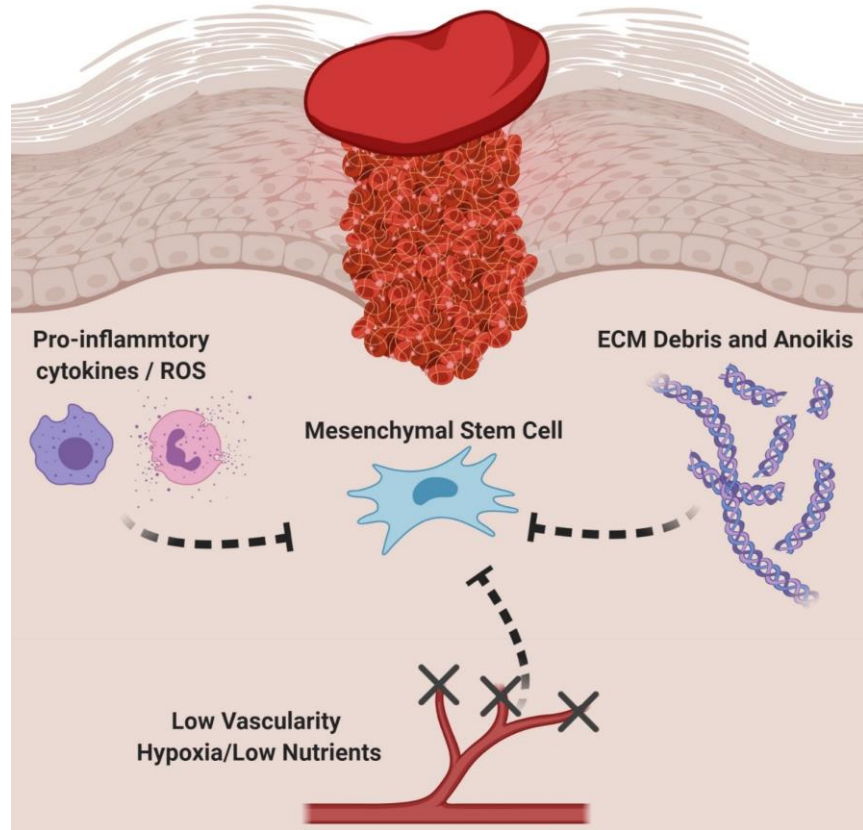


Figure 5: MSCs face a steep challenge when they enter the wound microenvironment. Several factors are in play that will limit their survival and therapeutic capacity. The innate immune response is responsible for destroying any foreign pathogens, but their methods of destruction can be non-discriminatory through their release of pro-inflammatory cytokines and reactive oxygen species (ROS). The insult will also cause tissue damage, leaving behind ECM debris, resulting in a lack of support to cells in the area, resulting in cell death via anoikis. Injury to the wound bed can also cause blood vessels to be severed, subsequently resulting in all damaged vasculature to be blocked off. This will cause the wound microenvironment to become ischemic leaving all cells with little to no oxygen or nutrients available. Biorender was used to design and create with figure. (<https://biorender.com/>)

### **2.3.3 MSC Delivery Strategies For Improved Survival And Efficacy**

Cutaneous wounds requiring interventional treatment options are often complex and require a multidisciplinary approach both at the macro level and micro levels of care. Where macro levels of care would be considered more general hospital methods of treatment such as site off-loading, compression bandages, and fluid control. Micro-level of care would be anything using a biological treatment focused on improving the wound at the microenvironment level. There are many elements clinicians and scientists must consider when utilizing and developing MSC therapeutic strategies. Cell source is often a significant consideration because there are multiple types of MSC-derived lineages that can behave differently under varying circumstances. In addition, there are some sources of MSCs that are easier to extract and with more significant numbers than with other locations of the body. The two most common sources of MSCs for clinical use are either derived from the bone marrow where 0.001-0.002% of cells harvested are MSCs; or from adipose tissue where MSCs are estimated to make up 1% of the total cell population [106]. Cell administration strategies is another key factor and will change depending on the patient's wound severity and type. But overall, the main goal of improving MSC survival percentages post-transplantation remains a focal point for enhancing MSC efficacy in wound healing. Here we highlight on some extracellular matrix approaches for improving MSC retention as most next generation cell based wound grafts and management systems will require the use of the ECM in one aspect.

#### **2.3.3.1 Matrix Components For MSC Delivery:**

The focus on the ECM is now regarded as crucial in the wound healing process as the cells themselves [61, 101]. The ECM is not just the primary support structure for each tissue within the

extracellular space but a combination of tension/mechanical forces with bioactive moieties that largely influence how cells function and behave. This was the original concept of “dynamic reciprocity” or the ongoing bidirectional interaction among cells and the surrounding matrix that regulated cellular function, coined by Paul Bornstein and colleagues [107, 108]. These observations would be further investigated and result in creating a subclass of ECM proteins called matricellular proteins, whose primary role was not to provide structural support but to interact and elicit a myriad of biological signals within the cell. Altogether, the ECM’s complex biochemical makeup, rigidity, and shape can be exploited to manipulate tissue replacement and wound healing therapies across many applications. Using ECM constructs that either resembles or impute the native matrix environment could help in promoting more physiological healing.

Collagen-1 is the most abundant ECM protein of the skin and is usually preferred for shovel-ready scaffolds as it is biocompatible, biodegradable, and can form highly organized 2-D and 3-D network like structures that allows it to incorporate a wide variety of biological components ranging from growth factors to matrix proteins to cells. Collagen-1 has been shown to improve MSC proliferation potential and prevent MSC anoikis through the binding of integrin receptors  $\alpha2/\beta1$ , and  $\alpha11/\beta1$  [109, 110]. Collagen-1 is also able to increase osteogenic differentiation through higher cell adhesion and enhance activation of RHO-A *in vitro* [109]. Another structural collagen, Collagen VI, has been used to enhance MSC proliferation and stemness for cartilage repair, while also displaying pro-survival capabilities in fibroblasts [111, 112]. Thus, encapsulating MSCs within structural collagen may augment the delivery of viable MSCs. However, Collagen-1 signals wound maturation and resolution, and thus would be suppressive during the early tissue replacement phase of healing; importantly collagen-1-dominant matrices limit angiogenesis [101].

A more immature matrix is likely needed to promote regenerative healing [113]. Previous work in our lab has shown that the matricellular protein tenascin-C (TNC) possesses epidermal growth factor receptor-like (EGF-L) repeats that can interact with the EGF receptor (EGFR) on MSCs in a low affinity/high avidity interaction; this restricts EGFR activation to the plasma membrane [48, 114]. The prolonged sequestration of EGFR enhances pro-survival signals, via low level tonic ERK and AKT signaling [98]. The addition of TNC to MSCs provides for survival of the transplanted cells for up to a month [49, 89]. Given that TNC is found naturally during the early phases of wound healing, coupling it with MSCs as a therapeutic delivery system is expected to not only provide for enhanced survival but also improve healing [49, 89]. Laminin V is another promising immature matrix protein that contains cryptic EGFR matrikines [115]. Combinational strategies using Laminin with MSCs have shown to enhance overall survival and improve wound healing outcomes through upregulated angiogenic capacity in diabetic rats and other models [116, 117]. The wound response matrix component fibronectin is another top candidate for MSC delivery. MSCs survival was enhanced in a rat hind limb model when encapsulated in agarose capsules containing fibronectin and fibrinogen pro-survival signals [118], in addition to increasing proangiogenic capacity of MSCs *in vitro* [117].

In addition to improving MSC survival and paracrine signaling, many of these immature matrices also promote the migration of cells around the wound bed. Tenascin-C, laminin, fibronectin, and thrombospondin all play vital roles in orchestrating the movement of distal proliferating resident cells to the center of the wound bed mainly through integrin binding mechanisms [119-121]. These properties add another facet to the overall capability of these MSC-ECM combinational therapies. Where the immature matrices improve the survival and growth factor secretion of MSCs, which then promotes enhanced proliferation of the resident tissue cells,

that in turn are able to migrate into the wound quicker due to the aforementioned present immature matrix. Further adding to this enhanced cycle of repair, MSCs have also shown that they can deposit ECM proteins such as fibronectin, tenascin-C, thrombospondin and others [122]. All together these matricellular proteins are highly regulated in adult tissues with restricted expression to areas of active remodeling, such as in wound healing [123]. Thus, by following the lessons from physiological healing, novel approaches can be designed employing the same matricellular proteins.

### **2.3.3.2 Matricellular Protein Tenascin-C**

Tenascin-C (TNC) is one of the original members of the matricellular protein group defined by Paul Bornstein in 1995 [124, 125]. Where matricellular proteins are defined as ECM proteins that modulate cell-ECM interactions but do not contribute to the structural integrity of the ECM in any way [124, 126]. Like the other matricellular proteins such as SPARC and thrombospondin 1, TNC is transient and becomes integrated with the ECM when tissues undergo remodeling such as in development, wound dealing, injury or stress [113, 126]. Within the context of normal unwounded human skin, TNC expression is limited to the epidermal-dermal junctions of hair buds and eccrine glands, as well as the intima of large blood vessels [127, 128]. TNC is also expressed at sparingly low levels in the papillary dermis beneath the basement membrane [129]. Upon injury or activation of acute inflammation, TNC expression levels are rapidly increased in the upper dermis [130, 131] as well as the deep dermis and muscle layers [132]. Upon an incision or abrasion to the skin, TNC was found to be heavily upregulated in the provisional matrix, the granulation tissue, the epidermal-dermal junctions, and the epidermis, where it is secreted by proliferating keratinocytes [128]. When TNC expression lasts past the tissue

replacement phase of repair and enters the resolution phase, it is usually found in scenarios of excessive scarring such as in keloids or hypertrophic scars [133].

TNC, by nature, is a substantial multimeric protein. It comprises two identical trimers that combine via disulfide bonds at the TNC assembly domain to create a hexameric glycoprotein structure [134]. Each arm monomer ranges in size from 180 to 320 kDa and is composed of four main domains: the TNC assembly domain, the EGF-L repeat domain, the fibronectin type III (FNIII) repeats domain, and a fibrinogen-like globular domain [121, 135]. Both its size and multiple domains allow it to interact with a myriad of different cell receptors, ECM proteins, growth factors and therefore be involved in numerous cellular responses. TNC is perhaps the most notable for its anti-adhesion properties by blocking fibronectin-mediated cell adhesion and spreading through competition of syndecan-4 [136]. TNC itself can be anti-adhesive through its FNIII A-D repeats [137]. However, all TNC's ability to modify cellular responses in one direction, such as say the ability to be non-adhesive, can just as easily revert the opposite way and become very adhesive and promote cell migration through binding through a different motif or by its modification via MMPs and other proteases. Of note, TNC in the wound healing processes is always being cleaved by MMPs (MMP 1,2,3,7 are the most notable) as this contributes to its turnover in tissue repair [137]. Its degradation also allows for a change in functionality as new cryptic binding sites are now accessible and more soluble, allowing them to interact easier with new partners [137].

As already stated throughout this dissertation, the domain of TNC our lab is the most focused on is the EGF-L repeat domain. The EGF-L repeats are notably able to bind the EGFR receptor with low affinity ( $K(D) \sim 74 \mu M$ ) [114], approximately three times weaker than sEGF to EGFR itself ( $K(D) \sim 20 nM$ ) [138]. This low-affinity interaction does not trigger EGFR

internalization nor its degradation, allowing the receptor to maintain its presence at the plasma membrane surface [114]. Additionally, due to there being 14.5 EGF-L repeats on each TNC arm and with the probable constraint of the ECM, this allows for repeated low-affinity interactions with the EGFR, thus creating a “low affinity/high avidity” interaction. TNC’s persistent signaling of EGFR without its internalization (as seen typically through sEGF interactions), results in prolonged activation of the AKT and ERK pro-survival signaling pathways [48]. We are now interested in whether the TNC-MSC interaction improves other areas of MSCs efficacy in wound healing, and it is what we are exploring in part 1 of this paper with relevance to chronic wound therapy.

### **3.0 Excessive Scarring**

#### **3.1 Clinical Significance**

Excessive scarring is a disfunction in the later stages of wound healing that results in the presence of excess fibrillar collagen disposition. Due to the gravity of repercussions non-healing chronic wounds present, the pathological problems created by excessive scarring events are often overlooked by many since they still hold the ability to "heal over". However, the occurrence rate for excessive scarring is still relatively high and comes with complications of their own. Excessive scarring will usually occur from either burns, severe trauma, or a surgical procedure. It is estimated that excessive scarring will affect 30-50% of individuals after a surgery or trauma event, whereas patients who suffer from burns will translate to 67-70% occurring excessive scarring [139-141]. The current medical cost for burn scar prevention and correction is up to 7.5 billion dollars annually in the United States and covers approximately 500,000 patients per year [142, 143]. Quality of life for these patients is dependent primarily on the location, the type, and the size or percent coverage of the scar. But those who suffer from excessive scarring are usually hindered in two main ways: restriction of movement and prolonged pain and itchiness to the area. The hard exterior and restriction of movement can be even more detrimental to the patient as scars appear epithelialized and 'healed'. However, these scars are dysfunctional and have an underlying dermis that is disfigured and compromised. The improper healing in these scars results in wounds that close but are structurally weaker and prone to re-ulceration. This can be a vicious cycle for some patients who can be forced into a continuous cycle between the open wound and excessive scarring. Another issue with scarring is that the resulted healing will cause disfiguration to the skin surface.

If these scars are in areas more accessible visible by the public, then these patients can have an immense psychological impact on their health [144, 145].

### **3.2 Excessive Scarring Microenvironment**

There are three main types of pathological scars: hypertrophic, keloid, and contracture. Hypertrophic scars are one of the most prevalent out of the three. They are defined as thick raised scars that remain confined to the borders of the original wound site [139]. Histological examination of hypertrophic scars reveals an excess of fine type III collagen fibers (Col-III>Col-I) tightly crosslinked and oriented parallel to the epidermal surface and containing an abundant amount of myofibroblasts resembling a more immature dermal state [143, 146]. Hypertrophic scars will typically appear within 1 month of insult, where they will grow for approximately 6 months and then either stop growing or regress in size over the following 6 months [139]. Keloid scars are less predominant but the extreme version of hypertrophic scars. They are defined as scars that will grow beyond the original wound margins and may continue to grow indefinitely. Histological examination of keloid scars reveals an excess of thick type I collagen fibers (Col-I>Col-III) disorganized in nature and lacking the abundances of myofibroblasts as seen in hypertrophic scars, but now have the addition of blood vessels widely scattered throughout the scar tissue [143, 146]. Keloid scars are more indiscriminate in appearance as they can appear three months after injury or three years after injury [139]. They are also harder to treat than hypertrophic scars as they never regress and will grow indefinitely, even after excision. The last type of scar is a contracture scar, most notable with burn victims and usually covers large areas of the body. It is defined by scar

formation that pulls and contracts the healthy, uninjured skin tissue adjacent to the scar, causing the skin to overtighten. If the contracture is too tight, this can cause a lack of motion issues and complications with underlying tissue and organs. These wounds are due to the excess of exuberant myofibroblasts within the wound bed [147].

Excessive scarring occurs from the failure to terminate the last two phases of the wound healing process, allowing the tissue replacement phase to persist into a weakened resolution phase (Figure 3 – Right Column). The initial stage of scarring appears as a sterile chronic inflammatory situation [148, 149]. The failure to end the tissue replacement phase of healing means a constant matrix turnover that generates the chemotactic fragments that further recruit macrophages (primarily M2) and naïve lymphocytes to the tissue, though at lower densities than that which is noted in the early inflammatory stage of healing [150]. These cells reinforce the matrix immaturity through secretion of pro-reparative growth factors (TGF- $\beta$ 1, TGF- $\beta$ 2, PDGF-CC, IL-4, IL-13), which maintains the fibroblasts in the synthetic state [146, 151]. Keratinocytes from the epidermis also exhibit hyperproliferation characteristics and increase expression of TGF- $\beta$  to promote further collagen synthesis of the underlying dermal fibroblasts [152]. Thus, the result is not the breakdown of the matrix and tissue but rather an excessive deposition of relatively immature matrix. This immature matrix will now contain higher levels of pro-reparative ECM proteins such as tenascin-C, fibronectin, and thrombospondin more resembling aspects of granulation tissue; while being relatively devoid of small leucine-rich proteoglycans (SLRP), such as decorin, which are the critical stop signals within the normal resolution phase of repair [61, 149]. Additionally, ECM degradation enzymes MMP-2 and MMP-9 are both active within the remodeling process of excessive scars may contribute to the ever-evolving immature matrix turnover in both regenerative and remodeling capacities [153, 154]. The immature matrix state, the upregulated pro-repair

signals, and the loss of stop/wound maturation signals will all lead to further fibroblasts proliferation and result in excess collagen production or differentiation into myofibroblasts for excess scar contracture [147, 153, 155]. All these processes culminate in a cycle that promotes excessive wound healing until the result of a scar is reached [26].

Most successful scar treatment strategies occur after the scar is formed through surgical excision or laser therapy. However, reoccurrence rates can be anywhere from 45% to 100% for keloids [143, 146], and other hypertrophic burn scars can be too massive to replace through a skin graft. In addition, current prophylaxis-style therapies such as pressure therapy or silicone gel sheeting therapy have varied results and will not work on already mature hypertrophic or keloid scars[146]. This has prompted researchers and clinicians to focus on TGF- $\beta$  drugs and applications to try and correct the ratio of TGF- $\beta$ 1 to TGF- $\beta$ 3 as this is one of the most notable growth factors in excessive scarring [156-158]. However, as many are finding out in cutaneous wound healing, the use of TGF- $\beta$  is a double-edged sword as it is found as a major regulator in all stages of wound healing [159-161]. With this last point for TGF- $\beta$ , we think the extracellular matrix protein decorin (DCN) may act as a better antifibrotic therapeutic. Decorin is only upregulated during the resolution phase of repair, and it is responsible for regulating collagen fiber-bundle organization, regressing angiogenesis, and suppressing the overall tissue growth factor response [162]. It is significantly downregulated in excessive scarring events and has decreased excessive skin contraction [155, 162].

### 3.3 Matricellular Protein Decorin

Decorin (DCN) is a small leucine-rich proteoglycan (SLRP) family member. Its name is derived from its proclivity to interact with or “decorate” collagen fibrils, as it can be found ubiquitously localized to collagen-rich connective tissues throughout the body. DCN is approximately 90-140 kDa in size and comprises three main domains. It has a central protein core of 12 leucine-rich repeats flanked by a set of conserved cysteine residue regions at the N-terminal and C-terminal [163, 164]. An additional distinct feature is a single glycosaminoglycan (GAG) chain containing either a chondroitin sulfate or dermatan sulfate side chain attached to a serine near the N terminal [163, 164].

Within the context of healthy, uninjured skin, DCN can be found within both the papillary dermis and reticular dermis but is entirely absent from the epidermis [165]. It was also observed that higher concentrations of DCN were in the papillary dermis compared to the reticular dermis, where papillary dermal fibroblasts secreted 5.9 times more DCN than reticular fibroblasts [165]. When the skin is injured, DCN protein levels are significantly reduced during the early phases of wound repair but will be reintroduced in the resolution phase from their production via myofibroblasts [166]. When looking at excessive scarring outcomes such as in keloids or hypertrophic scars, DCN productions levels from fibroblasts as well as overall DCN protein expression levels are significantly reduced, suggesting DCN is one of the major stop signals for scarring pathologies [155, 167-170].

The main functions of DCN have been slowly unveiled over the past couple of decades and are still being expanded on today. With its high-affinity attraction with collagen I, DCN has shown to be a major driver of collagen maturation during the resolution phase. It is primarily involved in collagen fibrillogenesis through its ability to bind collagen fibrils and regulate collagen fibril

diameter, organization, an spacing between collagen strands [168, 171-178]. When DCN is down-regulated or missing from this step, collagen maturation becomes significantly less organized and the overall tensile strength of the skin becomes much weaker [162, 168, 171]. It was subsequently discovered that DCN can bind to multiple growth factors and growth factor receptor tyrosine kinases. EGFR was the first receptor tyrosine kinase identified to bind directly with DCN[179], where further research has shown that the binding site of DCN within the EGFR is partially overlapping but distinct from the EGF-binding site [180]. When DCN binds and activates the EGFR, it will internalize and degrade via caveolar endocytosis to the lysosome, causing for EGFR down regulating and a potential mechanism of how DCN enacts its anti-proliferative tendencies during the resolution phase of repair [181, 182]. DCN has also been shown as an antagonist against the VEGFR2 of endothelial cells, inducing an autophagic response and suppressing angiogenesis during the resolution phase [183, 184]. Some notable wound healing growth factors that DCN can also inhibit are TGF- $\beta$ 1, TGF- $\beta$ 2, PDGF, and IGF-1[185]. The most notable growth factor is the TGF- $\beta$  family of growth factors, as their balance within the wound healing process is becoming more notable in the successful or unsuccessful outcomes of wound healing. DCN has been shown to bind and neutralize TGF- $\beta$ 1, TGF- $\beta$ 2 directly or by downregulating its production from hypertrophic scar fibroblasts [155, 166, 186].

## 4.0 Hypothesis

Matricellular proteins play a crucial role in cutaneous wound healing as their multifunctional nature allows for proper coordination of cells, growth factors, and other ECM components throughout the repair process. Further assessment of their biological roles in the context of abnormal wound healing outcomes is needed if they are going to be utilized in future wound healing applications. Due to their transient nature within the different phases of repair, we became interested in two specific matricellular proteins, Tenascin-C and Decorin, whose appearance and functional roles lay at opposite ends of the wound healing repair system. To that end, this thesis has two main parts, each with its own hypothesis. The first part of this thesis builds upon our lab's findings that Tenascin-C alleviates mesenchymal stem cell death both *in vitro* and *in vivo* [48, 49]. We now want to assess whether this TNC influence on MSCs improves their efficacy in wound repair. MSCs are naturally pro-angiogenic, and one of the biggest problems within treating chronic ulcers is overcoming the severe lack of angiogenesis; therefore, *we hypothesized that TNC would enhance the angiogenic and therapeutic effectiveness of MSCs and contribute to better wound healing outcomes.* For the second part of this thesis, we wanted to assess whether direct administration of matricellular proteins could improve pathological outcomes on their own. We have previously shown that mice lacking the CXCR3 receptor displayed a delayed and prolonged dermal wound healing phenotype that leads to hypertrophic scarring and that we could correct this defect through the use of cellular transplants. However, with the ability of DCN and other matricellular proteins to regulate many facets of wound repair, we reasoned we could avoid the complexity of a cell-based therapy if DCN can do it independently. Therefore, *we hypothesized that delivery of DCN would result in a reduced scarring phenotype*

*and an overall better healing outcome in our hypertrophic scarring mouse model.* Ultimately each hypothesis will test the utility of matricellular therapy and any promise for its use in the clinic.

## **5.0 Matricellular Protein Tenascin-C Enhances Mesenchymal Stem Cell Angiogenic And Wound Healing Ability.**

### **5.1 Summary:**

Human mesenchymal stem cells/multipotent stromal cells (MSCs) hold great promise in aiding wound healing through their ability to modulate all phases of repair, most notably their secretion of pro-regenerative paracrine factors. However, MSC clinical utility is significantly hindered by their poor survival rates post-transplantation due to the harsh microenvironment in injured tissue. Previous work in our lab has shown that the matricellular protein Tenascin-C (TNC) can provide survival signaling to MSCs via the epidermal growth factor receptor (EGFR) by restricting its activation at the plasma membrane. This prolonged sequestration of EGFR results in enhanced pro-survival signals via low-level tonic Erk and Akt signaling. Our lab is now investigating how these proximal signals from TNC influence MSC-mediated paracrine signaling during the wound healing process. This study examined the survival and angiogenic potential of MSCs cultured on TNC under ischemic duress *in vitro*. We also assessed the angiogenic and wound healing outcomes of MSC + TNC *in vivo* using a CXCR3 *-/-* mouse model that exhibits a delayed healing phenotype within the tissue replacement phase of repair. The study revealed that MSCs in the presence of TNC exhibit higher levels of angiogenic capability, collagen maturation, and an overall better wound healing outcome than just MSCs administered alone. These findings suggest the coupling of TNC to MSCs as a promising tool for future MSC-ECM type therapies for wound healing applications.

## 5.2 Introduction

Cutaneous wound healing is a dynamic and well-organized series of overlapping phases of repair that will culminate in forming newly intact dermal and epidermal tissue layers. Pathological ailments such as diabetes or vascular disease will obstruct the early phases of the wound healing process and form a chronic wound. Wounds become chronic when they fail to close after three months post-incident [60, 187]. One of the primary complications that lead to chronic wounds is disruptions to the blood supply. Rapid generation of new vasculature is necessary early within the wound healing process to deliver nutrients and oxygen, remove cellular and extracellular debris, and help with the transportation of cells into and out of the wound micro-environment [188, 189].

Mesenchymal stem cells/multipotent stromal cells (MSCs) have emerged as a promising candidate therapy for chronic skin wounds due to their genuine involvement in the early phases of routine wound healing. Upon injury, endogenous bone marrow MSCs will home to the site of injury and secrete paracrine signals to modulate the inflammation process and promote angiogenesis [52, 70, 190, 191]. Numerous pre-clinical and clinical studies have now been published looking at the utility of MSCs and the enhanced benefits of their use in treating a myriad of chronic wound conditions [192]. However, a significant challenge limiting overall MSC therapeutic potential is the poor survival rate and engraftment into the wound bed[52], with up to 90% of the introduced MSCs being lost within the first three days [193]. The chronic wound microenvironment is a hostile culmination of damaged extracellular matrix (ECM), cellular debris, hyper inflammation, and an impaired vasculature [97, 98]. These factors induce MSC death through various mechanisms, including anoikis, ischemic insult, or increased signaling from death cytokines [52, 99].

Our lab is interested in confronting this problem by taking cues from the normal wound healing response and utilizing a naturally occurring extracellular matrix protein called Tenascin-C (TNC). In unwounded skin, TNC is expressed at negligible levels in the papillary dermis just beneath the basement membrane [129]. Shortly after injury, TNC is significantly increased at all levels of the skin: in the epidermis through the secretion of epidermal keratinocytes [194], at the epidermal-dermal junction just under the basal lamina [131], as well as throughout granulation tissue within the dermis [128]. TNC is a six-armed glycoprotein composed of four main domains: the TNC assembly domain, the epidermal growth factor-like (EGF-L) repeat domain, the fibronectin type III (FNIII) domain, and a fibrinogen globe domain. The most intriguing element of the four has been the 14.5 EGF-like repeats found on each arm of the TNC hexamer [123]. Previous studies have noted that these EGF-like repeats can bind to the epidermal growth factor receptor (EGFR) through low affinity/high avidity interactions, allowing for the sequestering of the EGFR to the cell membrane preventing its internalization and degradation [114, 195]. We have previously reported that TNC promotes MSC survival in the face of Fas ligand-induced cell death by binding and sequestering the EGFR, resulting in prolonged activation of the AKT and ERK pro-survival signaling pathways [48, 98]. MSCs in a TNC-based polymer system *in vivo*, were able to survive out to 21 days post-transplantation within the wound bed [49]. This provides the rationale for using MSCs to promote healing.

In this study, we assessed whether the benefit of TNC is not just to promote MSC survival but also to improve the functional capacity of the wound bed. One of the significant hurdles within the chronic wound bed that newly transplanted cells must encounter is ischemia. Therefore, we first subjected MSCs cultured on TNC to *in vitro* hypoxia/nutrient deprivation (H/ND) growth conditions and assessed for survival advantages. We next evaluated TNC supported MSC culture

conditions subjected to H/ND for angiogenic influence on endothelial cells, as reestablishing new vasculature is necessary to overcome ischemia and progress the wound healing process forward. For the last set of experiments, we wanted to determine how TNC-MSC systems would translate *in vivo*. Since chronic wounds have a characteristically elevated quantity of metalloproteinases (MMPs) and other protein degrading enzymes compared to normal healing wounds [60], we decided to use a protein delivery system called coacervate to help protect TNC against early degradation post-implantation. This system is an injectable *in-vivo* delivery vehicle that uses a positively charged synthetic biodegradable poly (ethylene arginyl aspartate diglyceride) (PEAD) and a negatively charged heparin to form a 3-dimensional coacervate that will envelop around the protein cargo of choice [196-199]. The animal model we used for this study is an impaired wound healing CXCR3 *-/-* mouse model, which recapitulates an immature and delayed tissue replacement phase of repair [200]. This mouse model exhibits a delayed healing response within the dermal and epidermal layers of the skin, leading to an immature dermal matrix, a weakened basement membrane, and hypercellularity [148, 201]. Overall, we hypothesized that TNC would enhance the angiogenic and therapeutic effectiveness of MSCs and contribute to better wound healing outcomes.

## **5.3 Materials And Methods**

### **5.3.1 Cell Culture**

*MSC Cell Culture* – We used one Immortalized Bone Marrow Mesenchymal Stem Cells (IHMSCs) and three Primary bone marrow-derived MSCs (PrhMSCs). The IHMSC cell line was

a human bone marrow-derived cell line that was immortalized using human telomerase reverse transcriptase[202] and was kindly gifted to the lab by Dr. Junya Toguchida at Kyoto University. IHMSCs were cultured using the following proliferation media formulation: DMEM with L-Glutamine, 1g/L Glucose and Sodium Pyruvate from Corning (Cat. No.10-014-CV), supplemented with 10% FBS (Cat. No. 100-106, Gemini Bio-Products), 1 mM sodium pyruvate, 1 mM L-glutamine, 1  $\mu$ M non-essential amino acids, and 100 units per mL penicillin-streptomycin. PrhMSCs were obtained from the repository at the Darwin Prockop laboratory at Texas A&M University, a National Institute of Health-funded stem cell repository. PrhMSCs were cultured using the following proliferation media formulation:  $\alpha$ -MEM (Cat. No. 15-012-CV, Corning) supplemented with 16.5% FBS (Cat. No. S11550H, Atlanta Biologicals), 2 mM L-glutamine, and 100 units per mL penicillin/streptomycin.

For hypoxia and nutrient deprivation conditions (H/ND) to mimic ischemia *in vitro*. MSCs were expanded and seeded near confluence onto one of three treatment coatings (Plastic, Col-I or TNC+Col-I) and cultured in their fully supplemented DMEM for one day at ambient air conditions (37°C at 5% CO<sub>2</sub> and 21% O<sub>2</sub>) to stabilize after passaging. Meanwhile, basal DMEM and  $\alpha$ -MEM without supplementation or FBS were placed into BioSpherix incubators at 1% oxygen to acclimate the media 24 hours prior to adding to the cells. Upon the start of H/ND experiments of MSCs, the complete culture medias were aspirated, the plates were washed twice with PBS to remove residual media, and pre-equilibrated H/ND media was added to the MSCs. The MSCs were then placed into the BioShperix incubators at 1% oxygen. At no point in the culture of cells at 1% were the cells exposed to ambient oxygen conditions, as microscopes to monitor cells were also contained in the BioSpherix chamber. Positive confirmation of hypoxia on MSCs was confirmed

through a live cell green hypoxia dye (Cat. No. SCT033, EMD Millipore) as instructed by the company's protocol at the beginning stages of each H/ND experiment (Figure 6).

*Endothelial Cell Culture* – Immortalized Human Microvascular Endothelial Cells (HMEC-1) were obtained through ATCC[203] (Cat. No. CRL-3242) and cultured using the following proliferation media formulation: MCDB131 basal media without L-glutamine (Fisher Scientific) supplemented with 10% FBS, 10 ng/mL epidermal growth factor, 1 $\mu$ g/mL hydrocortisone, and 10mM glutamine. HMEC-1 were thawed and expanded up to passage 3 in proliferation media, then transitioned to either IHMSC or PrhMSC media conditions over a two-week period for functional endpoint experiments. By Passage 6 HMEC-1s were fully transitioned to MSC media conditions and used for cell migration and cord formation studies.

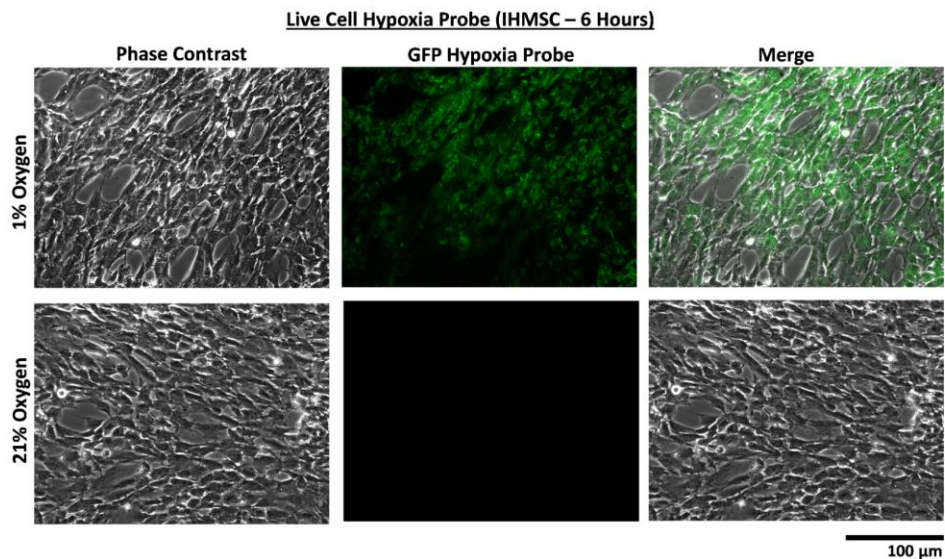


**Figure 6: Confirmation of hypoxia in BioSpherix culture system. MSCs were seeded onto either plastic, Col-I, or TNC+Col-I coated plates and placed under H/ND conditions. A live cell hypoxia probe was used on parallel plated IHMSC plates, one at 21% ambient oxygen levels and one at 1% hypoxic oxygen levels. Images were taken 6 hours post-exposure to hypoxia conditions. This served as a backup method for checking if the Biospherix instrumentation was working correctly. The sample images above are IHMSCs seeded onto plastic 6 well tissue cultures plates. The scale bar for all images is 100  $\mu$ m.**

### **5.3.2 Coating Culture Plates With Col-I And TNC**

Cell culture plate coating procedures and concentrations used for Tenascin-C (TNC) (Cat. No. CC065, EMD Millipore) and type 1 rat tail collagen (Col-I) (Cat. No. 354236, BD Biosciences) were as previously described in our lab [48]. In short, cell culture dishes were coated for 12 hours at 37°C with 1  $\mu\text{g}/\text{cm}^2$  Col-I, or 1  $\mu\text{g}/\text{cm}^2$  Col-I and 1  $\mu\text{g}/\text{cm}^2$  TNC diluted in PBS. After the incubation period, the PBS was aspirated, and the coated surfaces were placed under UV light for 30 minutes before seeding any cells. The Col-I was required for the TNC coated plates, as TNC is anti-adhesive and requires additional integrin-binding epitopes as provided by the collagens[48].

### **5.3.3 Apoptosis Assessment**

Two methods determined cell death. In the first method, flow cytometry combined with an Annexin V and propidium iodide (PI) kit (Cat. No. V13242, Thermo Fisher Scientific) were performed as per manufacturer's instruction. In brief, MSCs cultured under H/ND growth conditions on either plastic, Col-I, or TNC+Col-I were harvested by collecting adherent cells and floating cells in the supernatant. The floating and adherent cells were combined and stained for PI and Annexin V for 15 minutes at room temperature. An appropriate volume of 1X annexin-binding buffer and Counting beads (Cat. No. C36950, Thermo Fisher Scientific) were added and the tubes placed on ice. Samples were run through a BD FACSCanto II flow cytometer and analyzed using FlowJo\_V10. An unstained control for each cell type was used to determine positive and negative stained cells and counting beads were used to determine the absolute number of cells per treatment condition for quantification.

For the second method, MSCs were seeded onto 6-well plates for each condition (plastic, Col-I, or TNC+Col-I) and subjected to H/ND. Old media was removed, PBS with CellEvent caspase 3/7 green detection reagent (Cat. No. C10423, Thermo Fisher Scientific), and 5% FBS was added to each well and left to incubate for 30 minutes at 37°C. Cells were imaged and quantitated using ImageJ, where all images were converted to 8-bit format, and the threshold was reduced to highlight the green punctae in culture, using the same thresholding for all analyzed images. Particle analysis in ImageJ was set to detect fluorescent points with a radius greater than 50 pixels to exclude debris and background fluorescence. The number of caspase 3/7 positive and negative cells were calculated and expressed as a percentage of Caspase 3/7 positive staining. This second method procedure was also used to determine the survival time course during exposure to H/ND, but instead of using caspase 3/7, we initially used PI from the provided Annexin V/PI kit.

#### **5.3.4 Preparation Of Conditioned Media**

Conditioned media (CM) was harvested at 96-hour time point from the four MSC cells lines cultured under H/ND growth conditions on either plastic, Col-I, or TNC+Col-I. CM was then centrifuged for 10 min at 10,000 rpm to remove cells and cellular debris. The supernatant was collected and frozen for downstream assays.

#### **5.3.5 Cord Formation Assay**

Cord formation assays were performed using  $\mu$ -slide angiogenesis glass-bottom slides (Cat. No. 81507, Ibidi) as per manufacturers' instruction. In brief, growth factor reduced Matrigel (Cat. No. 356231, BD Biosciences) was seeded in the bottom well of the ibidi angiogenesis plates

and allowed to polymerize for 30 minutes at 37°C. While the gel was polymerizing, low passage fully transitioned HMEC-1 cells were trypsinized, counted, and mixed with a ratio of 50% basal media and 50% freshly thawed CM for each treatment condition. Basal media alone was used as the negative control, while basal media with 10% FBS was used as the positive control. Cells were then seeded into the Ibidi angiogenesis chamber at  $2 \times 10^5$  and placed into a 37°C incubator with ambient growth conditions. Cords were allowed to form over the next 6 hours before being quantified using ImageJ Angiogenesis Analyzer [204] and expressed as a total number of cords, total cord length, the total number of meshes, and total mesh area. Cords are the sum of segments (elements bordered by two junctions) and branches (elements bordered by a junction and one extremity); and a mesh is defined as an area enclosed by segments [204].

### **5.3.6 Scratch Assay**

Cell migration was assessed using the wound healing (or scratch) assay. HMEC-1 were seeded into 24 well plates and allowed to grow to confluence. Upon reaching confluence, the cells were washed in PBS and then cultured in basal media containing 1% dialyzed FBS for 24 hours to limit proliferation during the study. The next day using a 1000 mL pipette tip, scratches were made down the middle of each plate to create a denuded area. Each well was washed twice with PBS to remove cellular debris after the scratch was made. A mixture of 50% basal media with 1% dFBS and 50% CM from each treatment condition were added to their respective wells. Basal media alone was used as the negative control while basal media with 10% FBS was used as the positive control. Images were acquired at 0 and 24 hours, and the area unoccupied by the migrating cells was determined using Image J and expressed as % wound closure.

### **5.3.7 Cytokine Measurement**

MSCs were seeded onto 6-well plates for each condition (plastic, Col-I, or TNC+Col-I) and subjected to H/ND. At 96 hours, CM was collected, centrifuged to remove cellular debris, and frozen until ready to use. To determine angiogenic factors in the MSC CM, we used a semi-quantitative human angiogenesis antibody array (Cat. No. AAH-ANG-1000-2, RayBiotech) and followed instructions as outlined in their protocol. In brief, 1 mL of CM from each MSC treatment group was placed on a specialized PVDF membrane with specific angiogenic capture antibodies and incubated overnight at 4°. A series of washes and conjugation of biotinylated antibodies were performed following the incubation period. According to the kit's protocol, membranes were washed 3 times more and detected using labeled streptavidin and chemiluminescence. Radiographs were processed and analyzed using ImageJ Dot Blot analyzer plug-in.

### **5.3.8 RT-PCR Analysis**

MSCs were seeded onto 6-well plates for each condition (plastic, Col-I, or TNC+Col-I) and subjected to H/ND. At 48 hours, MSC treatment conditions were washed with PBS, trypsinized and pelleted, and RNA was isolated using RNeasy kit (Cat. No. 74004, Qiagen). Quality and concentration analysis of RNA samples was assessed using a nanodrop instrument and stored at -80°C. Next, the isolated RNA samples were synthesized into cDNA using The RT<sup>2</sup> First Strand c-DNA Synthesis Kit from Qiagen (Cat. No. 330404, Qiagen). MSC angiogenic and wound healing genes were assessed using Qiagen RT<sup>2</sup> Profiler Array System (Cat. No. PAHS-024ZA-12 and PAHS-121ZA-12, Qiagen) RT-PCR was performed on the Stratagene Mx3000P Real-Time PCR System with the Qiagen RT<sup>2</sup> SYBR Green qPCR Master Mix (Cat. No. 330523, Qiagen).

Samples were analyzed using the  $\Delta\Delta$ CT method plus or minus standard error and expressed in terms of fold regulation. MSCs grown on Col-I and TNC+Col-I were normalized back to MSCs grown on plastic, and GAPDH was used as the reference gene. Fold-regulation is similar to fold change in that positive values greater than one indicate up-regulation; however, fold-change values less than one that indicates down-regulation have now been transcribed to the negative inverse. For our analysis, we used 2 and -2 as our fold regulation cut-off numbers for anything of importance; and CT values more than 32 were seen as likely biologically irrelevant.

### **5.3.9 Animal Model**

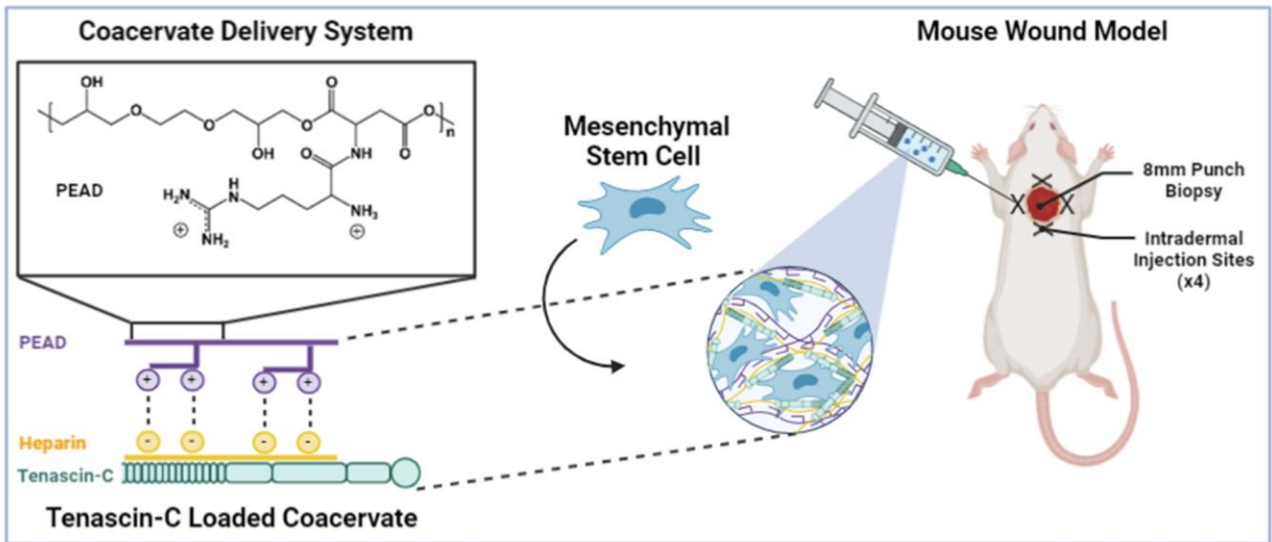
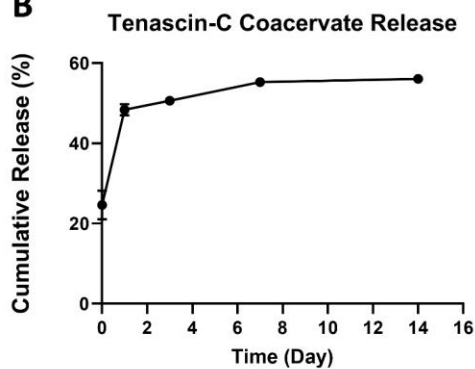
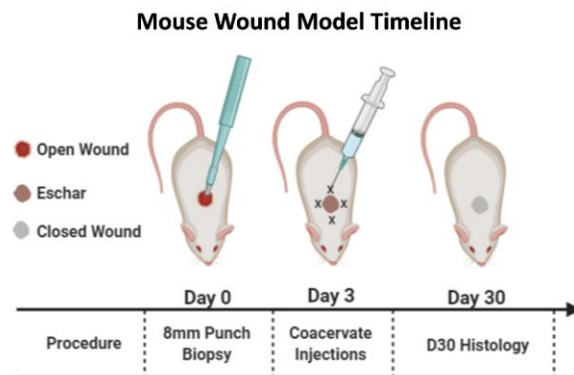
C57BL/6J CXCR3  $-/-$  mice were generated as previously described[205] and gifted to the lab by Bao Lui and William Hancock. The C57BL/6J CXCR3  $-/-$  mice were then bred to FVB strain mice for at least 20 generations to yield germline transmission of the targeted allele and create CXCR3 devoid mice on the FVB background. For this study, CXCR3  $^{-/-}$  female mice were bred with CXCR3  $^{-/-}$  males, and all offspring were screened for genotype through PCR before use. All studies on these animals were performed in compliance with and after approval by the Institutional Animal Care and Use Committees of the Veterans Administration and the University of Pittsburgh. These animals were housed in the Veteran's Affair Medical Center (Pittsburgh, PA) facility accredited by the Association for the Assessment and Accreditation of Laboratory Animal Care. Serological analyses did not detect blood-borne pathogens or evidence of infection. Mice were housed in individual cages after wounding, as allowed by the IACUC to limit fighting and further scarring and maintained under a 12-hour light/dark cycle following the guidelines approved by the Institutional Animal Care and Use Committee.

### **5.3.10 Mouse Wounding**

Male and female mice (8 to 9 months of age and weighing approximately 25 g) were anesthetized with an intraperitoneal injection containing ketamine (75 mg/kg) and xylazine (5 mg/kg). The backs were cleaned, shaved, and sterilized with betadine solution. Full-thickness wounds were performed using an 8mm diameter punch biopsy through the epidermal and dermal layers along one side of the dorsal midline of the mouse (Figure 7A). The contralateral uninjured skin served as unwounded control skin.

### **5.3.11 Coacervate Preparation And Mouse Injections**

PEAD was synthesized as previously described[206]. Stock solutions of PEAD and heparin (10mg/mL) were prepared in 0.9% saline solution using a 0.22  $\mu\text{m}$  sterile syringe filter. Human Tenascin-C purified protein (Cat. No. CC065, EMD Millipore) was reconstituted to 300  $\mu\text{g/mL}$  and mixed with heparin stock solution at their respective predetermined working dose of 10  $\mu\text{g}$  per animal. The heparin/TNC solution was then mixed with the PEAD stock solution to form protein-encapsulated coacervates at a final ratio of 1:100:500 mass ratio. Coacervation was determined by the rapid formation of a turbid solution once all components were added. The prepared coacervate mixture was then mixed with a prepared cell suspension of  $50 \times 10^4$  IHMSCs per mouse for a total injection volume of 300  $\mu\text{L}$  per mouse. Intradermal Injections were administered 72 hours post wounding. Each mouse received 300  $\mu\text{L}$  of one of five treatment options: CO only, CO+TNC, CO+MSC, TNC+MSC, or CO+TNC+MSC, through a series of 4 injections of 75  $\mu\text{L}$  around the wound bed to avoid tissue trauma (Figure 7A). Each treatment group comprised of 4 animals each.

**A****B****C**

**Figure 7: Coacervate delivery study of matricellular protein TNC and MSCs on delayed wound healing mouse model. (A) Overview schematic demonstrating the preparation of the coacervate-TNC + MSC delivery to an in-vivo mouse skin wound model. (B) ELISA exhibited a % cumulative release of TNC from coacervate over 14 days. (C) Overview of mouse wound healing timeline for wounding procedure and harvesting. There were 5 treatment groups (CO only, CO+TNC, CO+MSC, TNC+MSC, or CO+TNC+MSC), with each group comprising 4 animals.**

### 5.3.12 Coacervate Release

Coacervate was prepared as stated above to create three independent samples for coacervate containing TNC. Samples were incubated at 37°C for 14 days, and the supernatant was harvested on days 0, 1, 3, 7, and 14 through pelleting the coacervates by centrifugation (12,100g for 10 min). Supernatants were analyzed using pre-coated enzyme-linked immunosorbent assay (ELISA) kits (Cat. No. ab213831, Abcam), according to the manufacturer's specifications (Figure 7 B).

### 5.3.13 Histological Analyses

Wound bed biopsies were collected after euthanasia at day 30 using a 12mm punch biopsy and were immediately fixed in 10% buffered formalin. Samples were then sent to the University of Pittsburgh Neuropathology Histology Core for paraffin embedding (FFPE), sectioning into slides (6 µm), and sample staining for Hematoxylin and Eosin (H&E) and Masson's Trichrome staining (MT). Blank slides were also made for downstream Picrosirius Red (PSR) staining as directed by the manufacturer's protocol (Cat. No. 150681, Abcam) and follow up immunohistochemistry and immunofluorescent stains.

*Wound healing score assessment* – Histopathological examination of mouse tissues was performed in a double-blind approach among three investigators, and their scores averaged. Qualitative assessments were based on epidermal and dermal maturation as outlined in previously established protocols (Figure 8)[148, 201, 207]. In short, the samples were scored on a scale of 0 to 4 for both epidermal and dermal layers of tissue. For epidermal maturation scoring: 0 = no epidermal migration, 1 = partial epidermal migration, 2 = complete epidermal migration, 3 =

Partial keratinization and an intact basement membrane, 4 = complete keratinization and normal epidermis. For dermal maturation scoring: 0 = no healing, 1 = inflammatory infiltration, 2 = granulation tissue present – fibroplasias and angiogenesis, 3 = collagen deposition replacing granulation tissue > 50%, 4 = complete replacement of granulation tissue and complete healing.

*Skin thickness measurements* – H&E and MT sample images were analyzed using ImageJ line measurement tool to measure the thickness of the epidermal and dermal layers for each mouse specimen. The epidermal layers were measured from the stratum basale to the stratum granulosum (excluding the stratum corneum), and the dermal layer was measured from the top of the papillary layers to the bottom of the reticular layer. A total of 6 measurements per biological sample were scored for each layer.

*Collagen quantification* – Polarized PSR images were quantified using ImageJ version 1.53K (NIH; <https://imagej.nih.gov/ij>). Each image was split into red, green, and blue channels, from which the red and green channels were selected. The isolated red and green channels then underwent thresholding and follow-up measurements to determine the total staining area for each collagen type. Picrosirius Red birefringence under polarized light reveals tightly packed thick and long fibrils of type 1 collagen as either bright red-orange intense birefringence in tissue and thin short loose fibrils as yellow-green[208]. The overall ratio of type 1 collagen to type III collagen was analyzed by comparing the representative staining results for either collagen type back to the original image for total collagen content.

*Collagen orientation and alignment* – Polarized PSR images were quantified using ImageJ plug-in: OrientationJ version 2.0.5. Visual directional analysis using the color survey tool was performed with the following parameters: Hue is set for orientation, Saturation is set for coherency, and brightness is set to the original image[209]. The OrientationJ distribution tool was used to

create the distribution of orientation histograms to determine where patterns of alignment were within our samples[210]. The OrientationJ Dominant Direction tool was used to determine the quantitative orientation measurement for coherency across the whole image[211].

*Immunohistochemistry staining*– Skin sample tissue sections (6 µm) were rehydrated and placed into citrate acid buffer at 95°C for 10 minutes and cooled to room temperature for 1 hour. Samples were then washed in Phosphate-buffered saline (PBS) and quenched with 3% hydrogen peroxide. Following additional washes in PBS, samples were blocked in 20% goat serum for 1 hour and subsequently incubated with primary antibodies diluted in blocking buffer overnight at 4°C. Primary antibodies were at the following dilutions: CD31 (1:50, Cat. No. ab28364, Abcam). After primary antibody incubation, samples were washed in PBS and incubated in goat anti-rabbit HRP secondary antibody (1:2000, Cat. No. ab205718, Abcam) for 1 hour at room temperature. After final antibody incubations, samples were washed in PBS and then treated with ABC reagent (Cat. No. PK-6100, Vector Laboratories) for 30 minutes. Rewashed with PBS and developed with DAB reagent kit 27 (Cat. No. SK-4100, Vector laboratories), counterstained with H&E, clarified (Richard Alan Scientific), and dehydrated in ethanol and xylene. Samples were mounted (Cat. No. SP15-500, Fisher Scientific) and imaged using an Olympus Provis microscope. Image analysis was performed using Image J Colour Deconvolution 2 plug-in to acquire DAB positive staining area. The total DAB positive area was compared back to the total area of the original image to get a final percentage.

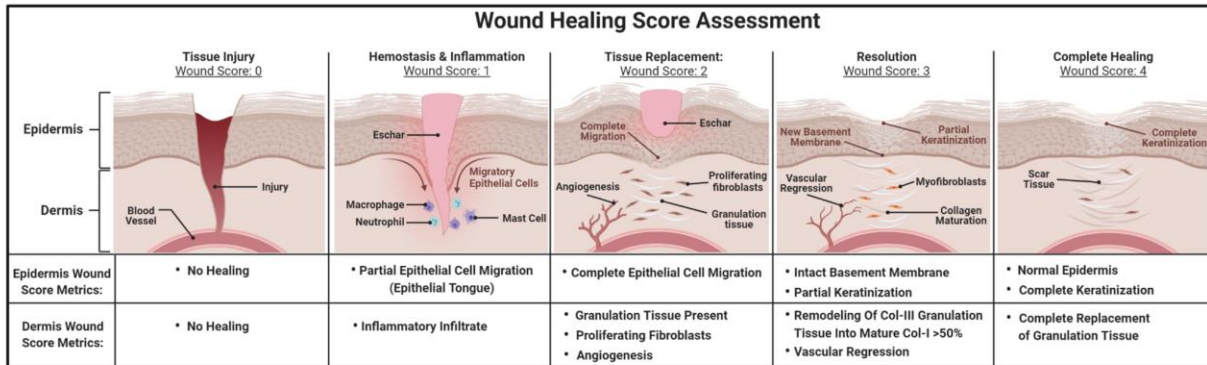


**Figure 8: Illustration overview of wound healing score assessment for cutaneous wound healing** Epidermal and dermal skin layers are assessed independently and given a score on a scale of 0 to 4, depending on the current wound healing phase being observed. Epidermal maturation scoring goes as follows: 0 = no epidermal migration, 1 = partial epidermal migration, 2 = complete epidermal migration, 3 = Partial keratinization and an intact basement membrane, 4 = complete keratinization and is now considered completely healed. Dermal maturation scoring goes as follows: 0 = no healing, 1 = inflammatory infiltration, 2 = granulation tissue present – fibroplasias and angiogenesis, 3 = collagen deposition replacing granulation tissue > 50%, 4 = complete replacement of granulation tissue and is now considered completely healed.

### 5.3.14 Statistical Analysis:

Data for the *in vitro* cell survival and cytokine array are presented as the mean  $\pm$  standard deviation, whereas the cord formation and cell migration assays are presented as the mean  $\pm$  s.e.m. All *in vitro* studies were performed using four biological replicates with at least 2 technical replicates. Results from animal wound healing score assessment and PSR staining assessment are expressed as mean  $\pm$  SD with at least a minimum of four mice per treatment group. Histological quantifications for skin layer thickness and immunohistological stains (CD31) were performed on five microscopic fields of each specimen and reported as mean  $\pm$  s.e.m. One-way ANOVA determined statistical analysis between treatment groups for all experiments except for the survival

time course for which two-way ANOVA was used to distinguish significance. Both ANOVA analyses were followed by posthoc Tukey HSD analysis using GraphPad Prism 9 software (GraphPad Software, San Diego, CA). Significance was claimed for  $P < 0.05$ . Significance is represented in all figures with symbols denoting  $*P < 0.05$ ,  $**P < 0.01$ ,  $***P < 0.001$ , and  $****P < 0.0001$

## 5.4 Results

### 5.4.1 Tenascin-C Protects MSCs Under Ischemic Conditions *In-Vitro*.

One of the major obstacles facing MSC survival and engraftment within chronic wounds is ischemia. We have previously shown TNC's ability to protect MSCs against inflammatory death signals [48], and now we wanted to determine whether this matricellular protein also ameliorated the ischemia due to the lack of angiogenesis. As previously described in the methodology, we have created an ischemic environment *in vitro* through our access to a Biospherix growth chamber and our previous experiments showing that MSCs were glycolytic in nature [101]. We first set out to make a cell survival time course using Propidium Iodide (PI) as a marker for dead cells and observed a significant difference at day 7 between our treatment groups (MSC on plastic, MSC on Col-I, or MSC on TNC+Col-I) under H/ND conditions (Figure 10 A,B). MSCs cultured on TNC+Col-I had much lower PI incorporation (80% survival) when compared to MSCs cultured on either plastic (34% survival) or Col-I alone (48% survival).

Additionally, MSCs cultured on Col-I showed better survival over MSCs cultured on plastic, though not to the degree of TNC+Col-I. We further analyzed the survival changes around

Day 7 using flow cytometry with a combination of PI and Annexin V cell death markers. In this system, PI can detect necrotic or late apoptotic cells through the loss in integrity of the plasma membrane, and Annexin V will signal early apoptosis through detection of plasma membrane flipped phosphatidylserine as well as late apoptosis. A snapshot of this transition at day 7 reveals that only 2.09% of the MSCs on plastic are not transitioning through apoptosis (PI-/Annexin V-); compared to the survival rates of MSCs on Col-I at 29.9% or MSCs on TNC+Col-I at 40.2%; the survival on TNC+Col-I was significantly higher than Col-I alone (Figure 9 A, B and 10B).

To confirm the flow cytometry data results, we performed an additional set of staining experiments with a live cell green caspase 3/7 stain and quantified it for apoptosis on day 7 (Figure 9 C, D). Once again, MSCs cultured on plastic were significantly limited in survivability, with mean positive staining for caspase 3/7 of 39%. While MSCs cultured on Col-I or TNC+Col-I had lower mean caspase 3/7 staining rates of 31% and 27%, respectively. With caspase 3/7, the difference between the Col-I and TNC+Col-I survival rates did not reach statistical significance; this could be due to the loss of dead cells floating off the bottom of the plate, where these were captured and quantified in the flow analysis. The data suggest that MSCs seeded on TNC+Col-I have significantly higher protection against the ischemic microenvironment than MSCs cultured on plastic alone and a slightly higher survival rate than MSCs cultured on Col-I.

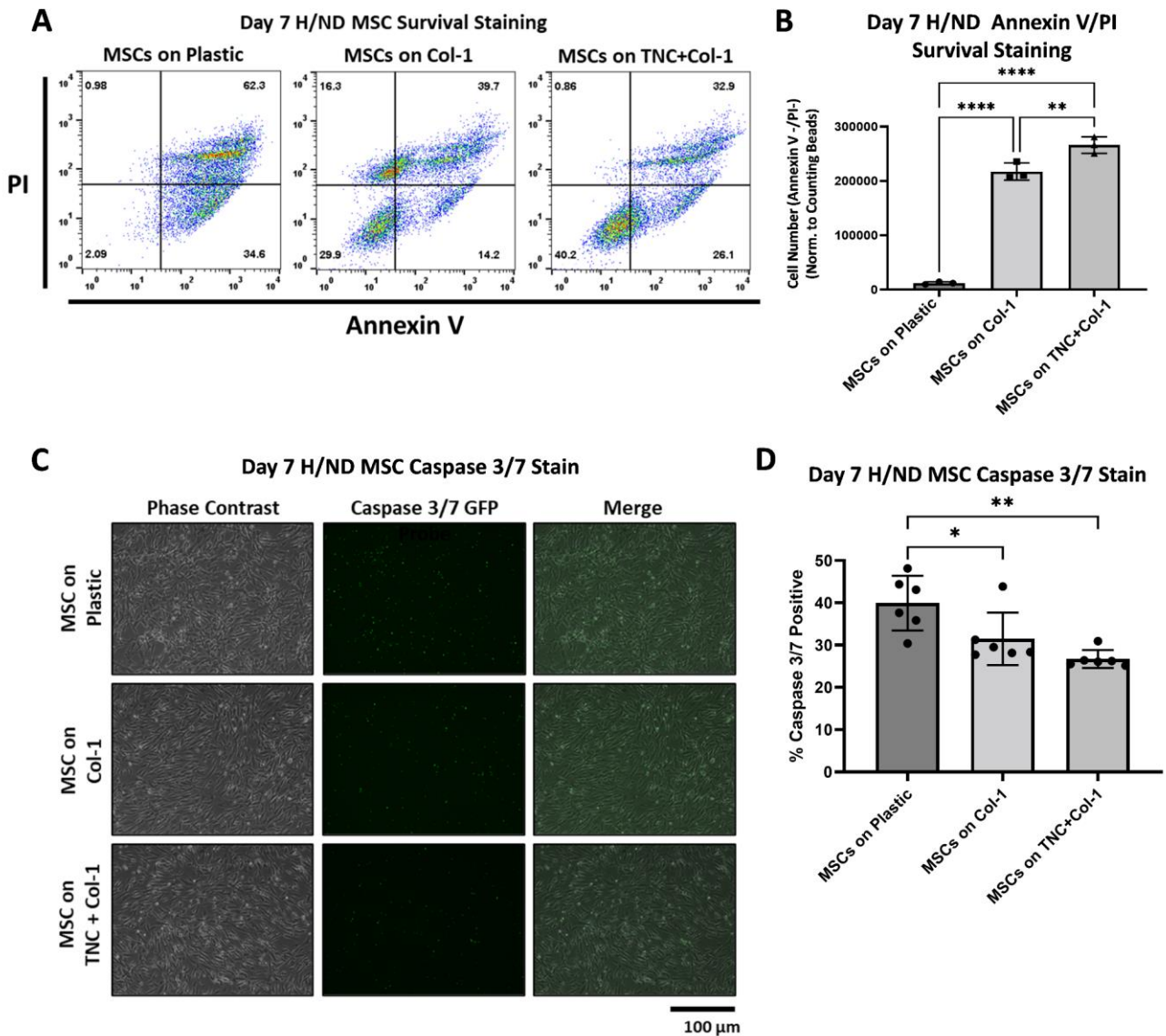


**Figure 9: TNC protects MSCs against ischemic conditions in vitro.** MSCs were seeded onto either plastic, Col-I, or TNC+Col-I coated plates and placed under H/ND conditions for up to 9 days. (A) Flow cytometry dot blot of MSCs stained with Annexin V and PI at day 7 H/ND where apoptosis begins to take effect. (B) Quantification of flow data normalized to counting beads expressed as cells negatively stained for Annexin and PI. (C) MSC live cell staining at day 7 for caspase 3/7 and (D) quantification using ImageJ software to find % positive caspase 3/7 staining. Quantification in C and D are shown as mean  $\pm$  SD. \* $p < 0.05$ , \*\* $p < 0.01$ , \*\*\* $p < 0.001$ . The scale bar for all images is 100  $\mu$ m.

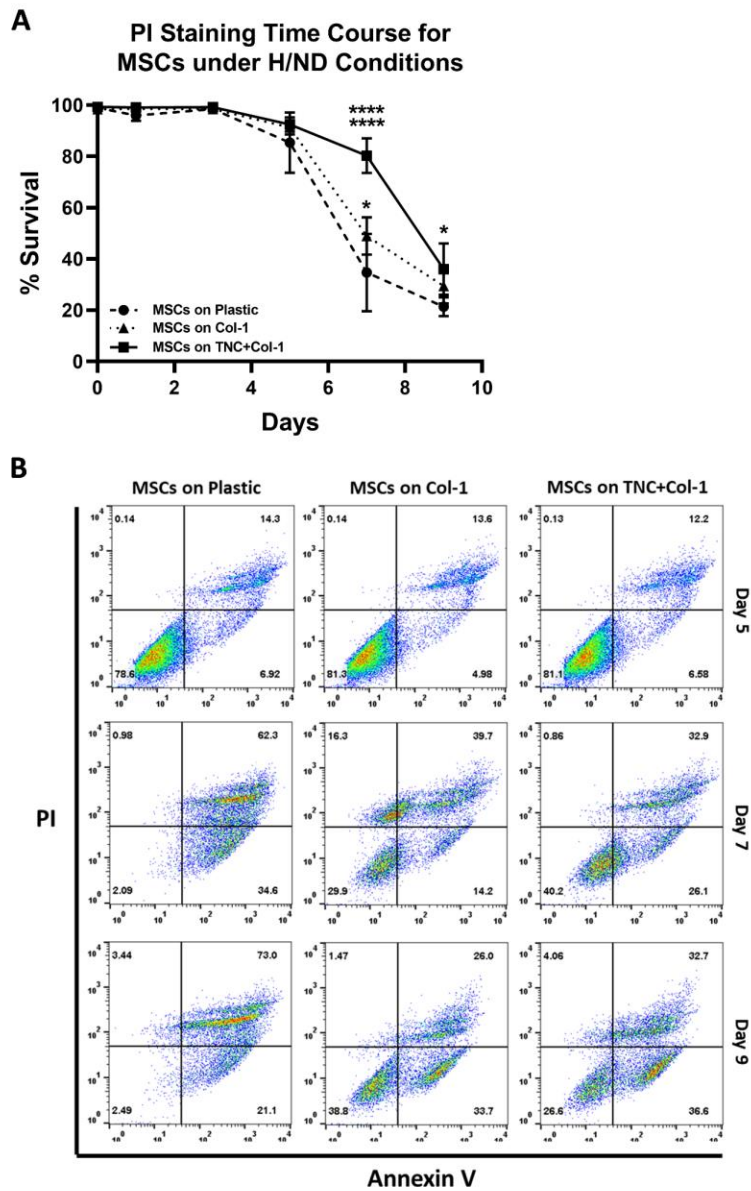


**Figure 10: Time course comparison of culture treatments on MSC cell survival during H/ND in vitro.** MSCs were seeded onto either plastic, Col-I, or TNC+Col-I coated plates and placed under H/ND conditions for up to 9 days. (A) PI analysis to assess percent survival among the different MSC treatment groups. (B) Flow cytometry dot blot of MSCs stained with Annexin V and PI at days 5, 7, and 9 where MSCs start to undergo apoptosis. Quantification using ImageJ software to find % positive PI staining in A and is expressed as mean  $\pm$  SD. Two-way ANOVA was used to distinguish significance during the time course. \* $p < 0.05$ , \*\* $p < 0.01$ , \*\*\* $p < 0.001$ , \*\*\*\* $p < 0.0001$ .

#### **5.4.2 Condition Media From MSCs Cultured On Tenascin-C Improves Endothelial Cord Formation And Motility.**

TNC can contribute to the angiogenic response by enhancing MSC-produced angiogenic factors. To assess TNC's influence on MSC's ability to modulate the ischemic wound environment and improve vascularization, we next wanted to look at the angiogenic effects of MSC conditioned media (CM) on endothelial cells *in vitro*. CM was harvested from MSCs cultured on either plastic, Col-I, or TNC+Col-I under H/ND conditions and used with HMEC-1 plated on a reduced growth factor Matrigel surface to commence cord formation (Figure 11 A). Overall, CM from all three treatment groups performed equal to or better than the positive control of basal media + 10% FBS across all metrics (Figure 11 B). More impressive, however, was the CM from MSC cultured on TNC+Col-I, as it scored significantly higher than MSCs cultured on plastic in total cord length, the total number of meshes, and total mesh area. Additionally, CM from MSCs cultured on TNC+Col-I had significantly longer length and a higher number of cords compared to CM from MCSs cultured on Col-I alone, and trended higher on the other metrics through the increases did not reach statistical significance.

After assessing the potential angiogenic influences, we next sought to examine the cell motility effects of the different culture conditions through a wound-healing/scratch assay. CM harvested from the varying MSC culture conditions (plastic, Col-I, TNC+Col-I) were placed into confluent HMEC-1 wells with a denuded strip in the center to allow for cell migration. Images were taken at 0 and 24 hours post addition of the CM, and cell migration into the denuded area was measured (Figure 11 C, D). Unlike in the cord formation assay, none of the MSC treatment groups outperformed the positive control group this time. The basal media negative control had a wound closure rate of 23%, while CM from both plastic and Col-I scarcely outperformed at 28%

and 30%. CM harvested from TNC+Col-I performed significantly better with a wound closure rate of 43%. Overall, TNC's interactions with MSCs look to have a pro-angiogenic effect.

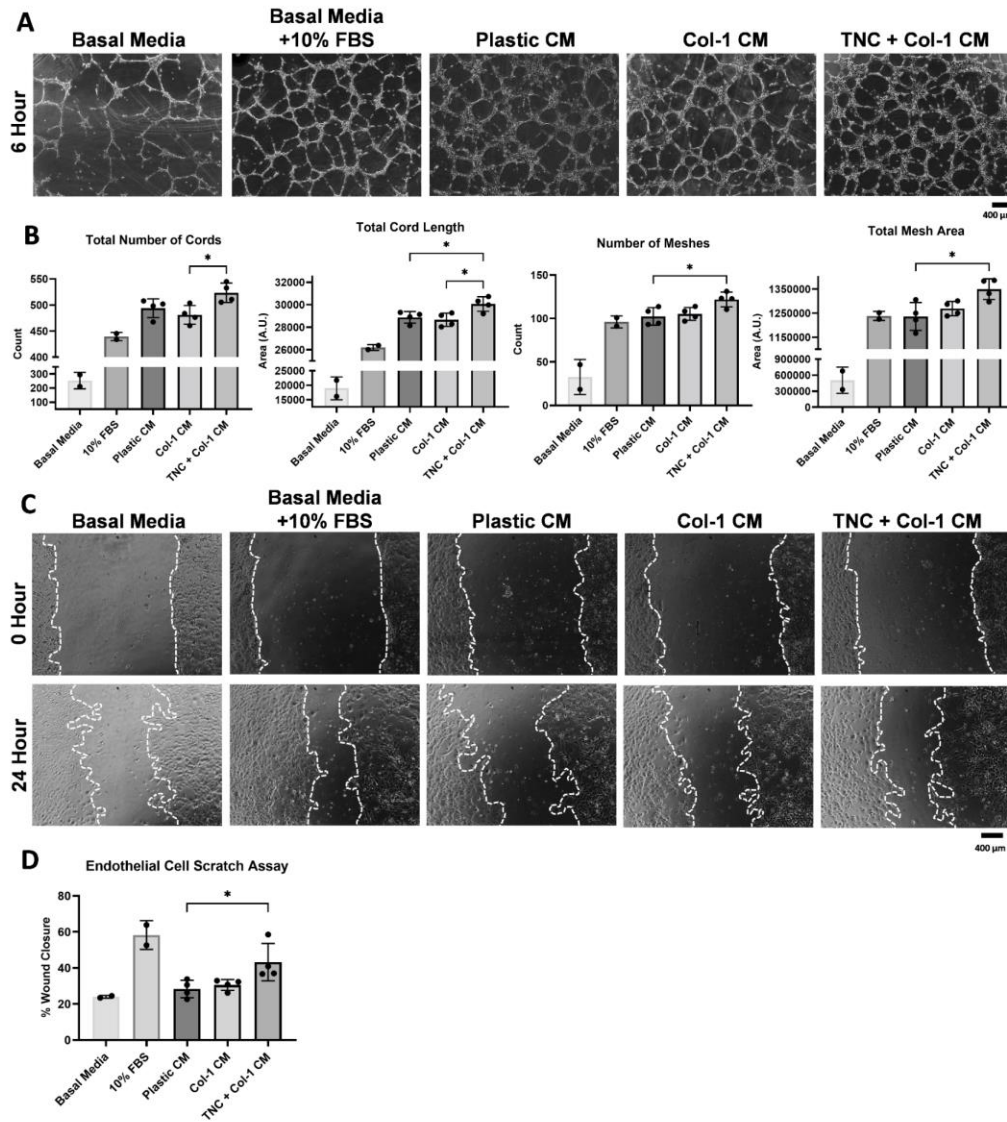
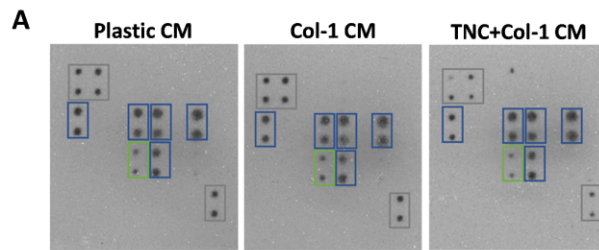


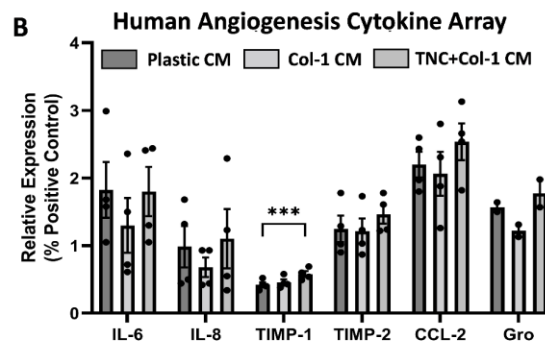
**Figure 11: MSC-TNC CM improves endothelial cell cord formation and motility.** BM-MSCs were seeded onto either plastic, Col-I, or TNC+Col-I coated plates and placed under H/ND conditions. (A) Cord assay was performed by collecting 96 hour CM and mixing with HMEC-1 at  $2 \times 10^5$  cells per well onto growth factor reduced Matrigel in ibidi angiogenesis slides. Images were taken 6 hours post-seeding and quantified using ImageJ Angiogenesis Analyzer for (B) the total number of cords, total cord length, number of meshes, total mesh area. (C) CM was also used to determine the pro-migration effects on HMEC-1 across a denuded area with images being taken at 0 and 24 hour time points and (D) ImageJ quantification for % wound closure for each treatment group. Quantification in B and D are shown as mean  $\pm$  s.e.m. \* $p < 0.05$ , \*\* $p < 0.01$ , \*\*\* $p < 0.001$ . The scale bar for all images is 400  $\mu$ m.

### **5.4.3 Assessment Of Culture Conditions On MSC Paracrine Activity And Gene Expression During H/ND Exposure.**

The physiological outcomes of CM on endothelial function prompted us to explore what factors could be at play. Utilizing an aliquot of CM from the different MSC culture conditions, we first tried to measure angiogenic cytokines utilizing an angiogenesis array for 43 protein targets. (Figure 12 A, B). Of the 43 targets, 6 proteins were substantially expressed including IL-6, IL-8 (CXCL8), TIMP-1, TIMP-2, CCL2 (MCP1-), and Gro alpha/beta/gamma (CXCL1, CXCL2, CXCL3). All protein hits were expressed by all three CM treatment groups, with only TIMP-1 exhibiting a significant difference between CM from Plastic and CM from TNC+Col-I, though the fold increase was minimal. Follow-up gene expression analysis for these 6 protein targets revealed no significant differences at the mRNA level between treatment groups (Figure 12 C). To explore other possible differences between the treatment groups, we ran each sample on two qPCR profilers to explore gene targets relating to angiogenesis and wound healing (Figure 13 A, B). Out of 138 unique genes in total from both arrays, there were 14 genes that either had an upregulation or downregulation of 2 or more, summarized in the table of Figure 13 C. However, only Col5A2 upregulated in CM from MSC on TNC+Col-I was statistically significant with a p-value of 0.027.



	A	B	C	D	E	F	G	H
1	POS	POS	NEG	NEG	Angiogenin	EGF	CXCL5	bFGF
2	POS	POS	NEG	NEG	Angiogenin	EGF	CXCL5	bFGF
3	GRO	IFN-gamma	IGF-1	IL-6	IL-8	Leptin	CCL2	PDGF-BB
4	GRO	IFN-gamma	IGF-1	IL-6	IL-8	Leptin	CCL2	PDGF-BB
5	PLGF	CCL5	TGF-B1	TIMP-1	TIMP-2	TPO	VEGF-A	VEGF-D
6	PLGF	CCL5	TGF-B1	TIMP-1	TIMP-2	TPO	VEGF-A	VEGF-D
7	Blank	Blank	Blank	Blank	Blank	Blank	NEG	POS
8	Blank	Blank	Blank	Blank	Blank	Blank	NEG	POS



**C** qPCR Analysis of MSCs in H/ND at 48hr (Norm. to GAPDH and Plastic)

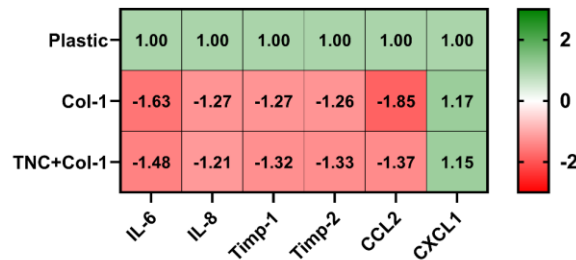
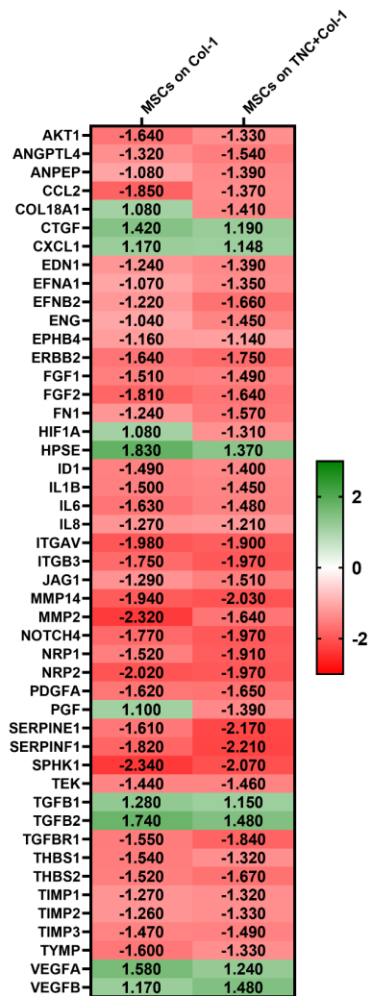
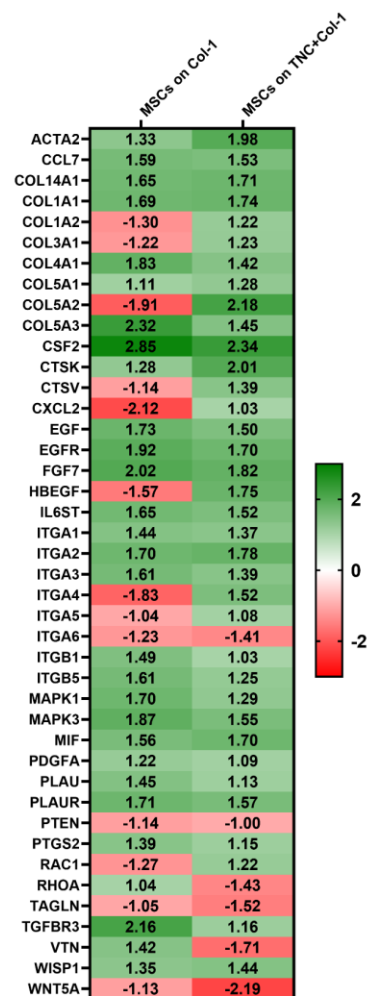


Figure 12: Evaluation and comparison of pro-angiogenic factors for MSC paracrine activity. MSCs were seeded onto either plastic, Col-I, or TNC+Col-I coated plates and placed under H/ND conditions. (A) CM was collected at 96 hours and analyzed using a Human Angiogenesis Array Kit and (B) quantified for relative expression compared to positive control spots (POS). (C) Parallel run treatment plates were harvested at 48 hours for mRNA, processed into cDNA, and quantified using qPCR for expression differences in cytokine targets found in the CM. Gene expression profiles are displayed in terms of fold-regulation. Quantification in B is shown as mean  $\pm$  SD. \* $p < 0.05$ , \*\* $p < 0.01$ , \*\*\* $p < 0.001$ .

**A Human Angiogenesis Profiler Array  
qPCR Analysis of MSCs in H/ND at 48hr  
(Norm. to GAPDH and Plastic)**



**B Human Wound Healing Profiler Array  
qPCR Analysis of MSCs in H/ND at 48hr  
(Norm. to GAPDH and Plastic)**



**C**

Gene	MSCs on Col-1		MSCs on TNC+Col-1	
	Fold Regulation	p-Value	Fold Regulation	p-Value
COL5A2	-1.91	0.357	2.18	0.027
COL5A3	2.32	0.503	1.45	0.650
CSF2	2.85	0.499	2.34	0.482
CTSK	1.28	0.425	2.01	0.460
CXCL2	-2.12	0.857	1.03	0.656
FGF7	2.02	0.431	1.82	0.694
MMP14	-1.94	0.814	-2.03	0.453
MMP2	-2.32	0.157	-1.64	0.351
NRP2	-2.02	0.388	-1.97	0.341
SERPINE1	-1.61	0.969	-2.17	0.534
SERPINF1	-1.82	0.595	-2.21	0.238
SPHK1	-2.34	0.422	-2.07	0.159
TGFBR3	2.16	0.105	1.16	0.275
WNT5A	-1.13	0.527	-2.19	0.882

**Figure 13: RT-PCR analysis of MSCs on different seeding conditions during H/ND. MSCs were seeded onto either plastic, Col-I, or TNC+Col-I coated plates and placed under H/ND growth conditions for 48 hours. mRNA was isolated and reverse transcribed to generate cDNA of each sample and run on a (A) human angiogenesis profiler array and a (B) human wound healing profiler array. Gene expression profiles are displayed in terms of fold-regulation. (C) Genes expression values larger than 2 or smaller than -2 are highlighted in the table.**

#### **5.4.4 Coacervate With TNC And MSC Improves Wound Healing *In Vivo* In Delayed Wound Healing Mouse Model.**

We next inquired whether our findings *in vitro* would improve the healing outcomes in our CXCR3 <sup>-/-</sup> mouse model of delayed wound healing [148, 201]. Wounds were made in the CXCR3 <sup>-/-</sup> mice, and one of five treatment groups (CO only, CO+TNC, CO+MSC, TNC+MSC, or CO+TNC+MSC) were administered 72 hours after the initial wounding. The wounds were harvested on D30 during the middle of the delayed tissue replacement phase of wound healing [52]. At this point in the wound healing process, histological stains using H&E and Masons Trichrome reveal complete migration and stratification of the epidermis, along with a fully intact basement membrane indicating complete wound healing of the epidermal layer with a wound score of a 4 (Figure 4 A, B, E). However, when looking at epidermal thickness as a restorative measure, treatment with CO+TNC+MSC was significantly thinner than CO Only, CO + TNC, and CO + MSCs. Interestingly, the treatment group with CO + MSCs trended much higher than all the rest in terms of epidermal thickness.

Transitioning to the dermal layer, we first noticed the higher cellularity in the mice treated with CO Only and CO + MSCs compared to the other treatments (Figure 14 A, B); this indicates the wound healing sequence being delayed with these treatments and implies a correction of the

defect with the other treatments. We next stained for platelet endothelial cell adhesion molecule (PECAM-1 or CD31) to assess differences in angiogenesis and capillary formation (Figure 14 C, D). We observed a statistically significant higher number of capillaries in mice treated with CO + TNC + MSCs and CO + TNC compared to CO Only control. When examining the Masson's Trichrome staining, the CO + TNC treatment group appeared to have the highest amount of granulation collagen due to the lightness of the blue color (Figure 14 B). The mice treated with CO + TNC + MSCs exhibited the darkest color of collagen, signifying higher collagen turnover from immature Col-III to mature Col-I.

Further quantification of collagen Col-I/Col-III ratio using Picrosirius Red stains (PSR) confirmed this observation, where mice treated with CO + TNC + MSC had a significantly higher Col-I/Col-III ratio compared to CO Only, CO + TNC, and CO + MSC (Figure 15 A, B, D). The CO Only, CO + TNC, and CO + MSC treatment groups had a Col-I/Col-III ratio close to 1, suggesting they were still early in the tissue replacement phase with a lot of granulation tissue. The CO + TNC + MSC mice had a Col-I/Col-III ratio above 1.5 and approaching 2, suggesting active collagen maturation and entry into the resolution phase of wound healing. Normal unwounded skin will have a Col-I/Col-III ratio of 2 or higher.

In addition to collagen content quantification, collagen alignment scoring can also help determine the maturity of collagen within the dermis. Upon healing a wound within the murine model who doesn't have rete ridges, the dermal layer alignment will become more horizontal as the collagen becomes more mature and contracted via the myofibroblasts. We first looked at the overall alignment of the collagen fibrils using the ImageJ color survey tool (Figure 15 C). This allows the PSR stain to be pseudo-colored according to their alignment orientation. From this view, we can analyze the orientation in two ways. The first collagen alignment method was to look at

the total distribution of all collagen fibrils relative to their degree of alignment (Figure 15 E). We see a skewed bimodal distribution in all treatment groups with one peak around the -50 degree orientation mark and the other around the +50 degree orientation mark. The mice treated with the CO + TNC + MSC group (green line) have the tallest peak out of all the treatment groups at the +50 mark, implying it has the most alignment in that location. It is also the highest peak out of all peaks on the graph, signaling it is the most aligned of all treatment groups. The two treatment groups with the lowest collagen alignment score are CO + TNC (orange line) and CO + MSCs (pink line). The second way to measure collagen alignment is through total measured coherency. This measures the overall coherency of the collagen fibrils within each image with a total coherency measure between 0 and 1, where 0 indicates complete isotropy and 1 would indicate complete alignment[210]. Similar to what we saw in the first collagen alignment method, the mice treated with CO + TNC + MSCs have a significantly higher coherency score compared to CO Only, CO + TNC, or CO + MSCs (Figure 15 F). The mice treated with TNC + MSC without coacervate also exhibited good alignment with coherency scores significantly higher than CO Only and CO + TNC treatment groups. For one last measure of collagen maturation in terms of contraction, mice treated with CO + TNC + MSCs and TNC + MSCs presented significantly thinner dermal thickness scores than the other three treatment methods (Figure 14 F). Overall, mice treated with CO + TNC + MSCs had the highest wound score, closely followed by TNC + MSCs without coacervate (Figure 4 E), whereas mice treated with CO Only and Co + MSCs exhibited the least amount of maturation in most metrics. These findings demonstrate that TNC inclusion improves the performance of MSCs in promoting maturation of wounds through the phases of healing.

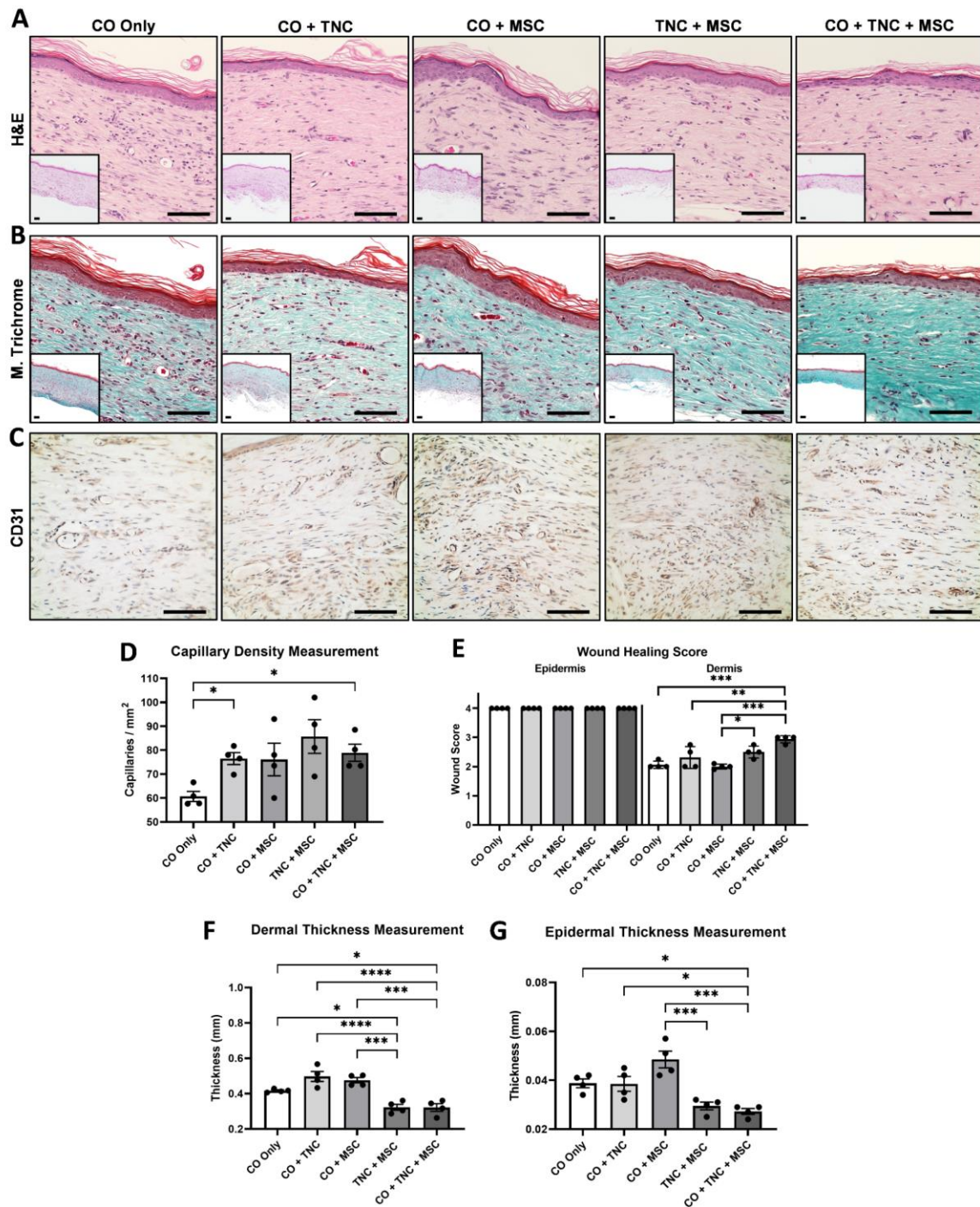


**Figure 14: Assessment of the tissue replacement phase of CXCR3<sup>-/-</sup> mice treated with matricellular protein TNC and MSCs embedded in coacervate. Representative histological sections of Day 30 wounds stained with (A) hematoxylin and eosin (H&E) and (B) Masson's trichrome (MT) at 10x and 40x magnification. (C) Immunohistochemistry of CD31 at 20x magnification to assess capillary density and (D) quantification of**

capillary density (Capillaries / mm<sup>2</sup>) using 5 sample images per treatment group. (E) Quantification of wound healing score and wound thickness measurement for (F) dermal and (G) epidermal skin layers. Quantification in E is shown as mean  $\pm$  SD, whereas D, F, and G are shown as mean  $\pm$  SEM. \*p<0.05, \*\*p<0.01, \*\*\*p<0.001. Scale bar for all images is 100  $\mu$ m. There were four mice per group.

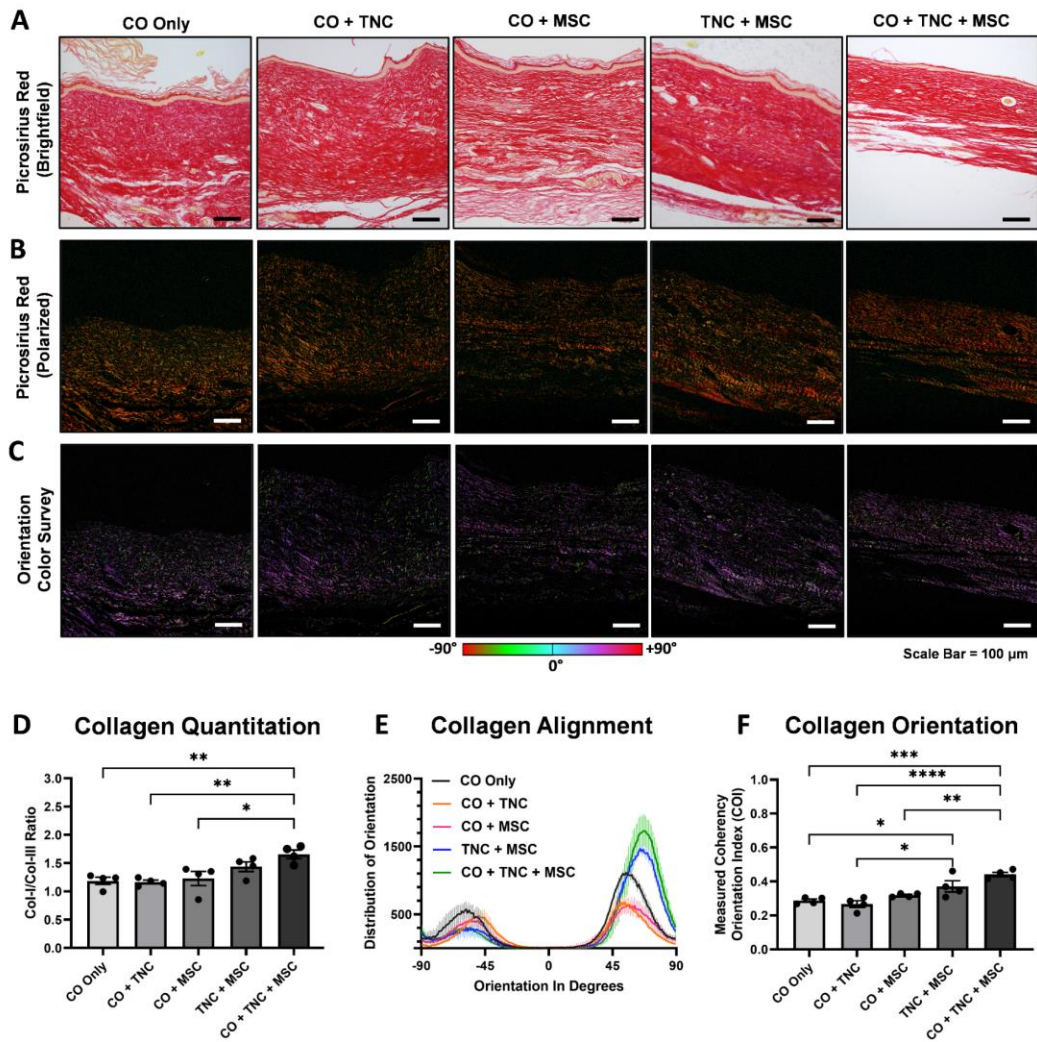


**Figure 15: Assessment of collagen alignment and maturation in CXCR3 <sup>-/-</sup> mice treated with matricellular protein TNC and MSCs embedded in coacervate. (A) Brightfield images of picosirius red (PSR) staining at 20x magnification. (B) Polarized light microscopy of picosirius red-stained sections reveals the birefringence properties of collagen type 1 (Red-Orange) and collagen type III (Green-Yellow). (C) OrientationJ color survey of PSR polarized images pseudo-colored for orientation alignment. (D) Image J Quantification of PSR polarized images to assess collagen maturation as displayed by the Col-I/Col-III ratio shown as mean ± SD (n = 4). (E) Distribution of collagen fibrils relative to their degree of alignment is shown as mean ± SD (n = 4). (F) Quantification of collagen orientation displayed as percent coherency where a score of 1 is total alignment and 0 is complete isotropy; shown as mean ± SD (n = 4). \*p<0.05, \*\*p<0.01, \*\*\*p<0.001. Scale bar for all images is 100 μm. There were four mice per group.**

## 5.5 Discussion

Mesenchymal stem cells remain a promising therapeutic for chronic wounds due to their ability to regulate two of the main obstructions of the wound healing process, inflammation and angiogenesis. However, the harsh environment of the chronic wound bed has limited the sought-after benefits of MSCs due to poor survival resulting in low engraftment rates post implantation [193]. Our previous studies have shown that prolonged signaling of the EGFR from the plasma membrane will promote survival of MSCs [48, 212]. A naturally occurring extracellular matrix protein prevalent during the cutaneous wound healing process, TNC, can signal via its EGF-L repeat domain in this manner and improve MSC survival [48, 195]. Thus, we proposed that coupling the application of TNC with MSCs could enhance the MSC function to counterbalance ischemia by improving angiogenesis.

As ischemia is one of the major deficits that must be overcome to heal chronic wounds, many MSCs preconditioning techniques have been explored in the realms of hypoxia, serum deprivation, nutrient deprivation, or combinations of each. However, this has led to variability in MSC performance outcomes both *in vitro* and *in vivo* depending on the technique and instrumentation used. In our *in vitro* culture system for ischemia, we utilized BioShperix growth incubators set at 1% oxygen in conjunction with unsupplemented basal DMEM to mimic both the low oxygen and nutrient levels of the wound bed prior to new vessel formation. Our results showed high survival rates of MSCs on all treatment culture conditions until day 5, where ischemia/starvation (H/ND)-induced apoptosis was noted. MSCs cultured on TNC+Col-I presented survival rates significantly higher than MSCs cultured on either plastic or Col-I under H/ND conditions. Additionally, the conditioned media from the MSCs on TNC+Col-I had significantly enhanced angiogenic and mitogenic capacity of endothelial cells *in vitro*. When

examining the CM for potential angiogenic paracrine drivers, no substantial differences could be determined among treatment groups. This suggests that either a combination of factors drive the enhanced angiogenic signal, or that elements not queried in this broad candidate approach (e.g. microRNAs in the exosomes) may be the critical signals. Such experiments lie beyond the scope of the present work but form the basis for future investigations.

Analysis of the *in vivo* data showed improved wound healing outcomes for mice treated with CO+TNC+MSC and TNC+MSCs treatment groups; with both groups significantly outscoring and the CO Only, CO+TNC, and CO+MSC treatment groups in dermal wound score, dermal thickness, and epidermal thickness. Surprisingly among the other treatment groups, the CO+MSCs performed the worse in almost every metric. This could have been due to the poor survival of the MSCs and secondary effects of apoptotic cells leading to inflammation, since the TNC survival signals weren't there to protect the MSCs. For the angiogenic component, all 4 treatment groups trended better than CO Only, however once again the CO+TNC+MSC group was consistently better than the other treatment groups.

A limitation of this study is the unknown encapsulation geometry of our TNC-coacervate mixture. Coacervate was originally designed to encapsulate and deliver smaller proteins such as HB-EGF (16kDA)[197] or Sonic Hedgehog (45kDA) [213]; whereas just one of TNC's six arms can be 180-250 kDA in size [121]. We were postulating that some parts of the TNC protein structure would be covered while others would be available to interact with the MSCs. This would be ideal as it would allow for partial protection against degradation of the harsh wound environment while also providing the pro-survival interactions needed with the MSCs. However, after performing our *in vitro* coacervate release study it seems that only 50% of the TNC protein was encapsulated to the point of co-precipitating with the coacervate (Figure 7 B). Additionally,

this encapsulation may have been extremely weak due to almost total release of TNC happening within just 24 hours. When examining the *in vivo* angiogenesis and wound healing results (Figures 14,15), the CO+TNC+MSC treatment group performed the best out of all treatment groups, however, it was always at the same level or just better than the TNC+MSC treatment group which performed the second best overall. Further analysis will be needed to determine if there are significant enhancement of coacervate usage with TNC. One additional area of interest would be whether the coacervate acts as a short-term docking and safe harbor site for growth factors and cytokines released by the adjacent MSCs. This could prolong the paracrine effects of the exogenous MSCs in very severe chronic wound situations.

In conclusion we find that TNC enhances MSC's ability to promote angiogenesis both *in vitro* and *in vivo*, while also improving the overall wound healing phenotype in mice with delayed dermal healing. TNC expression early in wound healing and absence later during the resolution phase offers clues to how it can be used as a jump start treatment for stalled healing. Understanding how it interacts and works with other physiological cellular components in the early stages of wound healing such as MSCs need to be built upon to help create the next generation in personalized wound care. These findings further the concept of utilizing natural occurring ECM elements that can be used in bioactive biomaterials to increase cell therapy applications in regenerative healing [214].

## **6.0 The Matricellular Protein Decorin Delivered Intradermally With Coacervate Improves Wound Resolution In A Mouse Model Of Hypertrophic Scarring.**

This chapter includes material excerpted from the following publications:

Sylakowski K., Hwang P., Justin A., Whaley D., Wang Y., Wells A. The extracellular protein decorin delivered intradermally with coacervate improves wound resolution in a mouse model of hypertrophic scarring. Wound Repair and Regeneration. 2022; ahead of print.

### **6.1 Summary**

Cutaneous wound healing is an intricate orchestration of three overlapping phases of repair that encompass numerous cell types, signaling cascades, and microenvironment modifications to reach a successful resolution. Disruption of any of these steps will create an abnormal healing response resulting in either ulceration or excessive scarring. It has become evident that the extracellular matrix and its associated components are key orchestrators during this process. One of these essential matrix proteins is decorin, a small leucine-rich proteoglycan (SLRP) that acts as a regulator of collagen fibrillogenesis and a non-competitive inhibitor of multiple growth factors signaling cascades. Decorin is a necessary shut-off switch for the pro-reparative mechanism of the tissue replacement phase and limits the occurrence of hypertrophic scarring by preventing excessive repair. we investigated the use of decorin as a therapeutic by administering the matrix protein anchored in a slow release coacervate in a hypertrophic scarring mouse model. Results

show that early wound healing phase measurements exhibit little difference in performance compared to our coacervate-only baseline or HB-EGF treated control mice. However, during the resolution phase of wound healing, the decorin-treatment significantly reduces cutaneous thickness, enhanced collagen alignment, and better overall wound scoring in the mice. Thus, mice treated with decorin display better healing outcomes and could limit the hypertrophic scarring phenotype still present in the coacervate only and HB-EGF controls. These results suggest that decorin may be a promising tool and alternative therapy for patients who suffer from over-exuberant matrix deposition during wound healing.

## **6.2 Introduction**

Cutaneous wound healing is a highly complex and dynamic process that requires a successful transition through three phases of repair to reach a successful resolution. This process relies critically on the timing and balance of key cell types, growth factors, and extracellular matrix (ECM) molecules to maintain proper outcomes. However, patients who have experienced extreme trauma or severe burns can disrupt this complex network of pro-fibrotic and anti-fibrotic interactions and signals, leading to an excessive deposition of collagen and the formation of hypertrophic scars (HTS) [215]. Patients with severe HTS are subject to high psychological and physical impairment levels, as these wounds are often found in areas of high skin tension and can be very resistant to treatment or therapy [216].

One of the critical elements of HTS is the imbalance of the ECM throughout the wound healing process. Early in the HTS wound healing process, the wound micro-environment is often plagued with chronic inflammation leading to an overabundance of matrix metalloproteinases

(MMPs) and disproportionate breakdown of ECM [146, 149, 215, 217]. This in turn, creates a response for fibroblasts in the next phase of repair to excessively proliferate and produce an overabundance amount of collagen, ultimately leading to HTS [146, 149, 215, 217, 218]. In addition to the changes observed to ECM structural proteins such as collagen in HTS patients, other non-structural ECM proteins called matricellular proteins are also affected. These specialized ECM proteins do not provide structure or scaffolding support for cells; instead, they directly interact with cell signaling through the interaction of growth factors, growth factor receptors, and other ECM proteins within the wound microenvironment, driving a variety of biological signaling cascades. One of these vital matricellular proteins is called decorin, and it acts as a critical stop signal within the resolution phase of wound healing.

Decorin (DCN) is a small leucine-rich proteoglycan roughly ~ 90-140 kDa in size. It consists of a core protein element composed of 10-12 tandem leucine-rich repeats (LRR) attached to a single N-terminal glycosaminoglycan chain (GAG) [219, 220]. Its name is derived by its ability to bind or "decorate" collagen fibrils and is found throughout the reticular dermis of the skin [220]. DCN's ability to interact with collagen allows for it to be a key component of collagen fibrillogenesis during wound healing as it helps to regulate collagen fibril diameter, organization, and spacing between collagen strands [171, 172]. Additionally, it can regulate other signaling cascades within the wound microenvironment, often acting as a non-competitive antagonist for a host of growth factors and growth factor receptors [56, 185, 186, 221]. One critical signaling receptor DCN will bind to during the resolution phase is the vascular endothelial growth factor (VEGF) receptor 2 of endothelial cells, inducing an autophagic response and suppressing angiogenesis during this repair phase [57, 222]. DCN has also been found to regulate transforming growth factor – beta-1 (TGF- $\beta_1$ ), a significant influencer of wound contraction, by either binding

and neutralizing the growth factor directly or by downregulating its production from hypertrophic scar fibroblasts [155, 166, 186].

CXCR3 is a seven transmembrane G-protein coupled receptor that is the sole receptor for CXCL4, CXCL9, CXCL10 and CXCL11, the latter two are expressed during wound healing at the time of the transition from tissue replacement to wound resolution. Our earlier work found that mice lacking the CXCR3 receptor displayed a delayed but prolonged dermal wound healing phenotype that leads to hypertrophic scarring [201, 223]. Correction of the scarring defect using cellular transplants reverses the matrix progression back towards near regenerative healing [49, 52, 89]. Thus, we asked if directly pharmacologically altering the matrix can achieve better healing as it would be easier than cellular transplants. DCN plays a crucial role in proper wound resolution, and since its protein levels are found to be decreased roughly 75% in HTS compared to regular wound healing patients [143, 146], we thought it makes a great matricellular candidate to test this premise. However, delivery of exogenous growth factors or other protein-based therapies is often limited in their efficacy due to extensive degradation once administered *in-vivo* into the harsh wound microenvironment [224]. To overcome this challenge, we have encapsulated DCN in a heparin-mediated coacervate system. This system is an injectable *in-vivo* delivery vehicle that uses a positively charged synthetic biodegradable poly (ethylene arginyl aspartate diglyceride) (PEAD) and a negatively charged heparin to form a 3-dimensional coacervate [196-198, 206]. This delivery approach allows for the protection of the DCN while also allowing for its controlled release over several days (Figure 1). As a control modulator, we used heparin-binding EGF-like growth factor (HB-EGF) as it has been shown to accelerate delayed healing in a mouse model of diabetic wounds [197]. We hypothesized that delivery of DCN would result in a reduced scarring phenotype and an overall better healing outcome in our hypertrophic scarring mouse model.

## 6.3 Materials And Methods

### 6.3.1 Animal Model

C57BL/6J CXCR3<sup>-/-</sup> mice were generated as previously described[205] and gifted to the lab by Bao Lui and William Hancock. The C57BL/6J CXCR3<sup>-/-</sup> mice were then bred to FVB strain mice for at least 20 generations to yield germline transmission of the targeted allele and create CXCR3 devoid mice on the FVB background. For this study, CXCR3<sup>-/-</sup> female mice were bred with CXCR3<sup>-/-</sup> males and all offspring were screened for genotype through PCR before use. All studies on these animals were performed in compliance with and after approval by the Institutional Animal Care and Use Committees of the Veterans Administration and University of Pittsburgh. These animals were housed in the Veteran's Affairs Medical Center (Pittsburgh, PA) facility accredited by the Association for the Assessment and Accreditation of Laboratory Animal Care. Serological analyses did not detect blood-borne pathogens or evidence of infection. Mice were housed in individual cages after wounding, as allowed by the IACUC to limit fighting and further scarring and maintained under a 12-hour light/dark cycle in accordance with the guidelines approved by the Institutional Animal Care and Use Committee.

### 6.3.2 Mouse Wounding

Male and female mice (6 to 8 months of age and weighing approximately 25 g) were anesthetized with an intraperitoneal injection containing ketamine (75 mg/kg) and xylazine (5 mg/kg). The backs were cleaned, shaved, and sterilized with betadine solution. Full-thickness wounds were performed using an 8mm diameter punch biopsy through the epidermal and dermal

layers along one side of the dorsal midline of the mouse. The contralateral uninjured skin served as unwounded control skin.

### **6.3.3 Coacervate Preparation**

PEAD was synthesized as previously described[206]. Stock solutions of PEAD and heparin (10mg/mL) were prepared in 0.9% saline solution and passed through a 0.22  $\mu\text{m}$  sterile syringe filter. Recombinant human HB-EGF (Cat. No. 50-398-861, PeproTech) and DCN (Cat. No. 143DE100 R&D Systems) were each reconstituted to 300  $\mu\text{g}/\text{mL}$  and mixed with heparin stock solution at their respective predetermined working doses of 1.45  $\mu\text{g}$  for HB-EGF[197] and 10  $\mu\text{g}$  for DCN[225]. The heparin/HB-EGF and heparin/decorin solutions were then each mixed with PEAD stock solutions to form protein-encapsulated coacervates at a final ratio of 1:100:500 (protein:heparin:PEAD) mass ratio. Coacervation proceeded rapidly with the formation of a turbid soliton once all components were mixed.

### **6.3.4 Coacervate Mouse Injections**

Intradermal Injections were administered once on day 7 for mice being harvested on day 14. Whereas mice that were harvested at day 30 or 90 received two rounds of injections, at day 7 and day 14. For each treatment, a mouse received a total of 200  $\mu\text{L}$  of either treatment coacervate or control coacervate through a series of 4 injections of 50  $\mu\text{L}$  around the wound bed to avoid tissue trauma (Figure 16A). Mice treated with HB-EGF coacervate would get a dose of 200  $\mu\text{L}$  containing a total of 1.45  $\mu\text{g}$  HB-EGF. While mice receiving DCN would get a dose of 200  $\mu\text{L}$  containing a total of 10  $\mu\text{g}$  DCN.

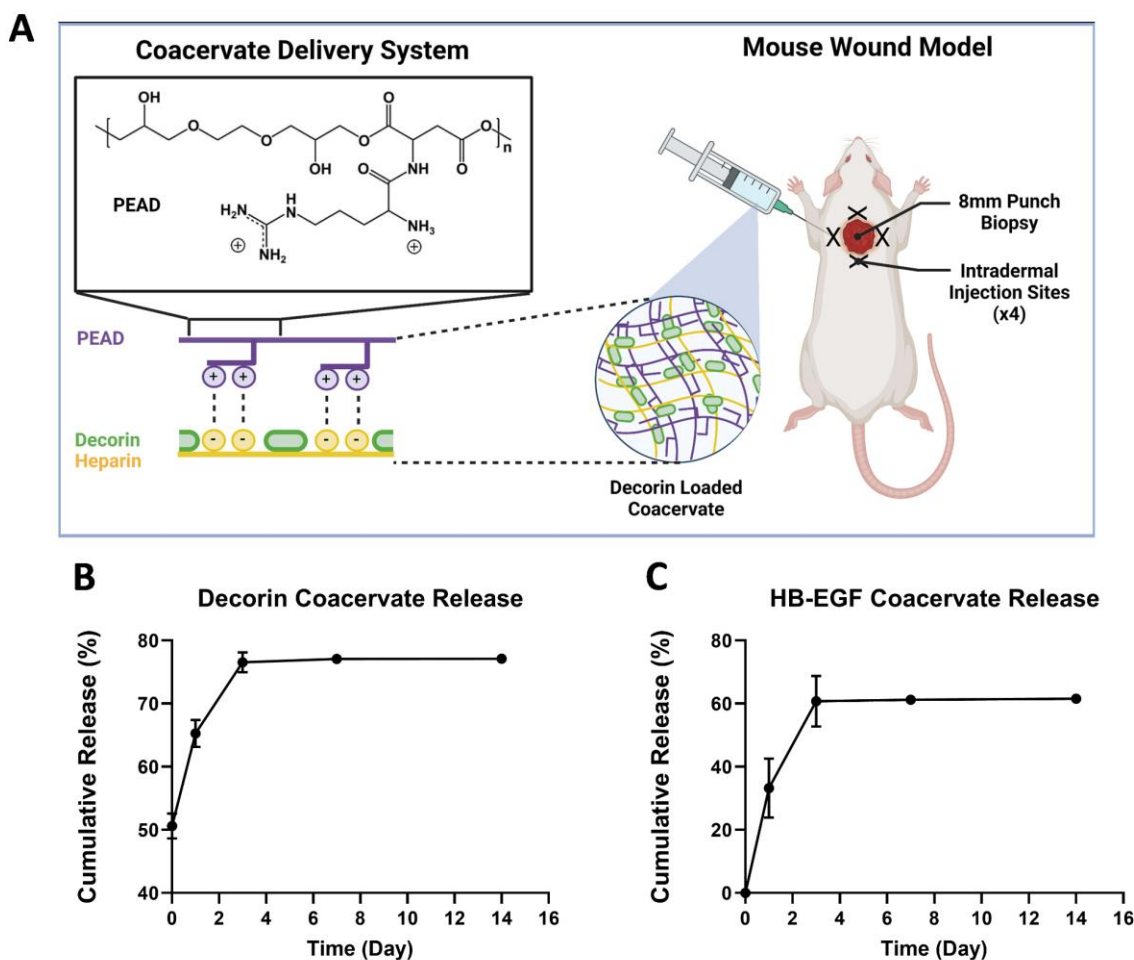


**Figure 16: Coacervate delivery study of matricellular proteins on hypertrophic mouse scarring model.**

(A) Overview schematic demonstrating the preparation of the coacervate-decorin delivery to an in-vivo mouse skin wound model. ELISA exhibited % cumulative release of (B) decorin and (C) HB-EGF from coacervate over 14 days.

### 6.3.5 Coacervate Release

Coacervate was prepared as stated above to create three independent samples for both HB-EGF and DCN. Samples were incubated at 37°C for 14 days, and the supernatant was harvested on days 0, 1, 3, 7, and 14 through pelleting the coacervates by centrifugation (12,100g for 10 min).

Supernatants were analyzed using pre-coated enzyme-linked immunosorbent assay (ELISA) kits (Cat. No. EHHBEGF and Cat. No. EHDCN, Thermo Fisher Scientific), according to the manufacturer's specifications. The release profiles were as previously published for HB-EGF (Figure 1C)[196], and slightly faster for DCN as it befits its larger size and lack of proteoglycan binding domain (Figure 16 B).

### **6.3.6 Histological Analyses**

Wound bed biopsies were collected after euthanasia at days 14, 30, and 90 using a 12mm punch biopsy and were immediately fixed in 10% buffered formalin. Samples were then sent to the University of Pittsburgh Neuropathology Histology Core for paraffin embedding (FFPE), sectioning into slides (6  $\mu$ m), and sample staining for Hematoxylin and Eosin (H&E) and Masson's Trichrome staining (MT). Blank slides were also made for downstream Picrosirius Red (PSR) staining as directed by the manufacturer's protocol (Cat. No. 150681, Abcam) and follow up immunohistochemistry and immunofluorescent stains.

*Wound healing score assessment* – Histopathological examination of mouse tissues was performed in a double-blind approach among three investigators, and their scores averaged. Qualitative assessments were based on epidermal and dermal maturation as outlined in Figure S1 and previously established protocols[148, 201, 207]. In short, the samples were scored on a scale of 0 to 4 for both epidermal and dermal layers of tissue. For epidermal maturation scoring: 0 = no epidermal migration, 1 = partial epidermal migration, 2 = complete epidermal migration, 3 = Partial keratinization and an intact basement membrane, 4 = complete keratinization and normal epidermis. For dermal maturation scoring: 0 = no healing, 1 = inflammatory infiltration, 2 =

granulation tissue present – fibroplasias and angiogenesis, 3 = collagen deposition replacing granulation tissue > 50%, 4 = complete replacement of granulation tissue and complete healing.

*Skin thickness measurements* – H&E and MT sample images were analyzed using ImageJ line measurement tool to measure the thickness of the epidermal layer and dermal layer for each mouse specimen. The epidermal layers were measured from the stratum basale to the stratum granulosum (excluding the stratum corneum); and the dermal layer was measured from the top of the papillary layers to the bottom of the reticular layer. A total of 6 measurements per biological sample were scored for each layer.

*Collagen quantification* – Polarized PSR images were quantified using ImageJ version 1.53K (NIH; <https://imagej.nih.gov/ij>). Each image was split into red, green, and blue channels, from which the red and green channels were selected. The isolated red and green channels then underwent thresholding and follow-up measurements to determine the total staining area for each collagen type. Picrosirius Red birefringence under polarized light reveals tightly packed thick and long fibrils of type 1 collagen as either bright red-orange intense birefringence in tissue and thin short loose fibrils as yellow-green[208]. The overall ratio of type 1 collagen to type III collagen was analyzed by comparing the representative staining results for either collagen type back to the original image for total collagen content.

*Collagen orientation and alignment* – Polarized PSR images were quantified using ImageJ plug-in: OrientationJ version 2.0.5. Visual directional analysis using the color survey tool was performed with the following parameters: Hue is set for orientation, Saturation is set for coherency, and brightness is set to the original image[209]. The OrientationJ distribution tool was used to create the distribution of orientation histograms to determine where patterns of alignment were

within our samples [210]. The OrientationJ Dominant Direction tool was used to determine the quantitative orientation measurement for coherency across the whole image [211].

*Immunohistochemistry staining*– Skin sample tissue sections (6 µm) were rehydrated and placed into citrate acid buffer at 95°C for 10 minutes and allowed to cool to room temperature for 1 hour. Samples were then washed in Phosphate-buffered saline (PBS) and quenched with 3% hydrogen peroxide. Following additional washes in PBS, samples were blocked in 20% goat serum for 1 hour and subsequently incubated with primary antibodies diluted in blocking buffer overnight at 4°C. Primary antibodies were at the following dilutions: CD45 (1:100, Cat. No. ab10558, Abcam), Col-IV (1:500, Cat. No. ab236640, Abcam). After primary antibody incubation, samples were washed in PBS and incubated in goat anti-rabbit HRP secondary antibody (1:2000, Cat. No. ab205718, Abcam) for 1 hour at room temperature. After final antibody incubations, samples were washed in PBS and then treated with ABC reagent (Cat. No. PK-6100, Vector Laboratories) for 30 minutes. Rewashed with PBS and developed with DAB reagent kit 27 (Cat. No. SK-4100, Vector laboratories), counterstained with H&E, clarified (Richard Alan Scientific), and dehydrated in ethanol and xylene. Samples were mounted (Cat. No. SP15-500, Fisher Scientific) and imaged using an Olympus Provis microscope. Image analysis was performed using Image J Colour Deconvolution 2 plug-in to acquire DAB positive staining area. The total DAB positive area was compared back to the total area of the original image to get a final percentage.

*Immunofluorescence staining* – Skin sample tissue sections (6 µm) were rehydrated and placed into citrate acid buffer at 95°C for 10 minutes and allowed to cool to room temperature for 1 hour. Samples were then washed in Phosphate-buffered saline (PBS) and quenched with 3% hydrogen peroxide. Following additional washes in PBS, samples were blocked in 20% goat serum for 1 hour and subsequently incubated with primary antibodies diluted in blocking buffer overnight

at 4°C. Primary antibodies were at the following dilutions: CD31 (1:50, Cat. No. ab28364, Abcam), Involucrin (1:500, Cat. No. 924401, Biolegend). After primary antibody incubation, samples were washed in PBS and incubated in goat anti-rabbit 488 secondary antibody (1:200, Cat. No. ab150077, Abcam) for 1 hour at room temperature in the dark. Samples were washed in PBS and mounted in Prolong Gold Antifade Mountant with DAPI (Cat. No. P36931, Invitrogen). Fluorescent images were obtained using an Olympus Provis microscope.

### **6.3.7 Statistical Analysis:**

Results for wound healing score assessment and PSR staining assessment are expressed as mean  $\pm$  SD with at least a minimum of four mice per treatment group. Histological quantifications for skin layer thickness and immunohistological stains (CD31, CD45, Col-IV) were performed on five microscopic fields of each specimen and reported as mean  $\pm$  SEM. Statistical differences between groups were determined by one-way ANOVA, followed by post-hoc Tukey HSD analysis using GraphPad Prism 9 software (GraphPad Software, San Diego, CA). Significance was claimed for  $P < 0.05$ .

## **6.4 Results**

### **6.4.1 Growth Factor Therapy Augments Initial Phases Of Healing**

Wounds made in the CXCR3<sup>-/-</sup> mice were treated 7 days after initial wounding using DCN or HB-EGF encapsulated in coacervate. These mice were then analyzed on day 14, during the later

stages of the inflammation phase of wound healing[26]. We observed mice treated with CO + HB-EGF to have increased epidermal closure compared to CO + DCN or CO Only treated mice (Figure 17 A-C). CO + HB-EGF treated mice exhibited complete epithelial cell migration in three of four mice, allowing for the early elimination of the eschar. We used an additional marker for determining epidermal maturation by examining a marker for keratinocyte cohesion, involucrin. In an early, less mature epidermis, the involucrin protein is localized in the cytoplasm of keratinocytes as exhibited in CO Only, and CO + DCN treated mice (Figure 17 D). However, in a more mature epidermis, keratinocytes will have secreted the involucrin outside the cell to help form a protective boundary and allow the complete formation of the keratinized stratified epithelium as exhibited by the CO + HB-EGF mice (Figure 17 D)[226]. These findings have resulted in CO + HB-EGF treated mice having significantly faster epidermal wound healing than CO + DCN treated mice (Figure 17 E).

Upon examining the dermal layer of tissue, histological stains H&E and Masons Trichrome revealed a high amount of cell infiltrate within each treatment group (Figure 17 A, B). We stained for leucocyte common antigen (CD45) to assess differences in immune cell infiltrate (Figure 17 G). However, no significant differences were found among treatment groups after quantification (Figure 17 H). We also measured the thickness of the dermis (Figure 17 F) and found no significance either. These findings showed no significant difference between treatment groups regarding the overall dermal wound healing score (Figure 2E). These findings suggest that the epidermal closure can be accelerated by upregulating the growth factor signaling early in wound healing. However, the dermal healing proceeds while introducing DCN, a healing 'stop' signaling, does not affect the inflammatory phases of wound healing.

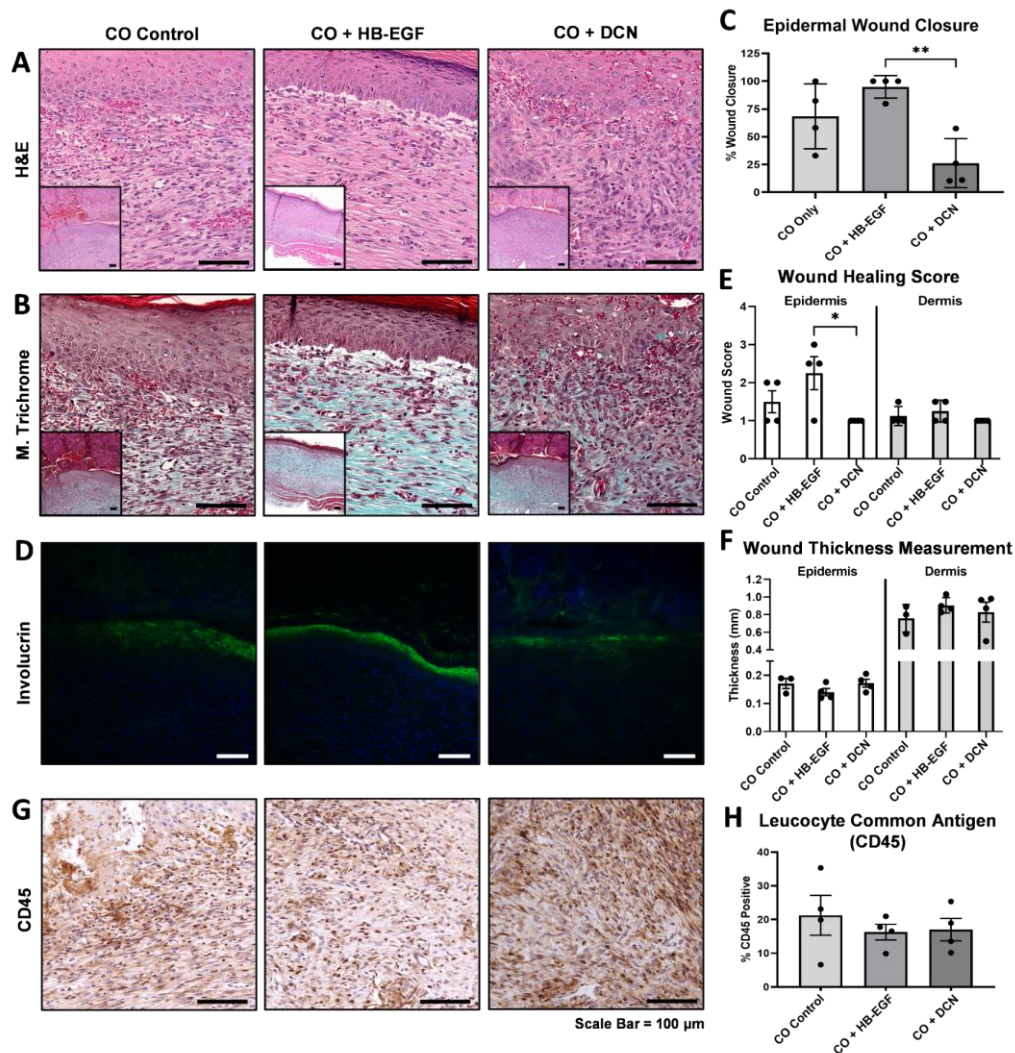


**Figure 17: Early wound healing phase assessment of CXCR3  $-/-$  mice treated with matricellular proteins embedded in coacervate. Representative histological sections of wounds stained with (A) hematoxylin and eosin (H&E) and (B) Masson's trichrome (MT) at 10x and 40x magnification. (C) Quantification of % wound closure obtained from ImageJ distance analysis on H&E and MT image sets between the leading edge of the epidermal tongues on each side of the eschar. (D) Immunofluorescent stain of Involucrin at 10x magnification for epidermal maturation evaluation. Quantification of (E) wound healing score and (F) wound thickness measurement for epidermal and dermal skin layers. (G) Immunohistochemistry of CD45 at 40x magnification for (H) inflammatory infiltrate quantification. Quantification in C and E are shown as mean  $\pm$  SD (n=4), whereas F and H are shown as mean  $\pm$  SEM (n=4). \* $p$ <0.05, \*\* $p$ <0.01, \*\*\* $p$ <0.001. Scale bar for all images is 100  $\mu$ m.**

#### **6.4.2 Modifying The Matrix Increased Vascularization During Tissue Replacement.**

Continuing onto our findings of delayed dermal maturation of CXCR  $-/-$  mice, we observed whether any coacervate treatment group helped to improve outcomes during the tissue replacement phase of repair by examining outcomes at 30 days. At this point in the wound healing process, histological stains using H&E and Masons Trichrome reveal complete migration and stratification of the epidermal layer, including eliminating the eschar in all three treatment groups (Figure 18 A, B). Additional staining with involucrin shows a complete protective barrier signifying the completion of the stratified corneum in the epidermis in all three treatment groups (Figure 18 F). The final stain of Col-IV revealing the formation of an intact basement membrane fully separating the epidermis from the dermis (Figure 18 E), informs that the epidermal layer has reached a total wound healing score of 4 in all three treatment groups (Figure 18 C).

Further histological examination of the dermal tissue layer did not reveal a significant difference, with all treatment groups averaging a wound healing score of 3 and the exact thickness measurement of roughly 0.50mm (Figure 18 C, D). In the Masson's Trichrome staining, the CO Only mice may have appeared to have slightly less collagen than the other two treatment groups (Figure 18 B). However, further quantification of collagen Col-I/Col-III ratio and alignment using Picrosirius Red stains revealed no significant differences (Figure 19 A-D). Histological examination also revealed an overall decrease in cellularity compared to D14 samples (Figure 18 A, B). We assessed the presence of immune cell infiltrate with CD45 but did not see a significant difference among treatment groups (Figure 19 F, G). However, one surprising discovery was the significant increase in capillary formation of CO + DCN treated mice compared to CO Only treated mice confirmed through CD31 and Col-IV staining (Figure 18 G, H; 19 E). However, even with increased vascularity, this did not change the overall wound scoring during this phase of repair.

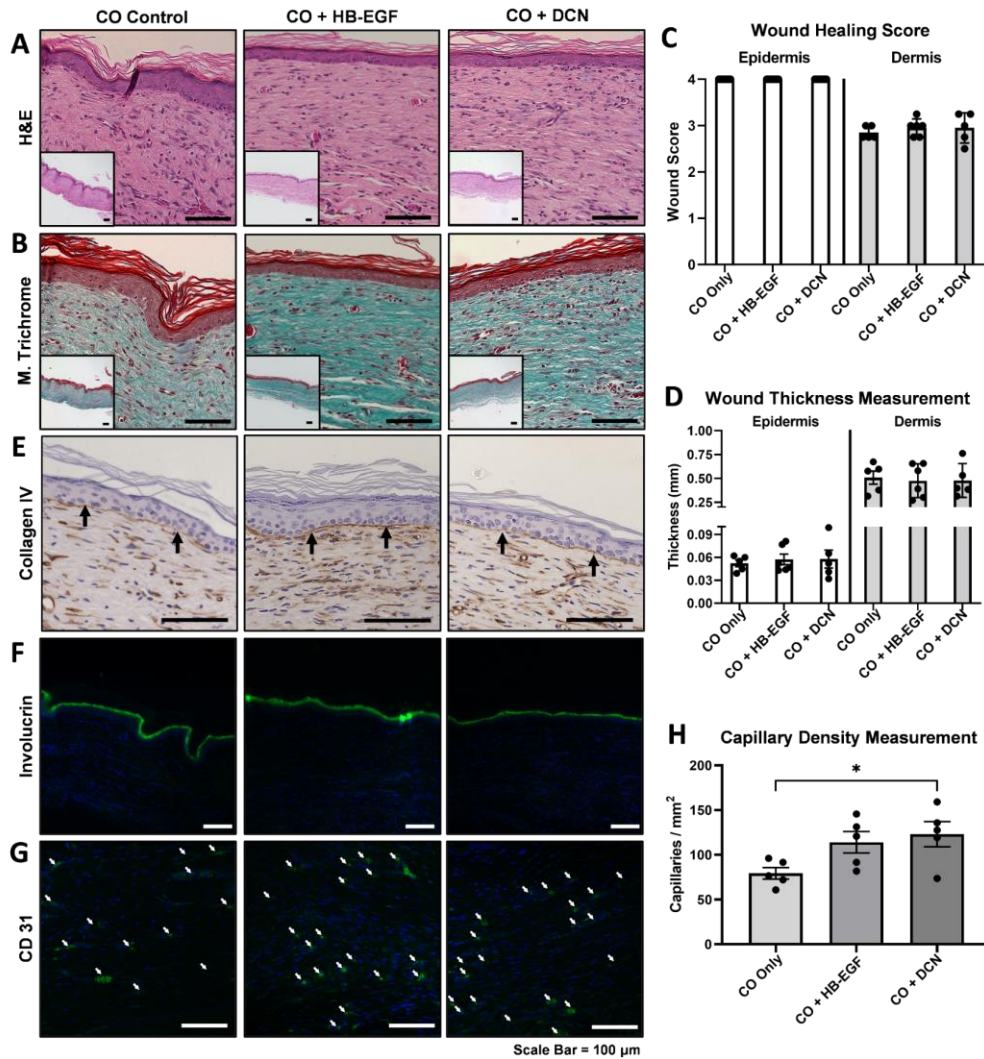


**Figure 18: Assessment of the tissue replacement phase of CXCR3 <sup>-/-</sup> mice treated with matricellular proteins embedded in coacervate. Representative histological sections of wounds stained with (A) hematoxylin and eosin (H&E) and (B) Masson's trichrome (MT) at 10x and 40x magnification. Quantification of (C) wound healing score and (D) wound thickness measurement for epidermal and dermal skin layers. (E) Immunohistochemistry of Collagen IV at 60x magnification to assess the formation of the basement membrane. (F) Immunofluorescent stain of Involutrin at 10x magnification for epidermal maturation evaluation. (G) Immunofluorescent stain of CD31 at 40x magnification with vasculature highlighted by white arrows. (H) Quantification of capillary density (Capillaries / mm<sup>2</sup>). Quantification in C is shown as mean ± SD (n ≥ 5), whereas D and H are shown as mean ± SEM (n ≥ 5). \*p<0.05, \*\*p<0.01, \*\*\*p<0.001. Scale bar for all images is 100 μm.**

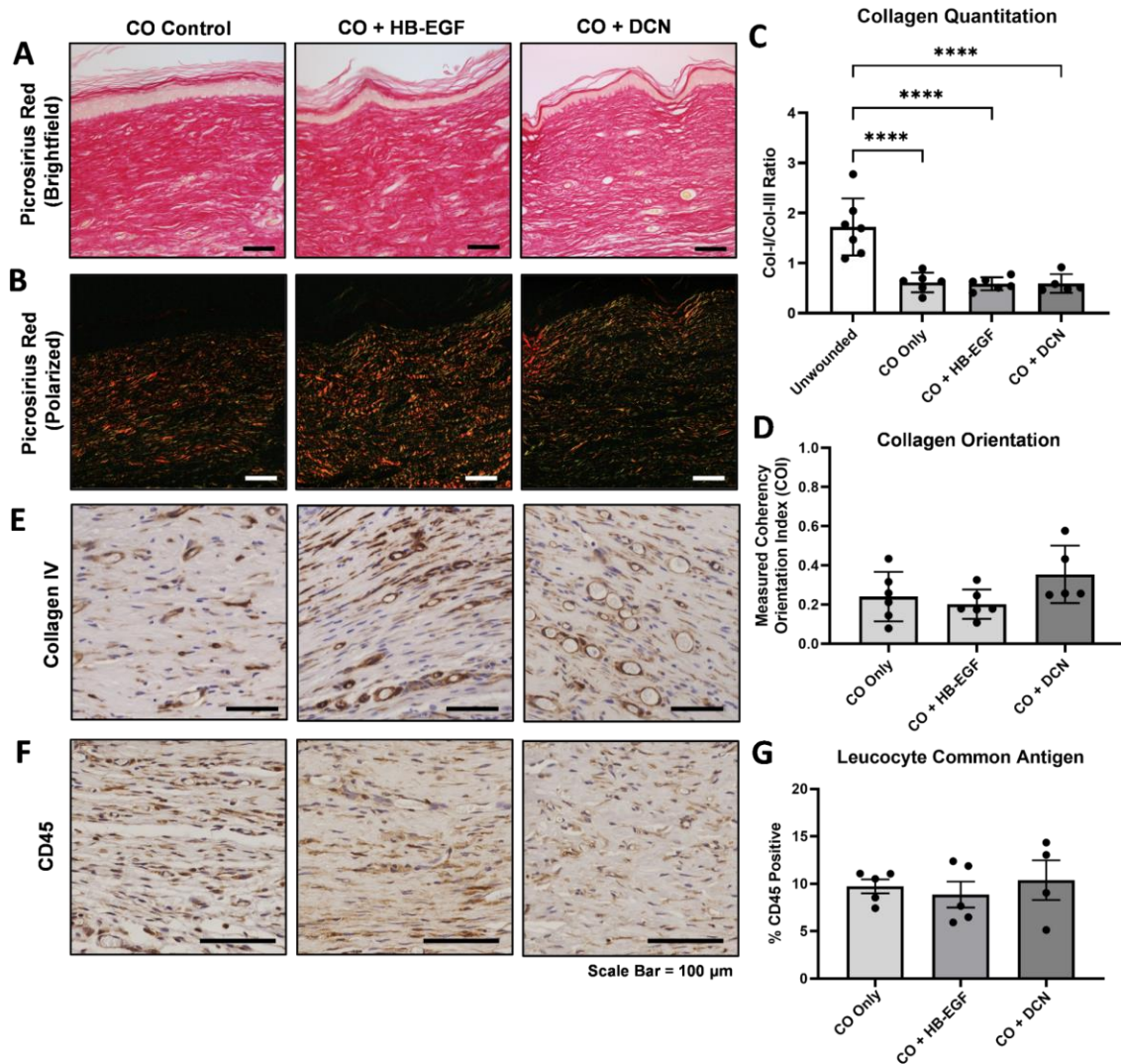


Figure 19: Additional staining to assess treatment groups on tissue replacement phase during wound healing. (A) Brightfield images of picosirius red (PSR) staining at 20x magnification. (B) Polarized light microscopy of picosirius red-stained sections reveals the birefringence properties of collagen type 1 (Red-Orange) and collagen type III (Green-Yellow). (C) Image J Quantification of PSR polarized images to assess collagen content displayed by the Col-I/Col-III ratio shown as mean  $\pm$  SD ( $n \geq 5$ ). (D) Quantification of collagen orientation displayed as percent coherency where a score of 1 is total alignment and 0 is complete isotropy; shown as mean  $\pm$  SD ( $n \geq 5$ ). (E) Immunohistochemistry of Collagen IV at 40x magnification as a supplemental assessment for vasculature. (F) Immunohistochemistry of CD45 at 60x magnification for (G) inflammatory infiltrate quantification (mean  $\pm$  SEM,  $n=4$ ). \* $p < 0.05$ , \*\* $p < 0.01$ , \*\*\* $p < 0.001$ . Scale bar for all images is 100  $\mu\text{m}$ .

### **6.4.3 Coacervate With Decorin Improves Wound Healing Outcomes In The Resolution Phase**

CXCR3 knockout mice exhibit hypertrophic scarring by day 90 after the initial wound [223]; this was predicted to be the time point during wound resolution that 'stop' signals would exert their most significant effects. To this point, we observed significantly improved wound healing scores in mice treated with CO + DCN as compared to CO Only mice (Figure 20). CO + DCN treated mice exhibited less overall cellularity within the dermal layer of tissue in addition to more organized collagen fibrils. Additionally, CO + DCN treated mice presented a significantly thinner epidermal and dermal wound thickness compared to CO-Only mice as these resolved back towards unwounded thicknesses (Figure 20D). CO + HB-EGF also exhibited a significantly higher dermal wound score over CO Only mice but did not significantly change the overall thickness measurement for either the epidermal or dermal layers, suggesting that this treatment did not drive resolution.

We further evaluated the collagen content and alignment of Picrosirius Red (PSR) staining (Figure 20E). Using polarized light microscopy on PSR stained samples, the natural birefringence of collagen fibers allows for the evaluation of collagen organization and separation into either collagen type I displaying a red-orange color or collagen type III with a green-yellow color (Figure 20F)[208]. Upon quantifying collagen content, we observed that the mice treated with CO + DCN had a significantly higher ratio of Col-I/Col-III compared to that of CO Only treated mice, returning the collagen content ratio to that observed in unwounded skin samples (Figure 20G). Conversely, both CO Only and HB-EGF treated mice had significantly lower ratios of Col-I/Col-III, suggesting these mouse populations are still in the process of turning over the remaining granulation tissue from the tissue replacement phase.

We next assessed the orientation of the collagen in our PSR stains. Utilizing the ImageJ plug-in OrientationJ, we were able to measure the overall profile alignment of collagen for an entire specimen as well as the overall coherency. First, we looked at the overall alignment of the collagen fibrils using the color survey analysis tool, allowing us to pseudo color our PSR images to hues that represent certain degrees of alignment (Figure 20H). This was further quantified in figure 20I, to show the total distribution of all collagen fibrils relative to their degree of alignment. Interestingly, all treatment groups displayed a skewed bimodal distribution with one smaller peak around the -50 degree orientation mark and one larger peak around the +50 degree orientation mark. This bimodal skew is attributed to the loss of rete ridges in the papillary dermis after a full-thickness wound. CO + DCN treated mice exhibited the highest collagen alignment around the +50 degree orientation mark compared to the other two treatments groups. The second measure we investigated was the overall coherency of the collagen fibrils within each image. Coherency measure between 0 and 1, where 0 indicates complete isotropy and 1 would indicate complete alignment[210]. Similar to what we saw in the collagen alignment, CO + DCN treated mice exhibited the highest coherency rate compared to the two other groups while significantly higher than CO Only treated mice (Figure 20J). Our results show that CO + DCN mice are further developed and more mature in their collagen content and alignment.

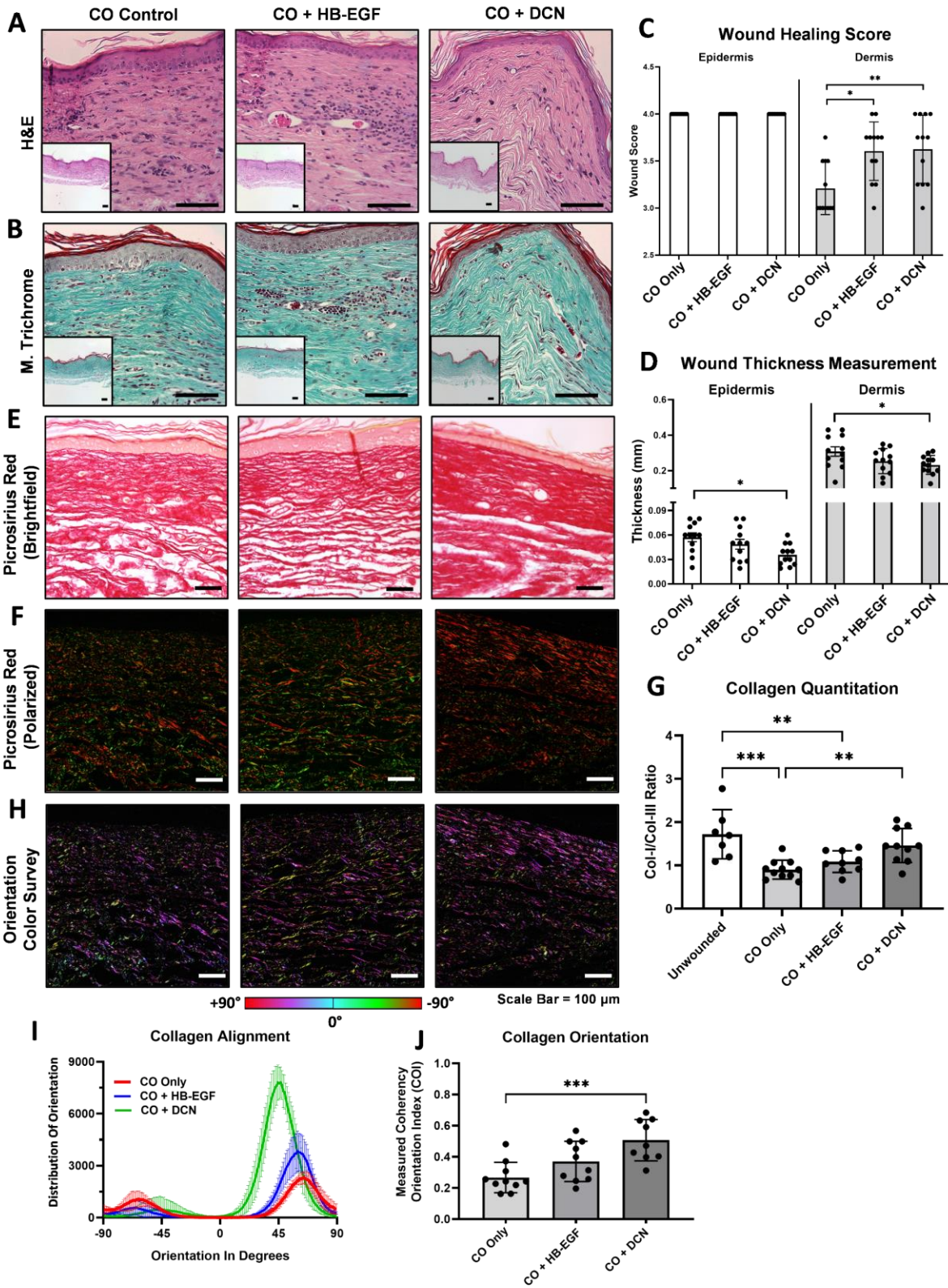


**Figure 20: Assessment of the resolution phase of CXCR3  $-/-$  mice treated with matricellular proteins embedded in coacervate. Representative histological sections of wounds stained with (A) hematoxylin and eosin (H&E) and (B) Masson's trichrome (MT) at 10x and 40x magnification. Quantification of (C) wound healing score and (D) wound thickness measurement for epidermal and dermal skin layers. Quantification in C is shown as mean  $\pm$  SD (n=12), D is shown as mean  $\pm$  SEM (n= 12). (E) Brightfield images of picrosirius red (PSR) staining at 20x magnification. (F) Polarized light microscopy of picrosirius red-stained sections revealing the birefringence properties of collagen type I (Red-Orange) and collagen type III (Green-Yellow). (G) Image J Quantification of PSR polarized images to assess collagen maturation as displayed by the Col-I/Col-III ratio shown as mean  $\pm$  SD (n  $\geq$  7). (H) OrientationJ color survey of PSR polarized images pseudo-colored for orientation alignment. (I) Distribution of collagen fibrils relative to their degree of alignment shown as mean  $\pm$  SD (n = 5). (J) Quantification of collagen orientation displayed as percent coherency where a score of 1 is total alignment and 0 is complete isotropy; shown as mean  $\pm$  SD (n = 10). \*p<0.05, \*\*p<0.01, \*\*\*p<0.001. Scale bar for all images is 100  $\mu$ m.**

## 6.5 Discussion

Cutaneous wound healing is a complex process that leads to either ulceration or excessive scarring when elements go awry. Unfortunately for those who suffer from the latter, most of the focus within the wound healing arena is concentrated around chronic wounds. This has left a large gap in available treatment options for patients who suffer from conditions such as HTS; especially for treatment options focused on early clinical interventions instead of post-scarring treatment methodologies. These circumstances are often validated as it is never certain when a patient will contract a HTS post-trauma or injury. However, the current numbers justify an investigation into preventative therapies for high conversion patients such as those who suffer from severe burns as they are 70-90% likely to contract HTS depending on severity and depth of the burn [143, 146].

Previous studies trying to decipher the underlying mechanisms and critical regulators of fibrosis and HTS have unearthed the potential of matricellular proteins as potent therapies [168, 220, 222, 227].

The main objective of this study was to determine whether scarring could be prevented by modulating the matrix composition by introducing matricellular signals. For this, DCN was chosen as the main leucine-rich proteoglycan in mature skins and a matricellular component whose appearance correlates with the transition to wound resolution [186, 220]. To provide for persistent signaling by limiting diffusion from the wound site and degradation, this was loaded into coacervate controlled release system [198, 206]. There was a concern that introducing this 'stop' signal might prevent the earlier stages of tissue replacement and thus yield a chronic ulcer or thin repair susceptible to dehiscence. The pro-reparative matricellular component HB-EGF served as a control [196, 197]. The result of the introduction of the DCN was evident only at the later stages of healing and resolution in the CXCR3  $-/-$  mouse model. During the late inflammatory stage and tissue replacement, the DCN-treated wounds were similar to those with coacervate alone and only slightly slower in healing than the HB-EGF treatment. However, at 90 days, when hypertrophic scars become evident, the DCN-treated wounds were more regenerative. Thus, this argues for matrix modulation as a new approach to limit scarring during wound healing.

This study is limited to a specific delivery of DCN at the earliest stages of tissue replacement and would need additional series of experiments prior to extrapolation to different uses. We did not pursue wound treatments in the absence of coacervates, as the earlier studies [197, 198, 206] demonstrated a benefit to timed-release of other various signaling factors. Thus, the benefit derived from the DCN-coacervate inoculations may also accrue to the function of the coacervate as a depot for other extracellular factors that are generated during the wound healing

process; in other words, the free coacervate may bind and then slowly release endogenous trophic factors. A DCN only treatment would not fully address this issue as the persistence of the DCN would be shortened.

Additionally, we introduced the DCN before evidence of fibrosis and scarring. This early treatment may not be warranted in all wounds as scarring is not a universal outcome. However, the concept is that it is easier to prevent scarring by maturing the collagen alignments in the first place than trying to revert scarring once fibrillar collagen is deposited [228]. Thus, it was essential to show that early introduction of DCN would not stall the healing process and result in an ulcer. The DCN treatments in the inflammation phase were only marginally slower than that in HB-EGF-treated wounds and equal during the tissue replacement phase; suggesting that DCN treatments could be translated to the clinic in such a manner for patients predisposed to scar. Whether DCN would function at later time points to help reverse early scarring lies beyond this first communication and will be the focus of future studies. Lastly, the murine wound model does not distinguish between hypertrophic scarring and keloid development, and thus we cannot comment on the universality of this approach in both clinical situations.

In conclusion, these findings further the concept that the outcome of wound healing can be directed by modulating the composition of the extracellular matrix components around the wound bed. DCN appears to be a facile 'stop' signal to prevent scarring and a promising candidate as an early clinical treatment option. Future developments will aim to integrate DCN with other extracellular matrix components such as HB-EGF, to generate combinational therapies that prevent stalled wounds and ulcers while also minimizing scar tissue when healed.

## **7.0 Concluding Remarks And General Discussion**

### **7.1 Significance**

As comorbidities such as obesity, diabetes, and cardiovascular disease continue to rise in conjunction with the increasing median age in the United States, the incidence of abnormal healing events will continue to grow to unprecedented new levels. Unfortunately, abnormal wound healing is still an unmet medical challenge due to the complexity and multiplicity of factors driving these adverse effects. This calls for the development of new wound management strategies and tools to orchestrate a better response for treatments of chronic wounds and excessive scarring pathologies. In this dissertation, we assessed the use of two matricellular proteins, Tenascin-C and Decorin, for their ability to modulate the wound healing response. We determined that TNC coupled with MSCs improved their protection against ischemic conditions and enhanced their ability to promote angiogenesis. This also improved wound healing scores within the tissue replacement phase of repair. These findings could indicate a potential therapy to treat patients with chronic wounds that result from ischemia. Additionally, we have found that direct administration of DCN in a model of hypertrophic scarring could alleviate this phenotype and enhance collagen maturation within the resolution phase of repair. These findings further uncover the potential effectiveness and treatment strategies that DCN may be applicable for in clinical contexts of excessive scarring. These findings are significant and exciting because they could help establish a new treatment strategy for chronic wounds and excessive scarring.

There is much to be done as we look at the bigger picture of matricellular proteins as a therapeutic avenue in cutaneous wound healing. The concept of matricellular proteins was first

established by Paul Borstein approximately 27 years ago [124, 126]. Since then, thousands of research studies have investigated matricellular proteins functionally, structure, occurrence in disease states, etc. However, when looking at their use in clinical trials (clinicaltrials.gov), very few studies actively use matricellular proteins as a primary intervention. For instance, Decorin only as 2 clinical trials where its antifibrotic features are assessed in vision repair and disorders. TNC has no clinical trials being used as a primary intervention as it is only used as a readout in serum analysis. Matricellular proteins offer many possibilities through their myriad of binding partners and impacts on both ECM and cellular function within the context of wound healing. Hopefully, the positive impact of matricellular proteins from this dissertation or, over the past 25 plus years of research, can begin to see use significantly in the clinical setting, as new treatments for adverse healing outcomes are as pertinent as ever.

## **7.2 Future Directions: Dual Delivery Of matricellular Proteins Tenascin-C And Decorin**

A future area we are interested in exploring is using matricellular proteins as a combinational strategy for wound healing purposes. Matricellular proteins within the wound healing paradigm are very transient in nature, allowing us in the wound healing community to further explore why that is and use nature as our guiding hand in new therapies. TNC and DCN would make a prime example for this novel approach as they are expressed at different points within the wound healing time course and juxtapose each other in many of their unique functions.

TNC is regarded as an on-switch for tissue repair, significantly increased in expression during the inflammation and early tissue replacement phase of repair. It promotes cell survival, angiogenesis, and positively regulates pro-regenerative growth factors such as TGF- $\beta$ 1, TGF- $\beta$ 2,

VEGF, and PDGF [121, 229-231]. While DCN is considered the off-switch increasing in expression during the resolution phase of repair. It involves refining the wound bed by promoting cell death of fibroblasts and endothelial cells, reducing excessive blood vessels, and negatively regulating the above-mentioned growth factors [185]. TNC is also known to be pro-fibrotic if expressed unusual in the last stage of wound healing where DCN is most notable as an anti-fibrotic agent, and its disappearance in the resolution phase also leads to excessive scarring [185, 232, 233].

When it comes to skin aging, both TNC and DCN levels are decreased over time [137, 234]. Additionally, they also decrease in molecular weight over time as TNC undergoes shortening through cleaving of proteases and DCN's single GAG chain becomes shorter in length [137, 234, 235]. In both instances, TNC and DCN wound healing capabilities decreases, and the skin becomes more fragile and more complex to heal upon insult. Therefore, a tremendous potential avenue for a combinational therapy such as this would be in the healing of elderly patients, as both extracellular proteins, if timed correctly, could prove beneficial at restoring lost functions and accentuating the wound healing process. In this regard, the therapy could be tuned to be more of a dimmer switch rather than a toggle switch.

### **7.3 Future Directions: Enhancing MSC Delivery Strategies For Improved Survival And Efficacy**

This section includes material excerpted from the following publications:

Sylakowski K., Bradshaw A., & Wells A. Mesenchymal stem cell/multipotent stromal cell augmentation of wound healing: lessons from the physiology of matrix and hypoxia support. The American Journal of Pathology. 2020; 190 (7): 1370-1381.

As the technology and expertise of creating bioactive and biomimetic scaffolds improve, the next step within the personalized medicine field will be to prime or manipulate the cell therapy of choice both using the interactions from the scaffold components and external manipulations. Special emphasis on coordinating and timing beneficial effects of cells in 3D matrices will become crucial for creating and utilizing the next generation wound management systems. Most of this dissertation focused on utilizing TNC in a 1-dimensional approach by only assessing the outcomes of MSC-TNC interaction in terms of angiogenic capacity. Now that TNC has been shown to improve both survival and angiogenic capacity of MSCs, the next step would be to add a second layer of complexity through the addition of pretreating the MSCs-TNC component prior to application in-vivo with the purposes of either improving survivability, improving therapeutic paracrine signaling, or both. Below we discuss one of the numerous ways of pretreating MSCs using hypoxia and how this may benefit MSC efficacy through the regulation of macroautophagy. It will be pertinent to understand the connection of these approaches (ECM, Cells, Hypoxia, etc) to make a more personalized and tunable wound treatment system.

### 7.3.1 Hypoxic Preconditioning For MSC Delivery:

Many MSCs reside in areas of low oxygen-tension from 3-9% depending on the tissue source [236, 237]. Hypoxia within the stem cell niche is thought to maintain self-renewal, proliferation, migration, and ultimately appears to augment their therapeutic potential [238-240]. Taking these cues from physiology, has led to experiments in which MSCs are grown at similarly low levels of oxygen to condition or acclimate them prior to wound implantation. However, when oxygen levels reach extreme levels of hypoxia (<1.5% O<sub>2</sub>) such as within a wound bed, MSCs can become over stressed and undergo apoptosis [239]. Further studies have shown that MSCs are innately glycolytic [101], and it is the combination of low oxygen tension and nutrient deprivation within the ischemic wound environment that severely challenges the cells. MSCs exposed to near-anoxic conditions (0.1% O<sub>2</sub>) for as little as three days were shown to rapidly consume all internal glucose energy reserves resulting in poor survival post implantation [241].

With both oxygen and nutrients being vital for MSC survival post implantation, researchers are focused on creating delivery methods that improves at least one of these bioenergetic challenges. The biggest and potentially easiest way to enhance MSC survival is to pre-condition MSCs in hypoxic conditions (1-4% O<sub>2</sub>) for 24 to 48 hours prior to implantation. MSCs pre-exposed to these hypoxic conditions respond by upregulating the hypoxia inducible factor 1 $\alpha$  (HIF-1 $\alpha$ ) [242]. HIF-1 $\alpha$  is a major regulator and response factor to oxygen tension within the cell, in which it will be post-translationally modified and marked for degradation under normal oxygen conditions. During hypoxia, HIF-1 $\alpha$  escapes degradation and translocates to the nucleus where it will then activate hypoxia response elements (HREs). Many of the genes that HREs target are involved in promoting angiogenesis (i.e. Vascular endothelial growth factor, VEGF), survival (Bcl-2, AKT), or regulate metabolism via increasing glycolytic potential (i.e. glucose transporter

1 - GLUT1, lactate dehydrogenase A – LDHA, phosphoglycerate kinase 1- PGK1) [243, 244]. The increase in glycolytic genes translates to increased MSC consumption of glucose and production of lactate in an oxygen-dependent manner [239, 245]. Further analysis of HRE targets genes have also found active mitochondrial repressors such as pyruvate dehydrogenase kinase 1 (PDK1); an inhibitor of pyruvate entrance into the TCA cycle. PDK1 inhibition of pyruvate effectively reduces mitochondrial oxygen consumption and thus allows cells to preserve their intracellular oxygen concentrations [246]. MSCs exposed to hypoxic conditions also utilize HIF-1 $\alpha$  to activate the AKT signaling pathway to enhance survival and proliferation [247]. However, when HIF-1 $\alpha$  is knocked-down, compensatory activation of the p53 pathway occurs resulting in a higher induction of apoptosis [244]. These manipulations appear to marginally improve the survival of the transplanted MSCs[245, 248]. Thus, the next steps would be to evaluate a combination of hypoxic preconditioning with delivery within matricellular components such as TNC.

### **7.3.2 Regulating Autophagy May Be Key Mechanism For Survival And Efficacy In MSC Combinational Therapies.**

Upon further investigation into the effects of hypoxic preconditioning on MSCs, upregulated HIF-1 $\alpha$  was shown to promote the initiation of macroautophagy [249]. Macroautophagy (hereafter, autophagy), is an evolutionarily conserved “self-eating” catabolic process that targets cellular components for degradation through the formation of double membraned organelles called autophagosomes that later fuse with lysosomes [250]. Under normal circumstances, autophagy is a highly selective process used to maintain cellular homeostasis by degrading the buildup of aggregate-prone proteins and dysfunctional organelles [251]. However, when cells are exposed to environmental stressors such as nutrient deprivation or hypoxia,

autophagy becomes a non-selective process indiscriminately sequestering large amounts of cytosolic cargo for degradation in the attempt to prolong survival [252]. The activation of non-selective autophagy quickly becomes a balancing act within a cell, as autophagy can play a role in both cell survival and apoptosis [253]. In addition, autophagy and apoptosis mutually inhibit each other until an undefined sensitivity threshold is reached and one process overtakes the other; subsequently resulting in either adaptation of the cell to the stress or stress induced death [104, 254]. It is through these threshold boundaries where MSCs can be further fine-tuned to escalate their efficacy as cell therapies.

MSC performance and function are tied to its ability to regulate autophagy [255]. To date, basal autophagy levels have been shown to be higher in MSC populations compared to differentiated cell types [256]. Additional studies suggest that autophagy is required for conservation of MSC stemness and self-renewal capabilities [257]. Even more interesting is that non-stressed MSCs accumulate arrested autophagosome, and their autophagic manipulation significantly alter the balance between renewal and differentiation [258]. MSC directed differentiation dynamics will change when autophagy is manipulated as early as 3 hours after induction into adipogenic and osteogenic lineages [258, 259]. This is due to the MSCs quickly consuming the arrested autophagosomes that were present prior to induction, and by speeding up or slowing down the autophagy process, this will either increase or decrease the overall differentiation efficiency outcomes [258].

MSC paracrine function has also been linked to autophagic manipulation. This has been reported mostly in conjunction with hypoxic preconditioning. As MSCs experience hypoxia, HIF-1 $\alpha$  becomes upregulated and allowed to translocate into the nucleus, it initiates the production of BNIP3/BNIP3L, a set of pro-autophagy proteins that interact with the Bcl-2 sequestration complex

allowing Beclin-1 to dissociate away and initiate the autophagic cascade [260]. In addition to BNIP3, hypoxia also positively influences autophagy induction through regulating the expression of MAP1LC3 $\beta$  and ATG5 via PERK-UPR pathway, as well as activating the AMPK pathway [261]. This upregulation in autophagic flux has been linked to increased expression of VEGF secretion through direct phosphorylation of ERK [51]. The combination of pretreating MSCs with hypoxia could enhance the therapeutic potential of MSCs even further especially by promoting angiogenesis [262]. In treating post MI hearts, MSCs that underwent hypoxic preconditioning exhibited higher rates of autophagic flux resulting in higher retention in cell number and a significant reduction in scar formation within the infarct wall [263].

The strong connection of autophagy to cellular processes such as angiogenesis has launched the cancer treatment and stem cell therapy fields to find additional upstream activation/regulation inputs. This has resulted in a large emphasis on the ECM as a point of interest for such studies [264]. The most recent studies have focused on proteoglycans, primarily the small leucine rich proteoglycan DCN [56, 265]. DCN becomes upregulated within the resolution phase of wound healing where mature matrix such as Collagen-1 becomes present again during this final stage of healing. DCN is considered an important shut off switch for the pro-reparative mechanism of the tissue replacement phase, as it binds to growth factor receptors such as EGFR, VEGFR2, and MET; and limits the occurrence of hypertrophic scarring through preventing excessive repair. Upon binding these receptors, DCN will induce autophagy and mitophagy responses within the cell [265, 266]. However, these actions have been shown in differentiated cells and not yet in stem cells. It is also unclear of the physiological roles DCN induced autophagy has in certain cell types [265]. When postulating what this could mean for MSCs, DCN could be helping to reset the stem cell niche back to its dormant state by downregulating the proliferation and angiogenic signals

once needed for early wound repair. And like other cells that remain in a quiescent state for long periods of time, they rely heavily on autophagy to clear out unwanted intracellular debris unlike higher proliferating cell types.

For early wound healing situations, the immature matricellular TNC has been linked to prompt Beclin-1 induction [267] which could possibly induce autophagic flux. This would either be a second mode of survival mechanism (in addition to the tonic AKT and ERK signaling) or an additional driver in producing the secretome for tissue replacement. TNC is also known as being an anti-adhesive matrikine, allowing for the migration and ECM detachment of cells during development and wound repair [267]. Loss of ECM attachment has been shown to induce autophagy to promote a survival mechanism against short term anoikis [268]. Thus, the anti-adhesive nature of TNC along with other ECM anti-adhesive glycoproteins could render a secondary method of action for inducing autophagy survival mechanism in MSC-ECM transplantation strategies. In order for majority of these anti-adhesive ECM proteins to be properly combined with MSC delivery strategies in 2D or 3D, Col-I is often used has a structural tether to keep everything together. However, there is evidence *in vitro* that Col-I actively down regulates autophagy [269], suggesting that further research will be needed to fine tune the ratio of matrix protein delivery strategies depending on the required outcome.

We conducted a couple of preliminary studies looking into the effects of TNC on the MSC arrested autophagy state under normal growth conditions of 1% oxygen and simulated preconditioning growth conditions of 4% oxygen with a 2-hour exposure (Figure 21). We found that IHMSCs grown on Col-I and TNC+Col-I had a significantly higher autophagosome number than cells grown on plastic when cultured under 21% oxygen levels. Inversely, IHMSCs grown on TNC+Col-I under 4% oxygen levels had a significantly lower number of autophagosomes

compared to cells grown on plastic (Figure 21). IHMSCs grown on plastic had a higher autophagosome count when cultured at 4% oxygen than at 21% oxygen. Whereas IHMSCs grown on TNC+Col-I matrices had a higher autophagosome count when cultured at 21% oxygen than at 4% oxygen. These early results suggest that TNC affects autophagic flux differently than MSCs cultured on plastic alone at 21% and 4 % oxygen levels.

Additionally, we performed another preliminary experiment looking at the autophagic flux of MSCs on the three culture conditions when placed under H/ND conditions for 7 days (Figure 22). We used a Tandem RFP-GFP-LC3 Autophagy Sensor to analyze live cell observation of autophagosome turnover. The plasmid is designed such that both RFP and GFP fluoresce when LC3-II is incorporated normally in the elongation-closure steps of autophagosomes formation. However, upon fusion of the autophagosomes to the lysosome, the acidic compartments of the lysosome will cause the GFP-LC3 to stop fluorescing, leaving only the RFP to continue to be expressed, indicating flux. Upon these initial observations, the autophagosome punctate in the MSC on TNC+Col-I conditions appeared to be larger in size and be fewer in number compared to the MSCs on Col-I and Plastic conditions. The mechanisms of controlling autophagosome size are still relatively unknown, but theoretically, this can be determined by the rate of membrane addition during the elongation step in conjunction with the spontaneous rate of closure [270-272]. With this theory, I postulate this is due to the stress received by the cell where cells under more stress have smaller autophagosomes than those under less stress. One caveat I would like to mention is that autophagy is a very dynamic and quick process, and both of these situations are just one snapshot of the whole process. These preliminary insights offer many future opportunities to explore and will be a vital part of understanding matricellular biology in cell therapy applications.

Altogether, both environmental stimuli of hypoxic preconditioning and matrix proteins are linked to autophagy in various ways (Figure 23). Further investigation into how to finetune their inputs in conjunction with autophagic flux could prove to be a critical insight into optimizing MSC therapeutic approaches. Especially in essential processes such as angiogenesis, where increased autophagic flux has been linked to upregulating angiogenesis through increased production of VEGFA in cutaneous wound repair [51].

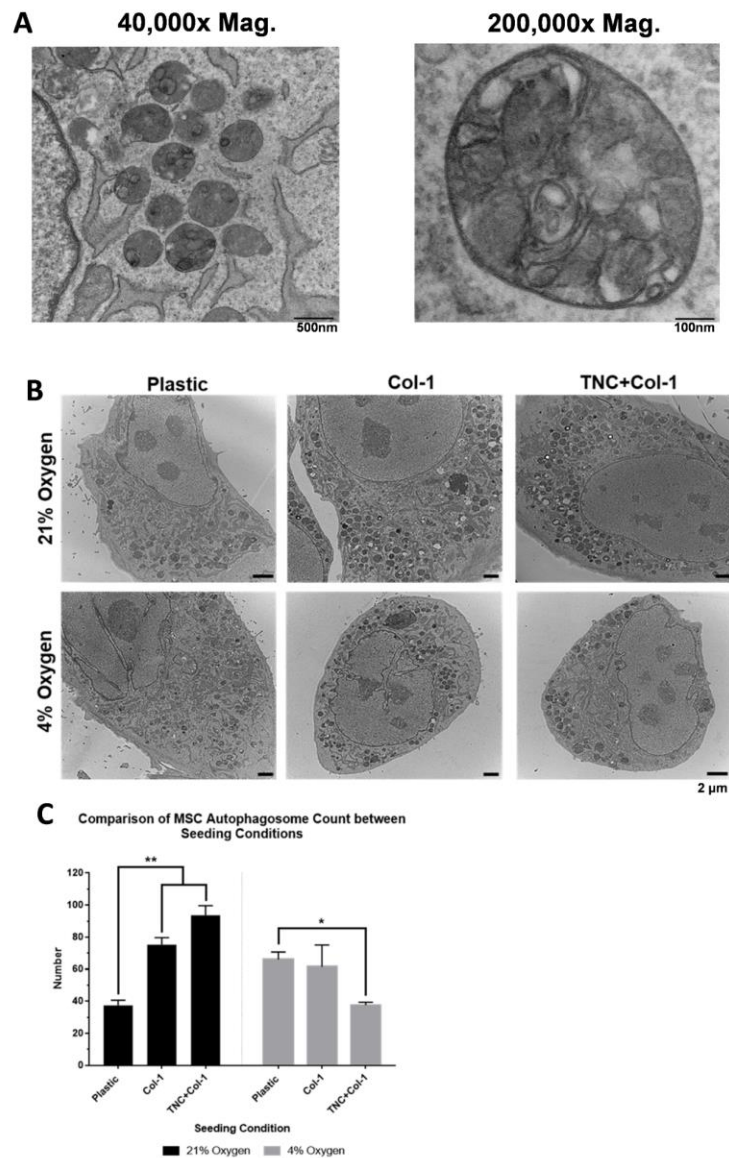


**Figure 21: Arrested autophagy phenotype in IHMSCs.** TEM micrographs of IHMSCs after 2 hours under different culture and growth conditions. (A) Representative images of arrested autophagosomes. The left panel exhibits a cluster of the varying autophagosome morphologies we typically see for our arrested autophagy phenotype in IHMSCs. The right panel is a highly magnified electron micrograph of a single autophagosome with the characteristic double membrane surrounding a diverse set of organelles. (B) Representative electron micrographs demonstrating different levels of autophagosome abundance under each culture condition. (C) Autophagosome number was compared for each matrix seeding condition within their relative oxygen level culture conditions.

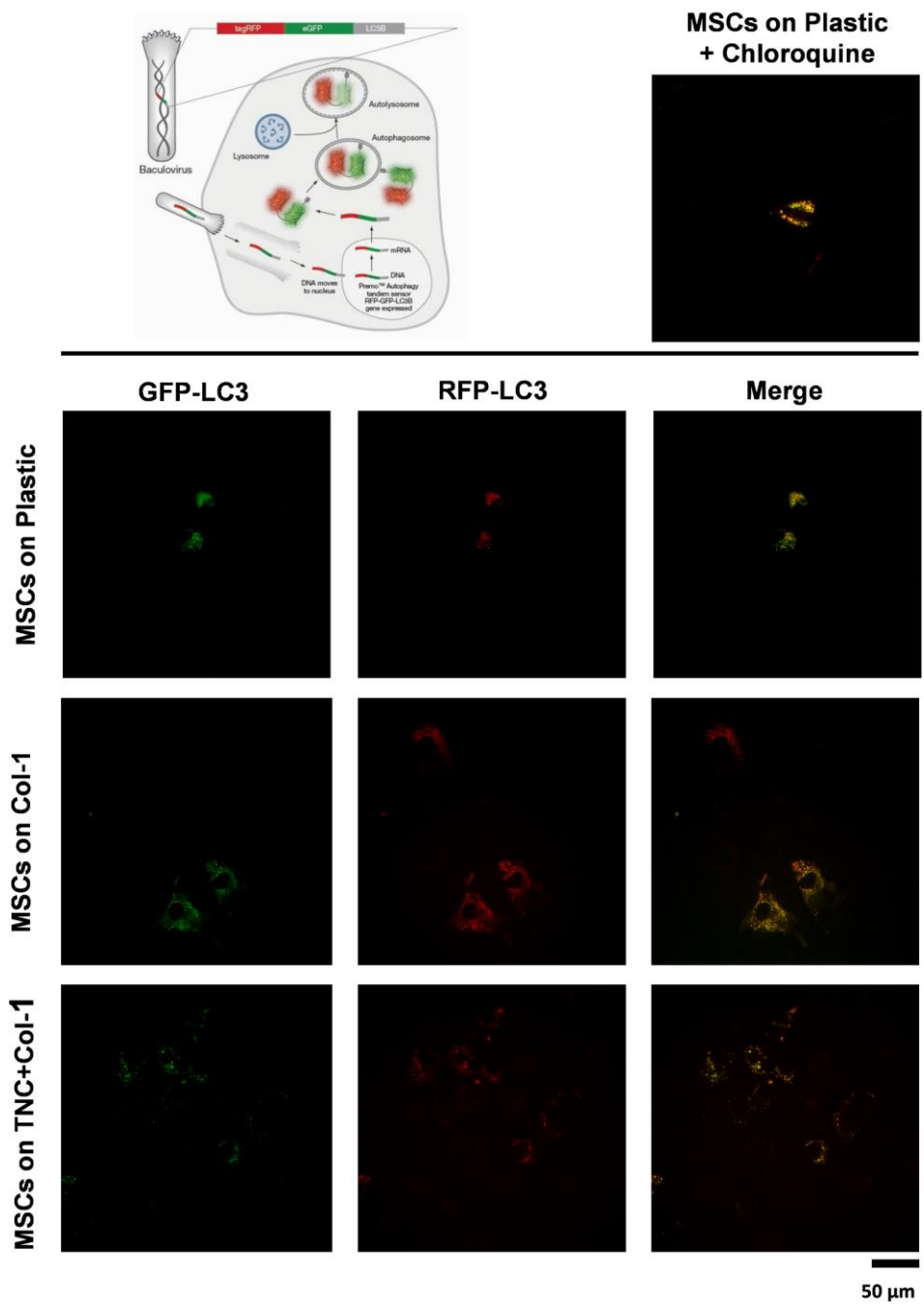


Figure 22: IHMSC autophagosome turnover at Day 7 exposure to H/ND IHMSCs cultured on plastic, Col-I, or TNC+Col-I were tagged with an autophagy tandem GFP-RFP LC3 reporter via transduction (see methods – Appendix A) and cultured under H/ND for 6 Days. IHMSCs cultured on plastic at normoxia were used for Chloroquine control group.

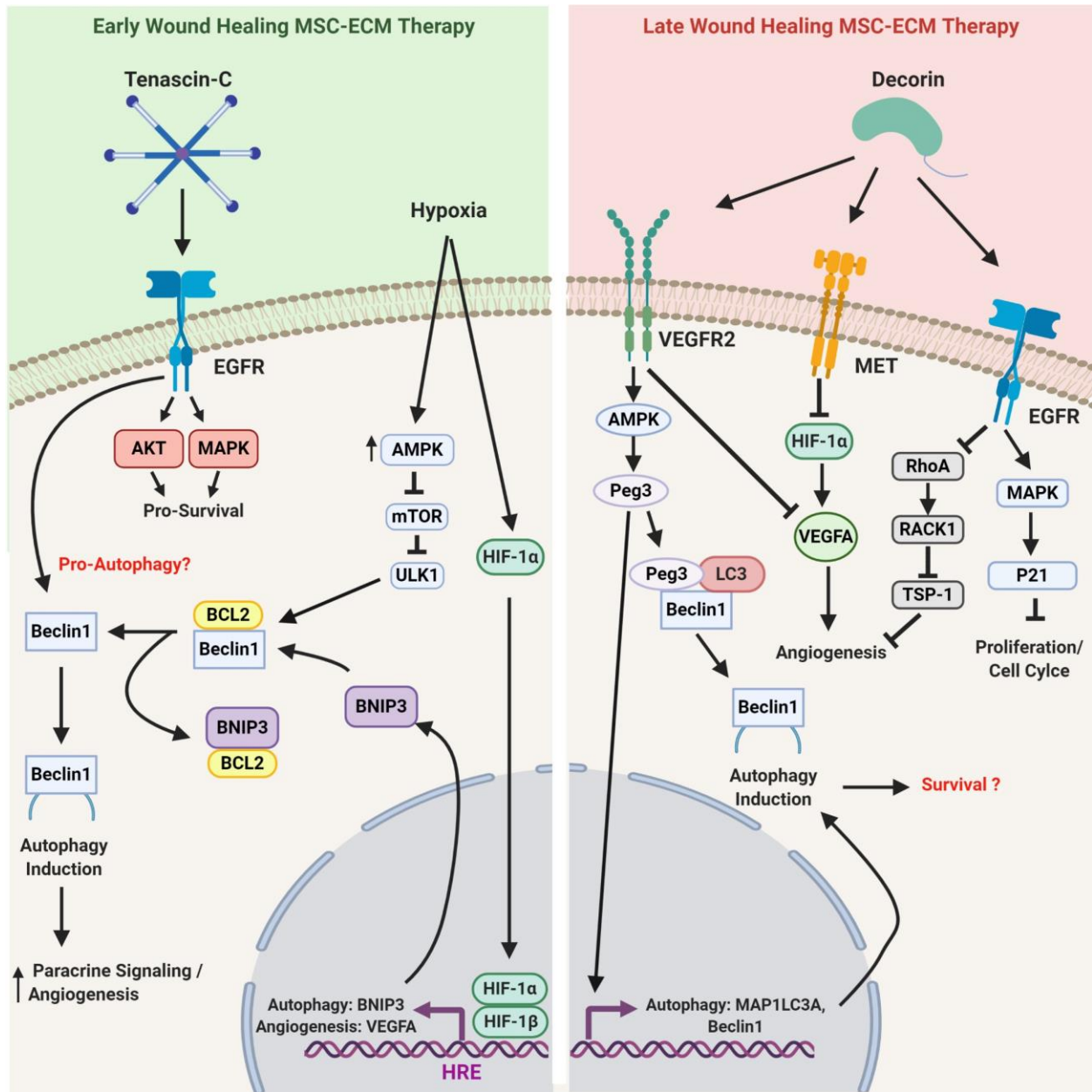


Figure 23: Concept of MSC-ECM therapeutic strategy to modulate downstream autophagy mechanisms in cutaneous wound healing. MSC-ECM combinational strategies need to be customized depending on the target stage of wound healing as they will have different intracellular influences on MSC performance. The left panel represents an MSC-ECM combinational therapy targeting the inflammatory and tissue replacement phases of wound healing such as in treating a chronic ulcer. Using a matrix protein that is naturally occurring during the early phases of wound repair, TNC will provide pro-survival signals through continual ERK and AKT signaling cascades. In conjunction with the TNC survival signals, the MSCs will be

exposed to hypoxia/ischemia. This will jump start the HIF-1 $\alpha$  signaling complex and result in an upregulated autophagic (BNIP3) and pro-angiogenic response (Hypoxia Response Elements such as VEGFA). TNC is also linked to the induction of Beclin1 and has been postulated as an influencer of autophagic expression. With the addition of the autophagic machinery the MSCs can utilize its output of nutrients / building blocks (amino acids, nucleic acids, fats, sugars) to further enhance its pro-angiogenic signaling properties. In the right panel we have an MSC-ECM combinational therapy that would be used to target the resolution phase of wound healing in hopes of stopping excess scar formation. Decorin is a naturally occurring matrix protein during the resolution phase and works as a major stop signal for all the pro-wound healing systems that were at play in the early phases of repair. It binds to various growth factors and receptors where it signals the surrounding cells to stop proliferating (EGF), and stop producing angiogenic factors (VEGFR2, MET, EGFR). However, Decorin is well known for inducing a robust induction of autophagy (VEGFR2) without a real clear understanding of how that effects the physiology of the cells moving forward. Biorender was used to design and create the figures. (<https://biorender.com/>)

## Appendix A

### Appendix A.1 Autophagy Analysis Methodology

#### Transmission Electron Microscopy

IHMSCs were cultured on either plastic, Col-I, or TNC+Col-I and subjected to either 21% oxygen or 1% oxygen for 2 hours before processing for Transmission Electron Microscopy (TEM). IHMSCs were processed for TEM as previously described in Stolz et al[273]. To harvest samples for TEM, we grew all IHMSC conditions in a six-well plate. The cells were washed with PBS to remove any residual media and fixed with 2.5% glutaraldehyde for 1 hour at room temperature. The cells were washed three consecutive times with PBS to remove any residual fixative and placed in 1% osmium tetroxide + potassium ferricyanide for 1 hour at room temperature to post-fix all lipid membranes. Osmium tetroxide reacts with unsaturated fatty acids to form covalent linkages, while also leaving behind osmium metal as part of the staining reaction. The samples were then washed three consecutive times with PBS to remove any residual Osmium tetroxide solution and placed in a series of escalating EtOH washes from 30-100% to slowly remove water from the cells. A final series of three 1-hour washes using 100% propylene oxide (Epon) was used to ensure all water is removed from the samples, and to prep the monolayers for Epon capsule embedding. Samples were embedded in propylene oxide:Polybed 812 epoxy resin (polysciences) and allowed to cure for three consecutive days. After the capsules harden, an ultramicrotome was used to cut ultrathin (70nm) sections for each sample. The sections were placed on specialized copper grids and stained with a couple of stains (2% uranyl acetate, and 1% lead citrate) to enhance

contrast of organelles within the EM image. Samples were imaged using a JEM 1011 Electron Microscope for autophagosome content.

#### Tandem Autophagy Sensor RFP-GFP-LC3B

IHMSCs were plated on either plastic, Col-I, or TNC+Col-I at a confluency of 80% and then transduced the next day using a Tandem RFP-GFP-LC3 Autophagy Sensor (Cat. No. P36239, Thermo Fisher Scientific). The following day the cells were switched to H/ND growth conditions and grown under these conditions (see previous methods) for 7 days. This system allows for the analysis of live cell observation of autophagosome turnover. The plasmid is designed such that both RFP and GFP fluoresce when LC3-II is incorporated normally in the elongation-closure steps of autophagosomes formation. However, upon fusion of the autophagosomes to the lysosome, the acidic compartments of the lysosome will cause the GFP-LC3 to stop fluorescing, leaving only the RFP to continue to be expressed indicating flux. Chloroquine was used as a negative control for autophagic turnover and used on IHMSCs cultured on plastic and subjected to normal growth conditions.

## **Appendix B**

### **Appendix B.1 CXCR3 Deficient Mouse Model for Wound Healing**

The intricate nature of cutaneous wound healing has led to numerous animal models and a myriad of techniques to mimic wound healing of a human. Porcine wound healing models are the closest resemblance to the human skin as the dermis is firmly attached to the tissue below [274, 275]. However, their slow reproduction rate and high cost per animal make them challenging in larger animal studies. This has led to murine animal models taking the lead for researchers studying cutaneous wounds healing over the past couple of decades [274, 275]. Mice are able to be bred quickly, have a low cost per animal, and are easier to genetically modify to better mimic pathological circumstances of the human body; all of which overshadow the macroscopic difference in their loosely attached skin.

In our studies over the past decade, we have discovered that CXCR3 deficient mice make a great animal model for studying delayed wound healing in addition to hypertrophic scarring. CXCR3 is a seven transmembrane G-protein coupled receptor found on many cell types involved in wound healing including smooth muscle cells, endothelial cells and inflammatory cells (T-cells, NK cells, monocytes). It is the sole receptor for ligands CXCL4, CXCL9, CXCL10 and CXCL11, the latter two are expressed during wound healing at the time of the transition from tissue replacement to wound resolution. CXCR3 signaling will result in the regulation of cell proliferation, cell migration, and cell survival; all biological processes crucial in repairing the wound and restoring homeostasis.

Our earlier work found that mice lacking the CXCR3 receptor recapitulates an immature and delayed tissue replacement phase of repair [200]. This mouse model exhibits a delayed healing response within the dermal and epidermal layers of the skin, leading to an immature dermal matrix, a weakened basement membrane, and hypercellularity [148, 201]. This results in CXCR3 KO mice having thicker dermal and epidermal layers and delayed wound score measurements when compared to FVB WT mice at day 30 (Figure 24 A-B). This prolonged immature tissue replacement phase of repair in CXCR3 KO mice will then lead to the formation of hypertrophic scarring [201, 223]. Where correction of the scarring defect using cellular transplants reverses the matrix progression back towards near regenerative healing[49, 52, 89]. This is once again observed with day 90 histology where CXCR3 KO mice have thicker epidermal layers and delayed dermal wound scores (Figure 24 A, C).

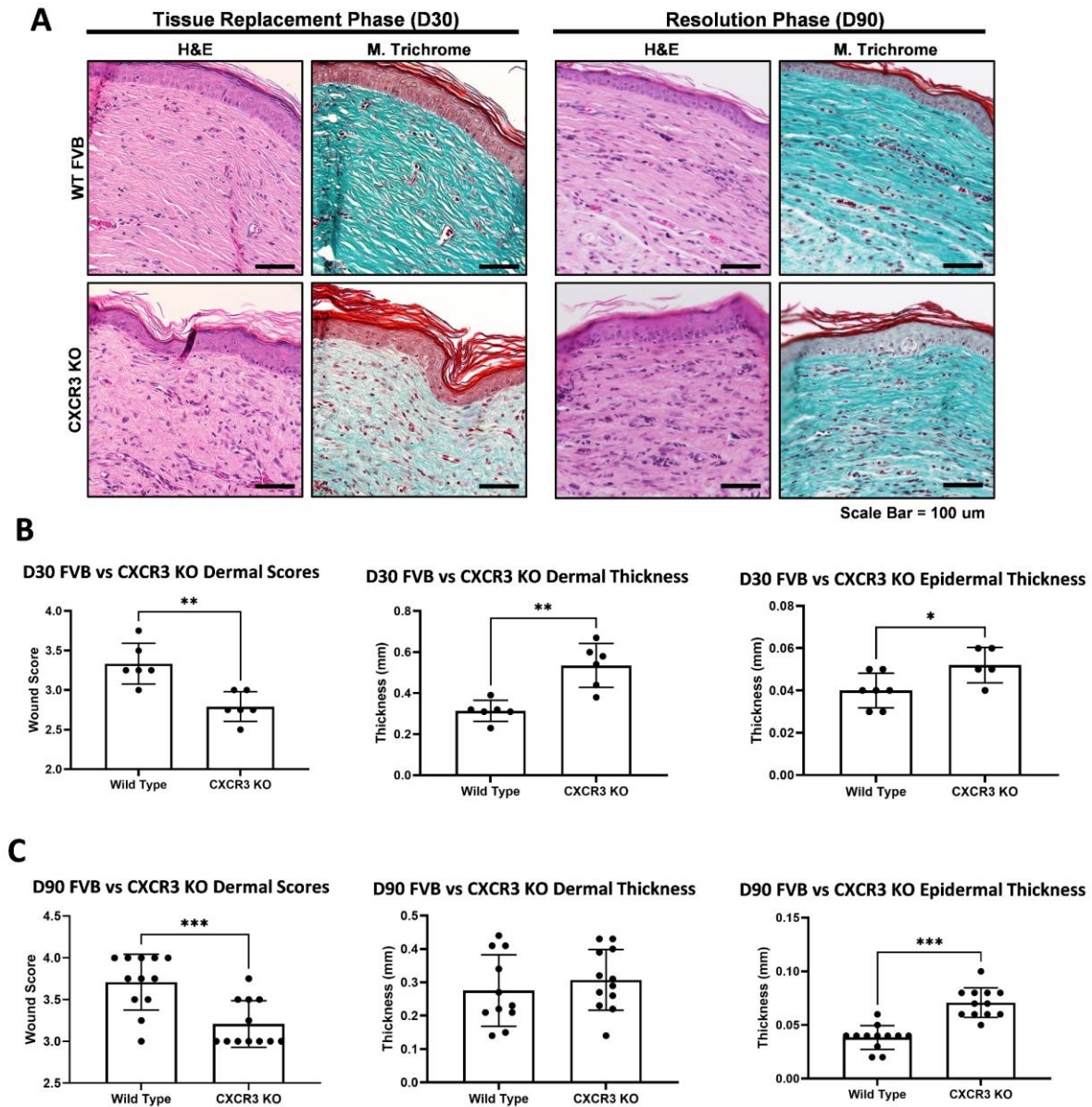


**Figure 24: FVB vs CXCR3 KO mouse comparison. Representative histological sections of wounds stained with hematoxylin and eosin (H&E) and Masson's trichrome (MT) at 40x magnification (A). Quantification of dermal wound healing score and wound thickness measurement for epidermal and dermal skin layers (B-C). Quantification in B and C are shown as mean  $\pm$  SD ( $n \geq 6$ ). \* $p < 0.05$ , \*\* $p < 0.01$ , \*\*\* $p < 0.001$ . Scale bar for all images is 100  $\mu$ m.**

## Appendix C

### Appendix C.1 Abbreviations

BM - Bone Marrow

CO - Coacervate

COI - Collagen Orientation Index

Col-I - Collagen Type 1

Col-III - Collagen Type III

CM - Conditioned Media

CXCR3 - Cysteine-X Amino Acid – Cysteine Receptor 3

ECM - Extracellular Matrix

EGFR - Epidermal Growth Factor Receptor

EGF-L - EGF-like Repeat

DCN - Decorin

H&E - Hematoxylin & Eosin

HMEC-1 - Human Dermal Microvascular Endothelial Cells

H/ND - Hypoxia and Nutrient Deprivation

HTS - Hypertrophic Scar

MMP - Matrix Metalloproteinase

MSC - Mesenchymal Stem Cell

MT - Masson's Trichrome

PBS - Phosphate-buffered Saline

PEAD - Poly (Ethylene Arginyl Aspartate Diglyceride)

PrhMSC - Primary Human Bone-Marrow Mesenchymal Stem Cell

PSR - Picrosirius Red

TEM - Transmission Electron Microscopy

TGF- $\beta$  - Transforming Growth Factor Beta

TNC - Tenascin-C

VEGF - Vascular Endothelial Growth Factor

## Bibliography

1. Goldsmith, L.A., *My organ is bigger than your organ*. Arch Dermatol, 1990. **126**(3): p. 301-2.
2. Proksch, E., J.M. Brandner, and J.M. Jensen, *The skin: an indispensable barrier*. Exp Dermatol, 2008. **17**(12): p. 1063-72.
3. Zhai, H. and H.I. Maibach, *Occlusion vs. skin barrier function*. Skin Res Technol, 2002. **8**(1): p. 1-6.
4. Ackerley, R., et al., *Touch perceptions across skin sites: differences between sensitivity, direction discrimination and pleasantness*. Front Behav Neurosci, 2014. **8**: p. 54.
5. Lumpkin, E.A. and M.J. Caterina, *Mechanisms of sensory transduction in the skin*. Nature, 2007. **445**(7130): p. 858-65.
6. Romanovsky, A.A., *Skin temperature: its role in thermoregulation*. Acta Physiol (Oxf), 2014. **210**(3): p. 498-507.
7. Hossein-nezhad, A. and M.F. Holick, *Vitamin D for health: a global perspective*. Mayo Clin Proc, 2013. **88**(7): p. 720-55.
8. Gurtner, G.C., et al., *Wound repair and regeneration*. Nature, 2008. **453**(7193): p. 314-21.
9. Thacher, T.D., P.R. Fischer, and J.M. Pettifor, *Vitamin D treatment in calcium-deficiency rickets: a randomised controlled trial*. Arch Dis Child, 2014. **99**(9): p. 807-11.
10. Sotiropoulou, P.A. and C. Blanpain, *Development and homeostasis of the skin epidermis*. Cold Spring Harb Perspect Biol, 2012. **4**(7): p. a008383.
11. Wong, D.J. and H.Y. Chang, *Skin tissue engineering*, in *StemBook*. 2008: Cambridge (MA).
12. Lechler, T. and E. Fuchs, *Asymmetric cell divisions promote stratification and differentiation of mammalian skin*. Nature, 2005. **437**(7056): p. 275-80.
13. Slominski, A.T., et al., *Local melatonergic system as the protector of skin integrity*. Int J Mol Sci, 2014. **15**(10): p. 17705-32.
14. Rawlings, A.V., et al., *Stratum corneum moisturization at the molecular level*. J Invest Dermatol, 1994. **103**(5): p. 731-41.

15. Bologna, J.L., J.L. Jorizzo, and J. Schaffer, *Dermatology: 2-Volume Set: Expert Consult Premium Edition-Enhanced Online Features and Print*. 2012, Philadelphia: Saunders.
16. Harding, C.R., *The stratum corneum: structure and function in health and disease*. *Dermatol Ther*, 2004. **17 Suppl 1**: p. 6-15.
17. Lippens, S., et al., *Death penalty for keratinocytes: apoptosis versus cornification*. *Cell Death Differ*, 2005. **12 Suppl 2**: p. 1497-508.
18. Ronfard, V., et al., *Long-term regeneration of human epidermis on third degree burns transplanted with autologous cultured epithelium grown on a fibrin matrix*. *Transplantation*, 2000. **70**(11): p. 1588-98.
19. Ushiki, T., *Collagen fibers, reticular fibers and elastic fibers. A comprehensive understanding from a morphological viewpoint*. *Arch Histol Cytol*, 2002. **65**(2): p. 109-26.
20. Sahota, P.S., et al., *Development of a reconstructed human skin model for angiogenesis*. *Wound Repair Regen*, 2003. **11**(4): p. 275-84.
21. Salcido, R., *Healing by Intention*. *Adv Skin Wound Care*, 2017. **30**(6): p. 246-247.
22. Chetter, I.C., et al., *Patients with surgical wounds healing by secondary intention: A prospective, cohort study*. *Int J Nurs Stud*, 2019. **89**: p. 62-71.
23. Barker, T.H. and A.J. Engler, *The provisional matrix: setting the stage for tissue repair outcomes*. *Matrix Biol*, 2017. **60-61**: p. 1-4.
24. Bodnar, R.J., et al., *Pericyte regulation of vascular remodeling through the CXC receptor 3*. *Arterioscler Thromb Vasc Biol*, 2013. **33**(12): p. 2818-29.
25. Martins-Green, M., M. Petreaca, and L. Wang, *Chemokines and their receptors are key players in the orchestra that regulates wound healing*. *Advances in Wound Care*, 2013. **2**(7): p. 327-347.
26. Wells, A., A. Nuschke, and C.C. Yates, *Skin tissue repair: Matrix microenvironmental influences*. *Matrix Biol*, 2016. **49**: p. 25-36.
27. Olczyk, P., L. Mencner, and K. Komosinska-Vassev, *The role of the extracellular matrix components in cutaneous wound healing*. *Biomed Res Int*, 2014. **2014**: p. 747584.
28. Mangin, P.H., et al., *Immobilized fibrinogen activates human platelets through glycoprotein VI*. *Haematologica*, 2018. **103**(5): p. 898-907.
29. Zuliani-Alvarez, L. and K.S. Midwood, *Fibrinogen-Related Proteins in Tissue Repair: How a Unique Domain with a Common Structure Controls Diverse Aspects of Wound Healing*. *Adv Wound Care (New Rochelle)*, 2015. **4**(5): p. 273-285.

30. Laurens, N., P. Koolwijk, and M.P. de Maat, *Fibrin structure and wound healing*. J Thromb Haemost, 2006. **4**(5): p. 932-9.
31. Soto-Pantoja, D.R., et al., *CD47 deficiency confers cell and tissue radioprotection by activation of autophagy*. Autophagy, 2012. **8**(11): p. 1628-42.
32. Isenberg, J.S., et al., *Gene silencing of CD47 and antibody ligation of thrombospondin-1 enhance ischemic tissue survival in a porcine model: implications for human disease*. Ann Surg, 2008. **247**(5): p. 860-8.
33. Kyriakides, T.R. and S. Maclachlan, *The role of thrombospondins in wound healing, ischemia, and the foreign body reaction*. J Cell Commun Signal, 2009. **3**(3-4): p. 215-25.
34. Kim, M.H., et al., *Dynamics of neutrophil infiltration during cutaneous wound healing and infection using fluorescence imaging*. J Invest Dermatol, 2008. **128**(7): p. 1812-20.
35. Park, J.E. and A. Barbul, *Understanding the role of immune regulation in wound healing*. Am J Surg, 2004. **187**(5A): p. 11S-16S.
36. Wang, J., *Neutrophils in tissue injury and repair*. Cell Tissue Res, 2018. **371**(3): p. 531-539.
37. O'Brien, X.M. and J.S. Reichner, *Neutrophil Integrins and Matrix Ligands and NET Release*. Front Immunol, 2016. **7**: p. 363.
38. Krzyszczyk, P., et al., *The Role of Macrophages in Acute and Chronic Wound Healing and Interventions to Promote Pro-wound Healing Phenotypes*. Front Physiol, 2018. **9**: p. 419.
39. Prame Kumar, K., A.J. Nicholls, and C.H.Y. Wong, *Partners in crime: neutrophils and monocytes/macrophages in inflammation and disease*. Cell Tissue Res, 2018. **371**(3): p. 551-565.
40. Frevert, C.W., et al., *Danger-Associated Molecular Patterns Derived From the Extracellular Matrix Provide Temporal Control of Innate Immunity*. J Histochem Cytochem, 2018. **66**(4): p. 213-227.
41. Muller, W.A., *Getting leukocytes to the site of inflammation*. Vet Pathol, 2013. **50**(1): p. 7-22.
42. Mahdavian Delavary, B., et al., *Macrophages in skin injury and repair*. Immunobiology, 2011. **216**(7): p. 753-62.
43. Wight, T.N., *Provisional matrix: A role for versican and hyaluronan*. Matrix Biol, 2017. **60-61**: p. 38-56.
44. Wight, T.N., et al., *Versican-A Critical Extracellular Matrix Regulator of Immunity and Inflammation*. Front Immunol, 2020. **11**: p. 512.

45. Garantziotis, S. and R.C. Savani, *Hyaluronan biology: A complex balancing act of structure, function, location and context*. Matrix Biol, 2019. **78-79**: p. 1-10.
46. Theocharidis, G., et al., *Type VI Collagen Regulates Dermal Matrix Assembly and Fibroblast Motility*. J Invest Dermatol, 2016. **136**(1): p. 74-83.
47. Cescon, M., et al., *Collagen VI at a glance*. J Cell Sci, 2015. **128**(19): p. 3525-31.
48. Rodrigues, M., et al., *The matrikine tenascin-C protects multipotential stromal cells/mesenchymal stem cells from death cytokines such as FasL*. Tissue Eng Part A, 2013. **19**(17-18): p. 1972-83.
49. Yates, C.C., et al., *Improved Transplanted Stem Cell Survival in a Polymer Gel Supplemented With Tenascin C Accelerates Healing and Reduces Scarring of Murine Skin Wounds*. Cell Transplant, 2017. **26**(1): p. 103-113.
50. Chen, P., M. Cescon, and P. Bonaldo, *Autophagy-mediated regulation of macrophages and its applications for cancer*. Autophagy, 2014. **10**(2): p. 192-200.
51. An, Y., et al., *Autophagy promotes MSC-mediated vascularization in cutaneous wound healing via regulation of VEGF secretion*. Cell Death Dis, 2018. **9**(2): p. 58.
52. Sylakowski, K., A. Bradshaw, and A. Wells, *Mesenchymal Stem Cell/Multipotent Stromal Cell Augmentation of Wound Healing: Lessons from the Physiology of Matrix and Hypoxia Support*. Am J Pathol, 2020. **190**(7): p. 1370-1381.
53. Wang, W., et al., *Osteopontin activates mesenchymal stem cells to repair skin wound*. PLoS One, 2017. **12**(9): p. e0185346.
54. Klingberg, F., B. Hinz, and E.S. White, *The myofibroblast matrix: implications for tissue repair and fibrosis*. J Pathol, 2013. **229**(2): p. 298-309.
55. Gubbiotti, M.A., et al., *Proteoglycan signaling in tumor angiogenesis and endothelial cell autophagy*. Semin Cancer Biol, 2020. **62**: p. 1-8.
56. Buraschi, S., T. Neill, and R.V. Iozzo, *Decorin is a devouring proteoglycan: Remodeling of intracellular catabolism via autophagy and mitophagy*. Matrix Biol, 2019. **75-76**: p. 260-270.
57. Buraschi, S., et al., *Decorin causes autophagy in endothelial cells via Peg3*. Proc Natl Acad Sci U S A, 2013. **110**(28): p. E2582-91.
58. Poluzzi, C., et al., *Endorepellin evokes autophagy in endothelial cells*. J Biol Chem, 2014. **289**(23): p. 16114-28.
59. Goyal, A., et al., *Endorepellin-evoked Autophagy Contributes to Angiostasis*. J Biol Chem, 2016. **291**(37): p. 19245-56.

60. Frykberg, R.G. and J. Banks, *Challenges in the Treatment of Chronic Wounds*. Adv Wound Care (New Rochelle), 2015. **4**(9): p. 560-582.
61. Yates, C.C., R. Bodnar, and A. Wells, *Matrix control of scarring*. Cell Mol Life Sci, 2011. **68**(11): p. 1871-81.
62. Jarbrink, K., et al., *Prevalence and incidence of chronic wounds and related complications: a protocol for a systematic review*. Syst Rev, 2016. **5**(1): p. 152.
63. Nussbaum, S.R., et al., *An Economic Evaluation of the Impact, Cost, and Medicare Policy Implications of Chronic Nonhealing Wounds*. Value Health, 2018. **21**(1): p. 27-32.
64. Richmond, N.A., A.D. Maderal, and A.C. Vivas, *Evidence-based management of common chronic lower extremity ulcers*. Dermatol Ther, 2013. **26**(3): p. 187-96.
65. Fearn, N., et al., *Placing the patient at the centre of chronic wound care: A qualitative evidence synthesis*. J Tissue Viability, 2017. **26**(4): p. 254-259.
66. Rohani, M.G. and W.C. Parks, *Matrix remodeling by MMPs during wound repair*. Matrix Biol, 2015. **44-46**: p. 113-21.
67. Davis, F.M., et al., *Dysfunctional Wound Healing in Diabetic Foot Ulcers: New Crossroads*. Curr Diab Rep, 2018. **18**(1): p. 2.
68. Krishnaswamy, V.R., D. Mintz, and I. Sagi, *Matrix metalloproteinases: The sculptors of chronic cutaneous wounds*. Biochim Biophys Acta Mol Cell Res, 2017. **1864**(11 Pt B): p. 2220-2227.
69. Uccioli, L., et al., *Non-healing foot ulcers in diabetic patients: general and local interfering conditions and management options with advanced wound dressings*. J Wound Care, 2015. **24**(4 Suppl): p. 35-42.
70. Bradshaw, A., K. Sylakowski, and A. Wells, *The Pro-reparative Engine: Stem Cells Aid Healing by Dampening Inflammation*. Curr Pathobiol Rep, 2018. **6**(2): p. 109-115.
71. Razyieva, K., et al., *Immunology of Acute and Chronic Wound Healing*. Biomolecules, 2021. **11**(5).
72. Friedenstein, A.J., R.K. Chailakhjan, and K.S. Lalykina, *The development of fibroblast colonies in monolayer cultures of guinea-pig bone marrow and spleen cells*. Cell Tissue Kinet, 1970. **3**(4): p. 393-403.
73. Benayahu, D., et al., *Bone marrow-derived stromal cell line expressing osteoblastic phenotype in vitro and osteogenic capacity in vivo*. J Cell Physiol, 1989. **140**(1): p. 1-7.
74. Bruder, S.P., et al., *Bone regeneration by implantation of purified, culture-expanded human mesenchymal stem cells*. J Orthop Res, 1998. **16**(2): p. 155-62.

75. Ferrari, G., et al., *Muscle regeneration by bone marrow-derived myogenic progenitors*. Science, 1998. **279**(5356): p. 1528-30.
76. Hauner, H., P. Schmid, and E.F. Pfeiffer, *Glucocorticoids and insulin promote the differentiation of human adipocyte precursor cells into fat cells*. J Clin Endocrinol Metab, 1987. **64**(4): p. 832-5.
77. Johnstone, B., et al., *In vitro chondrogenesis of bone marrow-derived mesenchymal progenitor cells*. Exp Cell Res, 1998. **238**(1): p. 265-72.
78. Pittenger, M.F., et al., *Multilineage potential of adult human mesenchymal stem cells*. Science, 1999. **284**(5411): p. 143-7.
79. Wakitani, S., T. Saito, and A.I. Caplan, *Myogenic cells derived from rat bone marrow mesenchymal stem cells exposed to 5-azacytidine*. Muscle Nerve, 1995. **18**(12): p. 1417-26.
80. Viswanathan, S., et al., *Mesenchymal stem versus stromal cells: International Society for Cell & Gene Therapy (ISCT(R)) Mesenchymal Stromal Cell committee position statement on nomenclature*. Cytotherapy, 2019. **21**(10): p. 1019-1024.
81. Singer, N.G. and A.I. Caplan, *Mesenchymal stem cells: mechanisms of inflammation*. Annu Rev Pathol, 2011. **6**: p. 457-78.
82. Madrigal, M., K.S. Rao, and N.H. Riordan, *A review of therapeutic effects of mesenchymal stem cell secretions and induction of secretory modification by different culture methods*. J Transl Med, 2014. **12**: p. 260.
83. Shin, L. and D.A. Peterson, *Human mesenchymal stem cell grafts enhance normal and impaired wound healing by recruiting existing endogenous tissue stem/progenitor cells*. Stem Cells Transl Med, 2013. **2**(1): p. 33-42.
84. Hu, M.S., et al., *Mesenchymal Stromal Cells and Cutaneous Wound Healing: A Comprehensive Review of the Background, Role, and Therapeutic Potential*. Stem Cells Int, 2018. **2018**: p. 6901983.
85. Chen, L., et al., *Paracrine factors of mesenchymal stem cells recruit macrophages and endothelial lineage cells and enhance wound healing*. PLoS One, 2008. **3**(4): p. e1886.
86. Di Ianni, M., et al., *Mesenchymal cells recruit and regulate T regulatory cells*. Exp Hematol, 2008. **36**(3): p. 309-18.
87. Vasandan, A.B., et al., *Human Mesenchymal stem cells program macrophage plasticity by altering their metabolic status via a PGE2-dependent mechanism*. Sci Rep, 2016. **6**: p. 38308.
88. Joel, M.D.M., et al., *MSC: immunoregulatory effects, roles on neutrophils and evolving clinical potentials*. Am J Transl Res, 2019. **11**(6): p. 3890-3904.

89. Yates, C.C., et al., *Multipotent stromal cells/mesenchymal stem cells and fibroblasts combine to minimize skin hypertrophic scarring*. *Stem Cell Res Ther*, 2017. **8**(1): p. 193.
90. Huang, S., et al., *Paracrine action of mesenchymal stromal cells delivered by microspheres contributes to cutaneous wound healing and prevents scar formation in mice*. *Cytotherapy*, 2015. **17**(7): p. 922-31.
91. Machado Cde, V., P.D. Telles, and I.L. Nascimento, *Immunological characteristics of mesenchymal stem cells*. *Rev Bras Hematol Hemoter*, 2013. **35**(1): p. 62-7.
92. Kornicka, K., J. Houston, and K. Marycz, *Dysfunction of Mesenchymal Stem Cells Isolated from Metabolic Syndrome and Type 2 Diabetic Patients as Result of Oxidative Stress and Autophagy may Limit Their Potential Therapeutic Use*. *Stem Cell Rev Rep*, 2018. **14**(3): p. 337-345.
93. Pittenger, M.F. and B.J. Martin, *Mesenchymal stem cells and their potential as cardiac therapeutics*. *Circ Res*, 2004. **95**(1): p. 9-20.
94. Yang, M., et al., *Changes in host blood factors and brain glia accompanying the functional recovery after systemic administration of bone marrow stem cells in ischemic stroke rats*. *Cell Transplant*, 2010. **19**(9): p. 1073-84.
95. Sagrinati, C., et al., *Stem-cell approaches for kidney repair: choosing the right cells*. *Trends Mol Med*, 2008. **14**(7): p. 277-85.
96. Toma, C., et al., *Human mesenchymal stem cells differentiate to a cardiomyocyte phenotype in the adult murine heart*. *Circulation*, 2002. **105**(1): p. 93-8.
97. Hu, M.S., et al., *Stem Cell-Based Therapeutics to Improve Wound Healing*. *Plast Surg Int*, 2015. **2015**: p. 383581.
98. Rodrigues, M., L.G. Griffith, and A. Wells, *Growth factor regulation of proliferation and survival of multipotential stromal cells*. *Stem Cell Res Ther*, 2010. **1**(4): p. 32.
99. Song, H., et al., *Modification of mesenchymal stem cells for cardiac regeneration*. *Expert Opin Biol Ther*, 2010. **10**(3): p. 309-19.
100. Rodrigues, M., et al., *Production of reactive oxygen species by multipotent stromal cells/mesenchymal stem cells upon exposure to fas ligand*. *Cell Transplant*, 2012. **21**(10): p. 2171-87.
101. Nuschke, A., et al., *Mesenchymal stem cells/multipotent stromal cells (MSCs) are glycolytic and thus glucose is a limiting factor of in vitro models of MSC starvation*. *Stem Cell Res Ther*, 2016. **7**(1): p. 179.
102. Zhu, W., et al., *Hypoxia and serum deprivation-induced apoptosis in mesenchymal stem cells*. *Stem Cells*, 2006. **24**(2): p. 416-25.

103. Potier, E., et al., *Prolonged hypoxia concomitant with serum deprivation induces massive human mesenchymal stem cell death*. Tissue Eng, 2007. **13**(6): p. 1325-31.
104. Marino, G., et al., *Self-consumption: the interplay of autophagy and apoptosis*. Nat Rev Mol Cell Biol, 2014. **15**(2): p. 81-94.
105. Li, L., et al., *How to Improve the Survival of Transplanted Mesenchymal Stem Cell in Ischemic Heart?* Stem Cells Int, 2016. **2016**: p. 9682757.
106. Otero-Vinas, M. and V. Falanga, *Mesenchymal Stem Cells in Chronic Wounds: The Spectrum from Basic to Advanced Therapy*. Adv Wound Care (New Rochelle), 2016. **5**(4): p. 149-163.
107. Raugi, G.J., et al., *Thrombospondin: synthesis and secretion by cells in culture*. J Cell Biol, 1982. **95**(1): p. 351-4.
108. Schultz, G.S., et al., *Dynamic reciprocity in the wound microenvironment*. Wound Repair Regen, 2011. **19**(2): p. 134-48.
109. Somaiah, C., et al., *Collagen Promotes Higher Adhesion, Survival and Proliferation of Mesenchymal Stem Cells*. PLoS One, 2015. **10**(12): p. e0145068.
110. Popov, C., et al., *Integrins alpha2beta1 and alpha11beta1 regulate the survival of mesenchymal stem cells on collagen I*. Cell Death Dis, 2011. **2**: p. e186.
111. Smeriglio, P., J. Lee, and N. Bhutani, *Soluble Collagen VI treatment enhances mesenchymal stem cells expansion for engineering cartilage*. Bioeng Transl Med, 2017. **2**(3): p. 278-284.
112. Castagnaro, S., et al., *Extracellular Collagen VI Has Prosurvival and Autophagy Instructive Properties in Mouse Fibroblasts*. Front Physiol, 2018. **9**: p. 1129.
113. Murphy-Ullrich, J.E. and E.H. Sage, *Revisiting the matricellular concept*. Matrix Biol, 2014. **37**: p. 1-14.
114. Iyer, A.K., et al., *Tenascin cytotactin epidermal growth factor-like repeat binds epidermal growth factor receptor with low affinity*. J Cell Physiol, 2007. **211**(3): p. 748-58.
115. Schenk, S., et al., *Binding to EGF receptor of a laminin-5 EGF-like fragment liberated during MMP-dependent mammary gland involution*. J Cell Biol, 2003. **161**(1): p. 197-209.
116. Wang, L., et al., *Mesenchymal Stem Cells Coated by the Extracellular Matrix Promote Wound Healing in Diabetic Rats*. Stem Cells Int, 2019. **2019**: p. 9564869.
117. Abdeen, A.A., et al., *Matrix composition and mechanics direct proangiogenic signaling from mesenchymal stem cells*. Tissue Eng Part A, 2014. **20**(19-20): p. 2737-45.

118. Karoubi, G., et al., *Single-cell hydrogel encapsulation for enhanced survival of human marrow stromal cells*. *Biomaterials*, 2009. **30**(29): p. 5445-55.
119. Margadant, C., et al., *Integrin alpha3beta1 inhibits directional migration and wound re-epithelialization in the skin*. *J Cell Sci*, 2009. **122**(Pt 2): p. 278-88.
120. Agah, A., et al., *The lack of thrombospondin-1 (TSP1) dictates the course of wound healing in double-TSP1/TSP2-null mice*. *Am J Pathol*, 2002. **161**(3): p. 831-9.
121. Midwood, K.S., et al., *Tenascin-C at a glance*. *J Cell Sci*, 2016. **129**(23): p. 4321-4327.
122. Ragelle, H., et al., *Comprehensive proteomic characterization of stem cell-derived extracellular matrices*. *Biomaterials*, 2017. **128**: p. 147-159.
123. Midwood, K.S. and G. Orend, *The role of tenascin-C in tissue injury and tumorigenesis*. *J Cell Commun Signal*, 2009. **3**(3-4): p. 287-310.
124. Bornstein, P., *Diversity of function is inherent in matricellular proteins: an appraisal of thrombospondin I*. *J Cell Biol*, 1995. **130**(3): p. 503-6.
125. Sage, E.H. and P. Bornstein, *Extracellular proteins that modulate cell-matrix interactions. SPARC, tenascin, and thrombospondin*. *J Biol Chem*, 1991. **266**(23): p. 14831-4.
126. Bornstein, P. and E.H. Sage, *Matricellular proteins: extracellular modulators of cell function*. *Curr Opin Cell Biol*, 2002. **14**(5): p. 608-16.
127. Schalkwijk, J., et al., *Tenascin expression in human dermis is related to epidermal proliferation*. *Am J Pathol*, 1991. **139**(5): p. 1143-50.
128. Mackie, E.J., W. Halfter, and D. Liverani, *Induction of tenascin in healing wounds*. *J Cell Biol*, 1988. **107**(6 Pt 2): p. 2757-67.
129. Lightner, V.A., et al., *Tenascin/hexabrachion in human skin: biochemical identification and localization by light and electron microscopy*. *J Cell Biol*, 1989. **108**(6): p. 2483-93.
130. Fassler, R., et al., *Differential regulation of fibulin, tenascin-C, and nidogen expression during wound healing of normal and glucocorticoid-treated mice*. *Exp Cell Res*, 1996. **222**(1): p. 111-6.
131. Filsell, W., et al., *Coordinate upregulation of tenascin C expression with degree of photodamage in human skin*. *Br J Dermatol*, 1999. **140**(4): p. 592-9.
132. Geffrotin, C., et al., *Unlike tenascin-X, tenascin-C is highly up-regulated in pig cutaneous and underlying muscle tissue developing fibrosis after necrosis induced by very high-dose gamma radiation*. *Radiat Res*, 1998. **149**(5): p. 472-81.
133. Dalkowski, A., et al., *Increased expression of tenascin C by keloids in vivo and in vitro*. *Br J Dermatol*, 1999. **141**(1): p. 50-6.

134. Kammerer, R.A., et al., *Tenascin-C hexabrachion assembly is a sequential two-step process initiated by coiled-coil alpha-helices*. J Biol Chem, 1998. **273**(17): p. 10602-8.
135. Chiquet-Ehrismann, R. and M. Chiquet, *Tenascins: regulation and putative functions during pathological stress*. J Pathol, 2003. **200**(4): p. 488-99.
136. Huang, W., et al., *Interference of tenascin-C with syndecan-4 binding to fibronectin blocks cell adhesion and stimulates tumor cell proliferation*. Cancer Res, 2001. **61**(23): p. 8586-94.
137. Giblin, S.P. and K.S. Midwood, *Tenascin-C: Form versus function*. Cell Adh Migr, 2015. **9**(1-2): p. 48-82.
138. Zhou, M., et al., *Real-time measurements of kinetics of EGF binding to soluble EGF receptor monomers and dimers support the dimerization model for receptor activation*. Biochemistry, 1993. **32**(32): p. 8193-8.
139. Arno, A.I., et al., *Up-to-date approach to manage keloids and hypertrophic scars: a useful guide*. Burns, 2014. **40**(7): p. 1255-66.
140. Nischwitz, S.P., et al., *Evidence-based therapy in hypertrophic scars: An update of a systematic review*. Wound Repair Regen, 2020. **28**(5): p. 656-665.
141. Lawrence, J.W., et al., *Epidemiology and impact of scarring after burn injury: a systematic review of the literature*. J Burn Care Res, 2012. **33**(1): p. 136-46.
142. Marshall, C.D., et al., *Cutaneous Scarring: Basic Science, Current Treatments, and Future Directions*. Adv Wound Care (New Rochelle), 2018. **7**(2): p. 29-45.
143. Finnerty, C.C., et al., *Hypertrophic scarring: the greatest unmet challenge after burn injury*. Lancet, 2016. **388**(10052): p. 1427-1436.
144. Reinholz, M., et al., *The dermatology life quality index as a means to assess life quality in patients with different scar types*. J Eur Acad Dermatol Venereol, 2015. **29**(11): p. 2112-9.
145. Oh, H. and S. Boo, *Quality of life and mediating role of patient scar assessment in burn patients*. Burns, 2017. **43**(6): p. 1212-1217.
146. Gauglitz, G.G., et al., *Hypertrophic scarring and keloids: pathomechanisms and current and emerging treatment strategies*. Mol Med, 2011. **17**(1-2): p. 113-25.
147. Van De Water, L., S. Varney, and J.J. Tomasek, *Mechanoregulation of the Myofibroblast in Wound Contraction, Scarring, and Fibrosis: Opportunities for New Therapeutic Intervention*. Adv Wound Care (New Rochelle), 2013. **2**(4): p. 122-141.
148. Yates, C.C., et al., *Delayed reepithelialization and basement membrane regeneration after wounding in mice lacking CXCR3*. Wound Repair Regen, 2009. **17**(1): p. 34-41.

149. Yates, C.C., P. Hebda, and A. Wells, *Skin wound healing and scarring: fetal wounds and regenerative restitution*. Birth Defects Res C Embryo Today, 2012. **96**(4): p. 325-33.
150. Ogawa, R., *Keloid and Hypertrophic Scars Are the Result of Chronic Inflammation in the Reticular Dermis*. Int J Mol Sci, 2017. **18**(3).
151. Wang, Z.C., et al., *The Roles of Inflammation in Keloid and Hypertrophic Scars*. Front Immunol, 2020. **11**: p. 603187.
152. Limandjaja, G.C., et al., *Increased epidermal thickness and abnormal epidermal differentiation in keloid scars*. Br J Dermatol, 2017. **176**(1): p. 116-126.
153. Fujiwara, M., Y. Muragaki, and A. Ooshima, *Keloid-derived fibroblasts show increased secretion of factors involved in collagen turnover and depend on matrix metalloproteinase for migration*. Br J Dermatol, 2005. **153**(2): p. 295-300.
154. Neely, A.N., et al., *Gelatinase activity in keloids and hypertrophic scars*. Wound Repair Regen, 1999. **7**(3): p. 166-71.
155. Zhang, Z., et al., *Recombinant human decorin inhibits TGF-beta1-induced contraction of collagen lattice by hypertrophic scar fibroblasts*. Burns, 2009. **35**(4): p. 527-37.
156. Ferguson, M.W., et al., *Prophylactic administration of avotermin for improvement of skin scarring: three double-blind, placebo-controlled, phase I/II studies*. Lancet, 2009. **373**(9671): p. 1264-74.
157. Occleston, N.L., et al., *Discovery and development of avotermin (recombinant human transforming growth factor beta 3): a new class of prophylactic therapeutic for the improvement of scarring*. Wound Repair Regen, 2011. **19 Suppl 1**: p. s38-48.
158. Bush, J., et al., *Therapies with emerging evidence of efficacy: avotermin for the improvement of scarring*. Dermatol Res Pract, 2010. **2010**.
159. Liarte, S., A. Bernabe-Garcia, and F.J. Nicolas, *Role of TGF-beta in Skin Chronic Wounds: A Keratinocyte Perspective*. Cells, 2020. **9**(2).
160. Walton, K.L., K.E. Johnson, and C.A. Harrison, *Targeting TGF-beta Mediated SMAD Signaling for the Prevention of Fibrosis*. Front Pharmacol, 2017. **8**: p. 461.
161. Pakyari, M., et al., *Critical Role of Transforming Growth Factor Beta in Different Phases of Wound Healing*. Adv Wound Care (New Rochelle), 2013. **2**(5): p. 215-224.
162. Scott, P.G., et al., *Chemical characterization and quantification of proteoglycans in human post-burn hypertrophic and mature scars*. Clin Sci (Lond), 1996. **90**(5): p. 417-25.
163. Iozzo, R.V., *The family of the small leucine-rich proteoglycans: key regulators of matrix assembly and cellular growth*. Crit Rev Biochem Mol Biol, 1997. **32**(2): p. 141-74.

164. Ramamurthy, P., A.M. Hocking, and D.J. McQuillan, *Recombinant decorin glycoforms. Purification and structure*. J Biol Chem, 1996. **271**(32): p. 19578-84.
165. Schonherr, E., et al., *Differences in decorin expression by papillary and reticular fibroblasts in vivo and in vitro*. Biochem J, 1993. **290** ( Pt 3): p. 893-9.
166. Zhang, Z., et al., *Recombinant human decorin inhibits cell proliferation and downregulates TGF-beta1 production in hypertrophic scar fibroblasts*. Burns, 2007. **33**(5): p. 634-41.
167. Sayani, K., et al., *Delayed appearance of decorin in healing burn scars*. Histopathology, 2000. **36**(3): p. 262-72.
168. Honardoust, D., et al., *Small leucine-rich proteoglycans, decorin and fibromodulin, are reduced in postburn hypertrophic scar*. Wound Repair Regen, 2011. **19**(3): p. 368-78.
169. Scott, P.G., et al., *Fibroblasts from post-burn hypertrophic scar tissue synthesize less decorin than normal dermal fibroblasts*. Clin Sci (Lond), 1998. **94**(5): p. 541-7.
170. Mukhopadhyay, A., et al., *Syndecan-2 and decorin: proteoglycans with a difference--implications in keloid pathogenesis*. J Trauma, 2010. **68**(4): p. 999-1008.
171. Danielson, K.G., et al., *Targeted disruption of decorin leads to abnormal collagen fibril morphology and skin fragility*. J Cell Biol, 1997. **136**(3): p. 729-43.
172. Kadler, K.E., A. Hill, and E.G. Canty-Laird, *Collagen fibrillogenesis: fibronectin, integrins, and minor collagens as organizers and nucleators*. Curr Opin Cell Biol, 2008. **20**(5): p. 495-501.
173. Mohan, R.R., et al., *Significant inhibition of corneal scarring in vivo with tissue-selective, targeted AAV5 decorin gene therapy*. Invest Ophthalmol Vis Sci, 2011. **52**(7): p. 4833-41.
174. Keene, D.R., et al., *Decorin binds near the C terminus of type I collagen*. J Biol Chem, 2000. **275**(29): p. 21801-4.
175. Zhang, G., et al., *Decorin regulates assembly of collagen fibrils and acquisition of biomechanical properties during tendon development*. J Cell Biochem, 2006. **98**(6): p. 1436-49.
176. Weber, I.T., R.W. Harrison, and R.V. Iozzo, *Model structure of decorin and implications for collagen fibrillogenesis*. J Biol Chem, 1996. **271**(50): p. 31767-70.
177. Reed, C.C. and R.V. Iozzo, *The role of decorin in collagen fibrillogenesis and skin homeostasis*. Glycoconj J, 2002. **19**(4-5): p. 249-55.
178. Reese, S.P., C.J. Underwood, and J.A. Weiss, *Effects of decorin proteoglycan on fibrillogenesis, ultrastructure, and mechanics of type I collagen gels*. Matrix Biol, 2013. **32**(7-8): p. 414-23.

179. Iozzo, R.V., et al., *Decorin is a biological ligand for the epidermal growth factor receptor*. J Biol Chem, 1999. **274**(8): p. 4489-92.
180. Santra, M., C.C. Reed, and R.V. Iozzo, *Decorin binds to a narrow region of the epidermal growth factor (EGF) receptor, partially overlapping but distinct from the EGF-binding epitope*. J Biol Chem, 2002. **277**(38): p. 35671-81.
181. Zhu, J.X., et al., *Decorin evokes protracted internalization and degradation of the epidermal growth factor receptor via caveolar endocytosis*. J Biol Chem, 2005. **280**(37): p. 32468-79.
182. Csordas, G., et al., *Sustained down-regulation of the epidermal growth factor receptor by decorin. A mechanism for controlling tumor growth in vivo*. J Biol Chem, 2000. **275**(42): p. 32879-87.
183. Neill, T., et al., *Decorin has an appetite for endothelial cell autophagy*. Autophagy, 2013. **9**(10): p. 1626-8.
184. Goyal, A., et al., *Decorin activates AMPK, an energy sensor kinase, to induce autophagy in endothelial cells*. Matrix Biol, 2014. **34**: p. 46-54.
185. Neill, T., L. Schaefer, and R.V. Iozzo, *Decorin: a guardian from the matrix*. Am J Pathol, 2012. **181**(2): p. 380-7.
186. Gubbiotti, M.A., et al., *Decorin interacting network: A comprehensive analysis of decorin-binding partners and their versatile functions*. Matrix Biol, 2016. **55**: p. 7-21.
187. Martin, P. and R. Nunan, *Cellular and molecular mechanisms of repair in acute and chronic wound healing*. Br J Dermatol, 2015. **173**(2): p. 370-8.
188. Veith, A.P., et al., *Therapeutic strategies for enhancing angiogenesis in wound healing*. Adv Drug Deliv Rev, 2019. **146**: p. 97-125.
189. DiPietro, L.A., *Angiogenesis and wound repair: when enough is enough*. J Leukoc Biol, 2016. **100**(5): p. 979-984.
190. Rustad, K.C. and G.C. Gurtner, *Mesenchymal Stem Cells Home to Sites of Injury and Inflammation*. Adv Wound Care (New Rochelle), 2012. **1**(4): p. 147-152.
191. Li, L. and J. Jiang, *Regulatory factors of mesenchymal stem cell migration into injured tissues and their signal transduction mechanisms*. Front Med, 2011. **5**(1): p. 33-9.
192. Huang, Y.Z., et al., *Mesenchymal Stem Cells for Chronic Wound Healing: Current Status of Preclinical and Clinical Studies*. Tissue Eng Part B Rev, 2020. **26**(6): p. 555-570.
193. Hu, X., et al., *Transplantation of hypoxia-preconditioned mesenchymal stem cells improves infarcted heart function via enhanced survival of implanted cells and angiogenesis*. J Thorac Cardiovasc Surg, 2008. **135**(4): p. 799-808.

194. Latijnhouwers, M., et al., *Human epidermal keratinocytes are a source of tenascin-C during wound healing*. J Invest Dermatol, 1997. **108**(5): p. 776-83.
195. Swindle, C.S., et al., *Epidermal growth factor (EGF)-like repeats of human tenascin-C as ligands for EGF receptor*. J Cell Biol, 2001. **154**(2): p. 459-68.
196. Johnson, N.R. and Y. Wang, *Controlled delivery of heparin-binding EGF-like growth factor yields fast and comprehensive wound healing*. J Control Release, 2013. **166**(2): p. 124-9.
197. Johnson, N.R. and Y. Wang, *Coacervate delivery of HB-EGF accelerates healing of type 2 diabetic wounds*. Wound Repair Regen, 2015. **23**(4): p. 591-600.
198. Park, U., et al., *Coacervate-mediated exogenous growth factor delivery for scarless skin regeneration*. Acta Biomater, 2019. **90**: p. 179-191.
199. Li, H., et al., *Sustained release of bone morphogenetic protein 2 via coacervate improves the osteogenic potential of muscle-derived stem cells*. Stem Cells Transl Med, 2013. **2**(9): p. 667-77.
200. Huen, A.C. and A. Wells, *The Beginning of the End: CXCR3 Signaling in Late-Stage Wound Healing*. Adv Wound Care (New Rochelle), 2012. **1**(6): p. 244-248.
201. Yates, C.C., et al., *Delayed and deficient dermal maturation in mice lacking the CXCR3 ELR-negative CXC chemokine receptor*. Am J Pathol, 2007. **171**(2): p. 484-95.
202. Shima, Y., et al., *In vitro transformation of mesenchymal stem cells by oncogenic H-rasVal12*. Biochem Biophys Res Commun, 2007. **353**(1): p. 60-6.
203. Ades, E.W., et al., *HMEC-1: establishment of an immortalized human microvascular endothelial cell line*. J Invest Dermatol, 1992. **99**(6): p. 683-90.
204. Carpentier, G., et al., *Angiogenesis Analyzer for ImageJ - A comparative morphometric analysis of "Endothelial Tube Formation Assay" and "Fibrin Bead Assay"*. Sci Rep, 2020. **10**(1): p. 11568.
205. Hancock, W.W., et al., *Requirement of the chemokine receptor CXCR3 for acute allograft rejection*. J Exp Med, 2000. **192**(10): p. 1515-20.
206. Chu, H., et al., *A [polycation:heparin] complex releases growth factors with enhanced bioactivity*. J Control Release, 2011. **150**(2): p. 157-63.
207. Yates, C.C., et al., *ELR-negative CXC chemokine CXCL11 (IP-9/I-TAC) facilitates dermal and epidermal maturation during wound repair*. Am J Pathol, 2008. **173**(3): p. 643-52.
208. Coelho, P.G.B., et al., *Evaluation of dermal collagen stained with picrosirius red and examined under polarized light microscopy*. An Bras Dermatol, 2018. **93**(3): p. 415-418.

209. Puspoki, Z., et al., *Transforms and Operators for Directional Bioimage Analysis: A Survey*. Adv Anat Embryol Cell Biol, 2016. **219**: p. 69-93.
210. Rezakhaniha, R., et al., *Experimental investigation of collagen waviness and orientation in the arterial adventitia using confocal laser scanning microscopy*. Biomech Model Mechanobiol, 2012. **11**(3-4): p. 461-73.
211. Fonck, E., et al., *Effect of aging on elastin functionality in human cerebral arteries*. Stroke, 2009. **40**(7): p. 2552-6.
212. Nuschke, A., et al., *Epidermal Growth Factor Tethered to beta-Tricalcium Phosphate Bone Scaffolds via a High-Affinity Binding Peptide Enhances Survival of Human Mesenchymal Stem Cells/Multipotent Stromal Cells in an Immune-Competent Parafascial Implantation Assay in Mice*. Stem Cells Transl Med, 2016. **5**(11): p. 1580-1586.
213. Johnson, N.R., et al., *Coacervate Delivery of Growth Factors Combined with a Degradable Hydrogel Preserves Heart Function after Myocardial Infarction*. ACS Biomater Sci Eng, 2015. **1**(9): p. 753-759.
214. Dash, B.C., et al., *Stem Cells and Engineered Scaffolds for Regenerative Wound Healing*. Bioengineering (Basel), 2018. **5**(1).
215. Zhu, Z., J. Ding, and E.E. Tredget, *The molecular basis of hypertrophic scars*. Burns Trauma, 2016. **4**: p. 2.
216. Bock, O., et al., *Quality of life of patients with keloid and hypertrophic scarring*. Arch Dermatol Res, 2006. **297**(10): p. 433-8.
217. Ghazawi, F.M., et al., *Insights into the Pathophysiology of Hypertrophic Scars and Keloids: How Do They Differ?* Adv Skin Wound Care, 2018. **31**(1): p. 582-595.
218. Oliveira, G.V., et al., *Hypertrophic versus non hypertrophic scars compared by immunohistochemistry and laser confocal microscopy: type I and III collagens*. Int Wound J, 2009. **6**(6): p. 445-52.
219. Chen, S. and D.E. Birk, *Focus on molecules: decorin*. Exp Eye Res, 2011. **92**(6): p. 444-5.
220. Pang, X., N. Dong, and Z. Zheng, *Small Leucine-Rich Proteoglycans in Skin Wound Healing*. Front Pharmacol, 2019. **10**: p. 1649.
221. Merline, R., R.M. Schaefer, and L. Schaefer, *The matricellular functions of small leucine-rich proteoglycans (SLRPs)*. J Cell Commun Signal, 2009. **3**(3-4): p. 323-35.
222. Sylakowski, K. and A. Wells, *ECM-regulation of autophagy: The yin and the yang of autophagy during wound healing*. Matrix Biol, 2021. **100-101**: p. 197-206.
223. Yates, C.C., et al., *Lack of CXC chemokine receptor 3 signaling leads to hypertrophic and hypercellular scarring*. Am J Pathol, 2010. **176**(4): p. 1743-55.

224. Hwang, J., M.O. Sullivan, and K.L. Kiick, *Targeted Drug Delivery via the Use of ECM-Mimetic Materials*. Front Bioeng Biotechnol, 2020. **8**: p. 69.
225. Krishna, P., et al., *Primed fibroblasts and exogenous decorin: potential treatments for subacute vocal fold scar*. Otolaryngol Head Neck Surg, 2006. **135**(6): p. 937-45.
226. Eckert, R.L., et al., *Involucrin--structure and role in envelope assembly*. J Invest Dermatol, 1993. **100**(5): p. 613-7.
227. Xue, M. and C.J. Jackson, *Extracellular Matrix Reorganization During Wound Healing and Its Impact on Abnormal Scarring*. Adv Wound Care (New Rochelle), 2015. **4**(3): p. 119-136.
228. Occleston, N.L., et al., *New therapeutics for the prevention and reduction of scarring*. Drug Discov Today, 2008. **13**(21-22): p. 973-81.
229. Aubert, A., et al., *Latent TGF-beta Activation Is a Hallmark of the Tenascin Family*. Front Immunol, 2021. **12**: p. 613438.
230. Katoh, D., et al., *Tenascin-C Induces Phenotypic Changes in Fibroblasts to Myofibroblasts with High Contractility through the Integrin  $\alpha$ v $\beta$ 1/Transforming Growth Factor beta/SMAD Signaling Axis in Human Breast Cancer*. Am J Pathol, 2020. **190**(10): p. 2123-2135.
231. De Laporte, L., et al., *Tenascin C promiscuously binds growth factors via its fifth fibronectin type III-like domain*. PLoS One, 2013. **8**(4): p. e62076.
232. Ummarino, D., *Systemic sclerosis: Tenascin C perpetuates tissue fibrosis*. Nat Rev Rheumatol, 2016. **12**(7): p. 375.
233. Bhattacharyya, S., et al., *Tenascin-C drives persistence of organ fibrosis*. Nat Commun, 2016. **7**: p. 11703.
234. Ruiz Martinez, M.A., et al., *Role of proteoglycans on skin ageing: a review*. Int J Cosmet Sci, 2020. **42**(6): p. 529-535.
235. Li, Y., et al., *Age-dependent alterations of decorin glycosaminoglycans in human skin*. Sci Rep, 2013. **3**: p. 2422.
236. Kimura, W. and H.A. Sadek, *The cardiac hypoxic niche: emerging role of hypoxic microenvironment in cardiac progenitors*. Cardiovasc Diagn Ther, 2012. **2**(4): p. 278-89.
237. Ivanovic, Z., *Hypoxia or in situ normoxia: The stem cell paradigm*. J Cell Physiol, 2009. **219**(2): p. 271-5.
238. Rosova, I., et al., *Hypoxic preconditioning results in increased motility and improved therapeutic potential of human mesenchymal stem cells*. Stem Cells, 2008. **26**(8): p. 2173-82.

239. Ejtehadifar, M., et al., *The Effect of Hypoxia on Mesenchymal Stem Cell Biology*. Adv Pharm Bull, 2015. **5**(2): p. 141-9.
240. Basciano, L., et al., *Long term culture of mesenchymal stem cells in hypoxia promotes a genetic program maintaining their undifferentiated and multipotent status*. BMC Cell Biol, 2011. **12**: p. 12.
241. Moya, A., et al., *Human Mesenchymal Stem Cell Failure to Adapt to Glucose Shortage and Rapidly Use Intracellular Energy Reserves Through Glycolysis Explains Poor Cell Survival After Implantation*. Stem Cells, 2018. **36**(3): p. 363-376.
242. Palomaki, S., et al., *HIF-1alpha is upregulated in human mesenchymal stem cells*. Stem Cells, 2013. **31**(9): p. 1902-9.
243. Wagegg, M., et al., *Hypoxia promotes osteogenesis but suppresses adipogenesis of human mesenchymal stromal cells in a hypoxia-inducible factor-1 dependent manner*. PLoS One, 2012. **7**(9): p. e46483.
244. Lv, B., et al., *Hypoxia inducible factor 1alpha promotes survival of mesenchymal stem cells under hypoxia*. Am J Transl Res, 2017. **9**(3): p. 1521-1529.
245. Beegle, J., et al., *Hypoxic preconditioning of mesenchymal stromal cells induces metabolic changes, enhances survival, and promotes cell retention in vivo*. Stem Cells, 2015. **33**(6): p. 1818-28.
246. Papandreou, I., et al., *HIF-1 mediates adaptation to hypoxia by actively downregulating mitochondrial oxygen consumption*. Cell Metab, 2006. **3**(3): p. 187-97.
247. Lee, J.H., Y.M. Yoon, and S.H. Lee, *Hypoxic Preconditioning Promotes the Bioactivities of Mesenchymal Stem Cells via the HIF-1alpha-GRP78-Akt Axis*. Int J Mol Sci, 2017. **18**(6).
248. Saini, U., et al., *Preconditioning mesenchymal stem cells with caspase inhibition and hyperoxia prior to hypoxia exposure increases cell proliferation*. J Cell Biochem, 2013. **114**(11): p. 2612-23.
249. Mazure, N.M. and J. Pouyssegur, *Hypoxia-induced autophagy: cell death or cell survival?* Curr Opin Cell Biol, 2010. **22**(2): p. 177-80.
250. Yang, Z. and D.J. Klionsky, *Mammalian autophagy: core molecular machinery and signaling regulation*. Curr Opin Cell Biol, 2010. **22**(2): p. 124-31.
251. Klionsky, D.J., et al., *How shall I eat thee?* Autophagy, 2007. **3**(5): p. 413-6.
252. Mizushima, N., et al., *Autophagy fights disease through cellular self-digestion*. Nature, 2008. **451**(7182): p. 1069-75.

253. Levine, B. and J. Yuan, *Autophagy in cell death: an innocent convict?* J Clin Invest, 2005. **115**(10): p. 2679-88.
254. Maiuri, M.C., et al., *Self-eating and self-killing: crosstalk between autophagy and apoptosis.* Nat Rev Mol Cell Biol, 2007. **8**(9): p. 741-52.
255. Hu, C., et al., *Modulating autophagy in mesenchymal stem cells effectively protects against hypoxia- or ischemia-induced injury.* Stem Cell Res Ther, 2019. **10**(1): p. 120.
256. Oliver, L., et al., *Basal autophagy decreased during the differentiation of human adult mesenchymal stem cells.* Stem Cells Dev, 2012. **21**(15): p. 2779-88.
257. Lee, Y., et al., *Increased SCF/c-kit by hypoxia promotes autophagy of human placental chorionic plate-derived mesenchymal stem cells via regulating the phosphorylation of mTOR.* J Cell Biochem, 2013. **114**(1): p. 79-88.
258. Nuschke, A., et al., *Human mesenchymal stem cells/multipotent stromal cells consume accumulated autophagosomes early in differentiation.* Stem Cell Res Ther, 2014. **5**(6): p. 140.
259. Pantovic, A., et al., *Coordinated time-dependent modulation of AMPK/Akt/mTOR signaling and autophagy controls osteogenic differentiation of human mesenchymal stem cells.* Bone, 2013. **52**(1): p. 524-31.
260. Bellot, G., et al., *Hypoxia-induced autophagy is mediated through hypoxia-inducible factor induction of BNIP3 and BNIP3L via their BH3 domains.* Mol Cell Biol, 2009. **29**(10): p. 2570-81.
261. Janji, B., et al., *The multifaceted role of autophagy in tumor evasion from immune surveillance.* Oncotarget, 2016. **7**(14): p. 17591-607.
262. Liu, J., et al., *Hypoxia regulates the therapeutic potential of mesenchymal stem cells through enhanced autophagy.* Int J Low Extrem Wounds, 2015. **14**(1): p. 63-72.
263. Zhang, Z., et al., *Autophagy mediates the beneficial effect of hypoxic preconditioning on bone marrow mesenchymal stem cells for the therapy of myocardial infarction.* Stem Cell Res Ther, 2017. **8**(1): p. 89.
264. Neill, T., L. Schaefer, and R.V. Iozzo, *Instructive roles of extracellular matrix on autophagy.* Am J Pathol, 2014. **184**(8): p. 2146-53.
265. Gubbiotti, M.A., et al., *Proteoglycan signaling in tumor angiogenesis and endothelial cell autophagy.* Semin Cancer Biol, 2019.
266. Wei, Y., et al., *EGFR-mediated Beclin 1 phosphorylation in autophagy suppression, tumor progression, and tumor chemoresistance.* Cell, 2013. **154**(6): p. 1269-84.

267. Wang, B., S. Ling, and W.C. Lin, *14-3-3Tau regulates Beclin 1 and is required for autophagy*. PLoS One, 2010. **5**(4): p. e10409.
268. Fung, C., et al., *Induction of autophagy during extracellular matrix detachment promotes cell survival*. Mol Biol Cell, 2008. **19**(3): p. 797-806.
269. Xu, Q., et al., *Type I collagen promotes primary cilia growth through down-regulating HDAC6-mediated autophagy in confluent mouse embryo fibroblast 3T3-L1 cells*. J Biosci Bioeng, 2018. **125**(1): p. 8-14.
270. Knorr, R.L., R. Dimova, and R. Lipowsky, *Curvature of double-membrane organelles generated by changes in membrane size and composition*. PLoS One, 2012. **7**(3): p. e32753.
271. Backues, S.K., et al., *Estimating the size and number of autophagic bodies by electron microscopy*. Autophagy, 2014. **10**(1): p. 155-64.
272. Xie, Z., U. Nair, and D.J. Klionsky, *Atg8 controls phagophore expansion during autophagosome formation*. Mol Biol Cell, 2008. **19**(8): p. 3290-8.
273. Stolz, D.B., et al., *Cationic colloidal silica membrane perturbation as a means of examining changes at the sinusoidal surface during liver regeneration*. Am J Pathol, 1999. **155**(5): p. 1487-98.
274. Parnell, L.K.S. and S.W. Volk, *The Evolution of Animal Models in Wound Healing Research: 1993-2017*. Adv Wound Care (New Rochelle), 2019. **8**(12): p. 692-702.
275. Masson-Meyers, D.S., et al., *Experimental models and methods for cutaneous wound healing assessment*. Int J Exp Pathol, 2020. **101**(1-2): p. 21-37.